2015

A multiplex self-referencing detection of pathogens using surface enhanced raman scattering nanoprobes with a nano-DEP microfluidic concentrator

Chao Wang
Iowa State University

A multiplex self-referencing detection of pathogens using surface enhanced raman scattering nanoprobes with a nano-DEP microfluidic concentrator

by

Chao Wang

A dissertation submitted to the graduate faculty

in partial fulfillment of the requirements for the degree of

DOCTOR OF PHILOSOPHY

Major: Environmental Science

Program of Study Committee:
Chenxu Yu, Major Professor
Jacek A. Koziel
Kurt A. Rosentrater
Xinwei Wang
Michelle L. Soupir

Iowa State University

Ames, Iowa

2015

TABLE OF CONTENTS

LIST OF FIGURES

LIST OF TABLES

CHAPTER 1. OVERVIEW OF THE CURRENT STATE OF RELEVENT RESEARCH

1.1. Waterborne pathogen identification

Environmental contamination by microorganisms may pose a serious threat to human health and sustainable development of society and economy. The presence of environmental pathogens and their toxins, and organic pollutants is a major issue that draws both scientific interests and public concerns. In terms of water safety, the presence of waterborne pathogens in drinking water, wastewater and recreational water can be a critical issue that demands attention from regulatory agencies, healthcare agencies, and industry sectors. For instance, some pathogenic strains of *Escherichia coli (E.coli)* in water contamination can cause diarrhea and death in immunocompromised individuals due to dehydration from prolonged illness; some species of *Staphylococci* bacteria cause food poisoning and toxic-shock syndrome while some species of *Streptococci* cause throat and middle ear infections and dental caries. The presence of these waterborne pathogens has threatened the quality and safety of the drinking water supply. Hence, it is an urgency to improve the current techniques of pathogen detection, monitoring, and characterization (Bentley and Meganathan. 1982; Ishige et al., 2005; Ryan and Ray. 2004; WHO. 2007).

Detection for microorganisms has come a long way since the microscope had been invented to investigate the microbial world. When it comes to microbial contamination of water systems, it remains to be challenging because most of drinking water outbreaks are caused by undetectable or unidentified agents by microscopic techniques (Reynolds.

2003). For instance, viruses are responsible for a significant portion of gastrointestinal illness in the United States. However, many of viruses cannot be cultured in the laboratory. Moreover, new strains of pathogens continue to emerge which present important additional challenges to both the water and public health sectors. Furthermore, the technical challenges and cost are always high in targeting and confirming a specific microbe as the causative agent of a disease. These are the major reasons why the indicator organisms are still the main monitoring tool used to measure both changes in environmental quality or conditions and the potential presence of hard-to-detect target pathogenic organisms. An indicator organism provides indirect evidences of the presence or absence of a pathogenic organism that may survive under similar physical, chemical, and nutrient conditions. However, viral, bacterial, parasitic protozoan pathogens are unlikely to all behave in the same way as a single indicator group, and certainly not in all situations. Therefore, there is no ideal or universal indicator which could directly reflect the exact correlation between numbers of any indicator and enteric pathogen (Guidelines for Drinking-water Quality. 1985; Bordner and Winter. 1978; Dutka. 1975; McFeters et al., 1974; Muller. 1964).

1.2. Traditional microbiological methods in water quality analysis

Traditional bacterial testing methods rely on specific media to enumerate and isolate viable bacterial cells in water samples (McFters et al., 1982). These methods are cheap and can give both qualitative and quantitative information on the number and the nature of microorganisms in water samples.

The most generally accepted method was the Multiple-Tube Fermentation test, which is referred to as the most probable number or MPN procedure. In this method a measured sub-sample (10 ml) is diluted with 100 ml of sterile growth medium and an aliquot of 10 ml is then decanted into each of ten tubes. The remaining 10 ml is then diluted again and the process repeated. At the end of 5 dilutions this produces 50 tubes covering the dilution range of 1:10 through to 1:10000. The tubes are then incubated at a pre-set temperature for a specified time and at the end of the process the number of tubes with growth showing is counted for each dilution. Statistical tables are then used to derive the concentration of organisms in the original sample. This method can be enhanced by using indicator medium which changes color when acid forming species are present, and by including a tiny inverted tube called a Durham tube in each sample tube. The Durham inverted tube catches any gas produced. The production of gas at 37 degrees Celsius is a strong indication of the presence of *E.coli* (EPAa. 2002).

Another common method is plate counting which relies on bacteria growing into a colony on a nutrient medium so that the colony becomes visible to the naked eye and the number of colonies on a plate can be counted. To ensure that an appropriate number of colonies will be generated several dilutions are normally cultured. This approach is widely utilized for the evaluation of the effectiveness of water treatment by the inactivation of representative microbial contaminants such as *E. coli* following ASTM D5465 (Hanaor and Sorrell. 2014; Hanaor et al., 2011). The laboratory procedure involves making serial dilutions of the sample (1:10, 1:100, 1:1000, etc.) in sterile water and cultivating these on nutrient agar in a dish that is sealed and incubated. Typical

media include plate counting agar for a general count or MacConkey agar to count Gram-negative bacteria such as *E. coli*. Typically one set of plates is incubated at 22°C and for 24 hours, and a second set at 37°C for 24 hours. The composition of the nutrient usually includes reagents that resist the growth of non-target organisms and make the target organism easily identifiable, often by a color change in the medium. Some recent methods include a fluorescent agent so that counting of the colonies can be automated. At the end of the incubation period the colonies are counted by visual inspection, a procedure that takes a few minutes and does not require a microscope as the colonies are typically a few millimetres across (Vial. 1977).

The third common method, membrane filtration, is widely used in modern laboratories for pathogen detection nowadays. Briefly, serial dilutions of the samples are vacuum filtered through membrane filters of sufficiently small pore size to retain the organisms sought. These filters are themselves placed on appropriate nutrient medium within sealed plates, or pad saturated with appropriate broth medium and incubated. If the organisms sought are present, colonies will grow on the membrane filter. Colonies are examined at 10–15X magnification with a stereoscopic microscope and then identified by size, color, shape and sheen. Typical colonies are counted and the number is reported as the number of colonies per 100 mL of sample. The methodology is otherwise similar to conventional total plate counts. Membranes have a printed millimetre grid printed on and can be reliably used to count the number of colonies under a binocular microscope (EPAb. 2002; Grant. 1997).

1.3. Advanced molecular detection methods

Even though the current standard detection methods can report elevated levels of indicator bacteria, more specific analysis is often needed to understand the behavior or presence of pathogenic bacteria specifically at strain level. Moreover, conventional methods usually take days to complete. Timing could be an important factor in water system pathogen detection and monitoring. The long procedure not only would not provide a sufficient protection from exposure to waterborne pathogens within water systems, but also would negatively affect tracking of contamination sources because the contamination signals can dissipate over the long incubation process. Furthermore, the required limit of detection (LOD) for pathogenic bacteria is very low, hence efficient separation and concentration techniques need to be used for specific detection of pathogens and to avoid false-negative results. Due to these critical requirements, advanced molecular pathogen detection methods have seen some rapid development in the recent decade.

1.3.1. Immunological assay

Immunological methods rely on the specific binding of an antibody to an antigen. Immunoassay refers to the qualitative and quantitative determination of antigen and antibody in a specimen by immunological reaction. This kind of techniques is considered to be highly sensitive, and reduces the tedious culture steps by using automatic mechanical devices. The specificity is also dramatically improved due to the development of monoclonal antibodies instead of polyclonal antibodies which actually contain a collection of antibodies having different cellular origin. Even though this kind

of molecular detection technique provides high degree of sensitivity and reproducibility, it is difficult to employ in field, such as at rivers and drinking water distributors, due to the requirement of complex instrumentation and well-trained operators. Enzyme-linked Immunosorbent Assay (ELISA) is the most common and commercially heterogeneous immunological assay. The LOD of conventional ELISA ranges from 10^5 CFU/mL for whole bacterial cells (Shen et al., 2014). Therefore, extreme low concentration bacteria water samples can still not be directly diagnosed using ELISA. Furthermore, expensive and short shelve half-life of certain reagents also limits the utility of ELISA or other immunological assays in rural areas of developing countries. Moreover, extensive sample preparation and long readout time are still required, resulting in delayed response and disease containment (Mandal et al., 2011; Lazcka et al., 2007; Skottrup et al., 2009).

1.3.2. Nucleic acid assay

The polymerase chain reaction (PCR) is a technology in molecular biology that amplifies a single copy or a few copies of a piece of DNA across several orders of magnitude, generating thousands to millions of copies of a particular DNA sequence (Bartlett and Stirling. 2003). Since nucleic acid sequences are the fingerprinting properties for a specific type of bacterial pathogen, PCR is an excellent method to detect and identify a single infectious microbiological target. However, PCR might produce either false negative or false positive results, due to the presence of inhibitory compounds or cross-contamination, respectively. In addition, it also involves multi-step

processing, well-trained personnel, considerable time and expensive instrumentation and reagents (Ashimoto et al., 1996; Burg et al., 1989; Josephson et al., 1993).

1.4. Pathogen detection biosensor

Although molecular techniques have significantly improved the sensitivity and specificity of waterborne microbes' detection, they are not without their own weaknesses. Certain methods look good and work well if used in pilot or lab scale by skillful technicians, but are not practical enough for routine testing of real water samples on-site or in field.

Biosensors are widely used today in health care and food industry as well as environmental monitoring. International Union of Pure and Applied Chemistry (IUPAC) now define a biosensor as a self-contained integrated device that provides quantitative analytical information using a biological recognition element (biochemical receptor) in contact with a transduction element. Biosensors can be classified into various groups, based either on signal transduction mechanism, or bio-recognition principle. On the basis of the signal transducing elements, biosensors can be categorized as electrochemical, optical, piezoelectric or thermal sensors. According to the bio-recognition principles, biosensors are classified into immunochemical, enzymatic, non-enzymatic receptor, and whole-cell and DNA biosensors (Fig. 1).

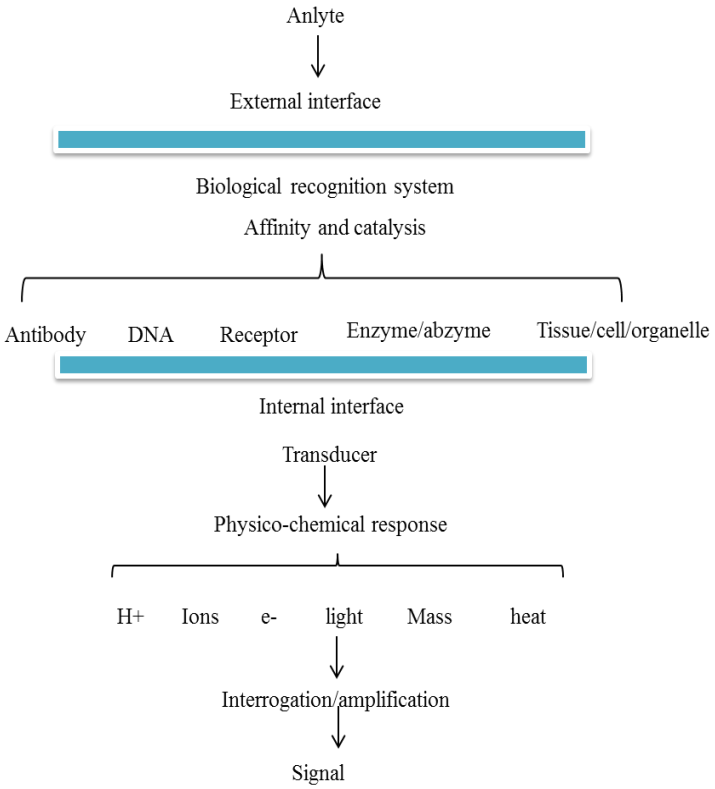

Fig. 1.1 Schematic diagram of possible biosensor analyte recognition

The need for disposable systems or tools for environmental monitoring has encouraged the development of new technologies and more suitable methodologies, which could give highly sensitive and reliable detection results, and even allow on-site field monitoring without trained operators. In this respect, biosensors have demonstrated a great potential to complement standard analytical methods for a number of environmental monitoring applications such as ground water screening, ocean monitoring, and global environmental monitoring. First of all, biosensor-based techniques usually do not involve serial dilutions, so that they are simple to perform and faster than the traditional detection methods. High throughput biosensor systems are capable of analyzing hundreds of samples over a short time span since the instrument is computer-driven and automated to enable continuous monitoring. Furthermore, biosensors have the possibility of portability, of miniaturization and

working on-site, and the ability to measure pollutants in complex matrices with minimal sample preparation. Equally important, they offer the possibility of determining not only specific chemical but also the biological effects, such as toxicity, cytotoxicity, and genotoxicity.

1.5. Review of current study in pathogen detection biosensors

1.5.1. Bioluminescence sensor

Bioluminescence is the production and emission of light by a living organism. It is a form of chemiluminescence and this phenomenon is used in microbiological targets detection. Among various bioluminescence sensors, ATP and bacterial bioluminescence are the major two applications in water pathogen detection. The first one utilizes enzyme and coenzyme complex (Luciferase-Luciferin) to react with the common ATP molecule existed in the living target cells. The total light output is directly proportional to the amount of ATP present and can be quantified by luminometers. However, in order to produce a minimal readable signal, at least 1000 bacterial cells are needed, which blocks the possibility of further lowering the detection limit. The later one uses the gene which is responsible for bacterial bioluminescence. DNA segment carrying this gene can by introduced into host-specific phages. After infection to the host bacterium, the lux gene could trigger the light emission in the host, which can be easily detected by luminometers. This technique can detect 100 cells in 60 min and the specificity of this assay depends on the phage specificity.

1.5.2. Fluorescence biosensor

Typically, the fluorephore, used in fluorescence biosensor applications, is excited by a specific wavelength of light and then it emits light at a different wavelength. Reporter molecules, labeled with fluorescent dyes, are required in sensitive detection of the target analytes presented at a trace level in the sample. Fluorescent labeling reagents include: organic dyes, nanoparticles, and rare-earth elements. Generally, molecular emission such as fluorescence and phosphorescence is about 1000 times superior in sensitivity than most spectrophotometric methods, and hence archiving lower limits of detection for the desired analytes (Guilbault, 1990; Yu et al., 2015).

1.5.3. Surface Plasmon Resonance (SPR) sensor

SPR is a phenomenon that occurs during optical illumination of a metal surface and it can be used for biomolecular interaction analysis. In a typical SPR biosensor, the specific antibodies are immobilized on a gold or silver coated thin slide, which is called the sensing surface. The sensing surface is located above a high index-resonant layer and a low index coupling layer. When a visible or near-IR external source is passed through the waveguide in such a way, it causes an internal total refection on the surface of the waveguide. At a certain wavelength in the red or near-IR region, the light interacts with plasma or cloud of electrons on the high index-metal surface and the resonance effect causes a strong absorbance. The presence of antigens interacting with the receptor or antibody causes a shift in the resonance to longer wavelengths and the amount of shift can be related to the concentration of the bound molecules (Bhunia. 2007; Rasooly and Herold. 2006; Taylor et al., 2008).

1.5.4. Electric impedance sensor

Impedance biosensor detects the ions or carbon dioxide produced from metabolic end products. Microbial metabolism usually results in an increase in both conductance and capacitance, causing a decrease in impedance. To be more specific, if lactose, one kind of nutrients, is provided to microbes, they will convert the lactose to lactic acid in ionic form which could change the impedance measured by a bridge circuit. It is considered that impedance sensor is well suited for detection of bacteria in water samples and to monitor water quality. However, this technique is not suited for testing samples with low number of microorganisms and that the sample matrix may interfere with the analysis (Yang et al., 2004; Sun et al., 1995).

1.5.5. Piezoelectric sensor

Piezoelectric sensor could detect the bacteria in water sample after coating the surface of the sensor with a selective binding substance, for example, antibodies. The bacteria will bind to the immobilized antibodies and the mass of gold-plated piezoelectric crystal will increase while the resonance frequency of oscillation will decrease proportionally. This technique offers a real time output, simplicity of use and cost effectiveness (Su and Li. 2004; Janshoff et al., 2000; He et al., 1994).

1.6. Thesis scope

Although a great advance has been made in the realm of biosensors in the past decade, many challenges remain for biosensors to truly become field-deployable tools for pathogen detection. Among them the most significant ones are the sample handling at low concentrations, and the consistency of highly sensitive detection.

In my PhD research, I aim to create a biosensor that can detect pathogens at extremely low level with high consistency and user-friendly operation protocols, and can be used to rapidly process water samples for easy sample preparation. I developed a concept of self-referencing mechanism that utilizes Surface enhanced Raman scattering (SERS) molecular probes to achieve target bacteria detection in one single step with high reliability brought by a novel multiplex targeting scheme, and integrated the detection methodology with a microfluidic sample preparation platform for easy interrogation of water samples. The technique I developed is a major step forward towards developing a real field-deployable biosensor for rapid pathogen detection.

1.7. Reference

Ashimoto A, Chen C, Bakker I, Slots J 1996 Polymerase chain reaction detection of 8 putative periodontal pathogens in subgingival plaque of gingivitis and advanced periodontitis lesions *Oral Microbiology and Immunology*. 11 266-273

Bartlett, JM Stirling D 2003 A short History of the Polynerase Chain Reaction *PCR Protocals. Methods in Molecular Biology*. 226 3-6

Bentley R, Meganathan R 1982 Biosynthesis of vitamin K (menaquinone) in bacteria *Microbiol. Rev*. 46 241-280

Bhunia AK 2007 Biosensors and bio-based methods for the separation and detection of foodborne pathogens *Adv. Food Nutr. Res*. 54 1-44

Bordner R. Winter J 1978 Microbiological methods for Monitoring the Environment: Water and Wastes *EPA-600/8-78-017*. Cincinnati, Ohio

Burg JL, Grover CM, Pouletty P, Boothroyd JC 1989 Direct and sensitive detection of a pathogenic protozoan, Toxoplasma gondii, by polymerase chain reaction *J. Clin. Microbiol.* 27 1787-1792

Dutka, BJ 1975 Coliforms are an Inadequate Index of Water Quality *J. Environ. Health.* 36 39-46

Grant MA 1997 A New Membrane Filtration Medium for Simultaneous Detection and Enumeration of *Escherichia coli* and Total Coliform *Appl. Environ. Microbiol*. 63 3526-3530

Guilbault GG 1990 Practical fluorescence New York. *CRC Publisher and Distributor*.

Guidelines for Drinking-water Quality Vol. 1. 1985 World Health Organization. Geneva

Hanaor DH, Sorrell CC 2014 Sand Supported Mixed-Phase TiO_2 Photocatalysts for Water Decontamination Applications *Advanced Engineering Materials* 16 (2): 248–254

Hanaor D, Michelazzi M, Leonelli C, Sorrell CC 2011 The effects of firing conditions on the properties of electrophoretically deposited titanium dioxide films on graphite substrates *Journal of the European Ceramic Society* 31 (15): 2877–2885

Ishige T, Honda K, Shimizu S 2005 Whole organism biocatalysis *Current Opinion in Chemical Biology*. 9 174-180

He F, Geng Q, Zhu W, Nie L, Yao S, Meifeng C 1994 Rapid detection of Escherichia coli using a separated electrode piezoelectric crystal sensor *Anal. Chimica. Acta*. 289 313-319

Janshoff A, Galla HJ, Steinem C 2000 Piezoelectric Mass-Sensing Devices as Biosensor---An Alternative to Optical Biosensors? *Angew. Chem. Int. Ed*. 39 4004-4032

Josephson KL, Gerba CP, Pepper IL 1993 Polymerase chain reaction detection of nonviable bacterial pathogens *Appl. Environ. Microbiol*. 59 3513-3515

Lazcka O, Javier F, Del Campo D, Xunoz FX 2007 Pathogen detection: A perspective of traditional methods and biosensors *Biosensors and Bioelectronics*. 22 1205-1217

Mandal PK, Biswas AK, Choi K, Pal UK 2011 Methods for Rapid Detection of Foodborne Pathogen: An Overview *American Journal of Food Technology*. 6 87-102

McFeters GA et al. 1974 Comparative Survival of Indicator Bacteria and Enteric Pathogens in Well Water *Appl. Environ. Microbiol.* 27 823-829

McFeters GA, Cameron SC, LeChevallier MW 1982 Influence of Diluents, Media and Membrane Filter on the Detection of Injured Waterborne Coliform Bacteria *Appl. Environ. Microbiol.* 43 97-103

Muller G 1964 What are the Lessons of the Hamburg Flood for Drinking Water Hygiene Standards? *Arch. Hyg. Bakterilo.* 148 321-326

Rasooly A and Herold KE 2006 Biosensors for the analysis of food and waterborne pathogens and their toxins *J. AOAC. Int.* 85 984-995

Skottrup PD, Micolaisen M, Justesen AF 2009 Towards on-site pathogen detection using antibody-based sensors *Biosensors and Bioelectronics*. 24 339-348

Su XL, Li Y 2004 A Self-assembled monolayer-based piezoelectric immunosensor for rapid detection of Escherichia coli O157:H7 *Biosensors and Bioelectronics*. 19 563-574

Sun F, Rogers CA, Liang C 1995 Structural frequency response function acquisition via electric impedance measurement of surface-bonded piezoelectric sensor/actuator *Proceedings of 36th AIAA/ASME/ASCE*. 3450-3458

Taylor AD, Ladd J, Homola J, Jiang S 2008 Surface Plasmon Resonance (SPR) Sensors for the Detection of Bacterial Pathogens *Principles of Bacterial Detection: Biosensors, Recognition Receptors and Microsystems*. Springer New York. 83-108

U.S. Environmental Protection Agency (EPAa). 2002. Method 1680: Fecal Coliforms in Biosolids by Multiple-Tube Fermentation Procedures. Washington, D. C.

U.S. Environmental Protection Agency (EPAb). 2002. Method 1106.1: Enterococci in Water by Membrane Filtration Using membrane-Enterococcus-Esculin Iron Agar (mE-EIA)

Via J 1977 Bacteriological Analysis of Drinking Water *Commission of the European Communities Luxembourg*.

Yang L, Li Y, Griffis C, Johnson MG 2004 Interdigitated microelectrode (IME) impedance sensor for the detection of viable *Salmonella typhimurium Biosensors and Bisoelectronics*. 19 1139-1147

Yu Q, Wang Q, Li B, Lin Q, Duan Y 2015 Technological development of antibody immobilization for optical immunoassays: progress and prospects *Anal. Chem*. 45 62-75

CHAPTER 2. LITERATURE REVIEW ON MICROFLUIDIC SERS BIOSENSING

2.1. Introduction of Raman Spectroscopy and SERS

Surface-Enhanced Raman scattering (SERS) based detection/analysis systems utilizing high-throughput microfluidic sampling have been gaining popularity in biomedical, pharmaceutical, diagnostic, and analytical applications due to the advantages offered by the miniaturized reactors/processors to a nano and micro scale. The SERS-microfluidics systems aim to solve the problems associated with the conventional SERS detection mode, such as varying mixing time and scattering geometry that lead to inconsistency in enhancement factors, localized heating and photodissociation that lead to alteration of the analytes. Furthermore, for biochemical analysis, the low excitation power intensity achieved in on-chip SERS allows non-destructive detection of living cells (Lai et al., 2014). Easy access to a variety of commercially available colloidal nanoparticles has made SERS-based detection suitable for microfluidics, and its utilization has been demonstrated for detecting trace amount analytes such as 4-aminobenzenethiol (Piorek et al., 2007) and crystal violet (Strehle et al., 2007). In this chapter, I will review the most recent advance in this exciting field. In most cases the review is limited to literatures published in the last five years.

2.1.1. Mechanism for Raman spectroscopy and SERS

Traditional instrumentations widely used in environmental screening and detection include thin layer chromatography (TLC), high-pressure liquid chromatography

(HPLC), gas chromatography-mass spectrometry (GC-MS), liquid chromatography-mass spectrometry (LC-MS), and immunoassay. TLC is a simple and economic method in contaminant determination but its sensitivity is low. Other instrumentation techniques show higher reliability, however, they are time-consuming and high-cost due to the complicated sample preparation. Hence, these methods are inappropriate for on-site routine monitoring of numerous samples. Hence, there is a compelling need for the development of easy-to-use instrumentation technique that could give highly sensitive and reliable detection results, and even allow on-site field monitoring.

Raman spectroscopy has emerged as a powerful whole-organism fingerprinting tool for the rapid identification of different chemical and biological analytes in recent years (Kudelski. 2008). Raman spectroscopy enables the label-free, non-destructive and dynamic chemical analysis of living cells based on the inelastic scattering of photons reflecting specific molecular vibrational and rotational modes of the analyte molecules. However, Raman scattering is a rare event which results in low signal intensity. Typical Raman cross sections are between 10^{-30}-10^{-25} cm^2 per molecule with the larger values occurring only under favorable resonance-Raman conditions when the excitation light matches the related electronic transition energy in the molecules (Soga. 2000; Kneipp et al 2008). Therefore, long signal collection time (i.e., more laser exposure) and high laser power are usually needed for the acquisition of high quality Raman signals, which leads to photo-induced damages to the samples, especially when living cells are being interrogated.

Surface-enhanced Raman scattering (SERS) is a unique phenomenon that can amplify molecular Raman cross-sections to the level of fluorescence cross sections (10^{-17}-10^{-16} cm^2 per molecule), and enormously enhances Raman signal intensity, due to the localized surface plasmon resonance (LSPR) between the excitation light, the analyte molecules, and a noble metal nanostructure (Moskovits. 1985; Campion and Kambhampati. 1998). SERS was first observed by Fleischmann et al. (Fleischmann et al., 1974). They reported that the intense vibrational spectra of pyridine, sodium carbonate, formic acid, and potassium formate could be observed when the target molecules were adsorbed to redox-cycled silver or copper electrodes (Paul et al., 1975; Mcquillan et al., 1975). Basically, roughened noble metal surface (especially gold and silver) could generate localized surface plasmon resonances when excited by a laser, and the resulted plasmon fields could enhance the intensity of Raman signals from chemicals at the vicinity of the metal surface (Plieth et al., 2005). Soon after, Jeanmaire and Van Duyne verified the remarkable sensitivity of SERS and examined various factors, such as surface features, the potential of the electrode, and the solution-phase analyte concentration, that affect the intensity of the Raman bands of target molecules (Jeanmaire and Van Duyne. 1977). Since then, various noble metal structures with roughened surfaces or nanoscale patterns have been reported to enhance Raman signals, with enhancements as high as 10^{13-14} (Liao et al., 1981; Bantz et al., 2011).

Two independent mechanisms have been attributed to SERS: electromagnetic (EM) enhancement and chemical enhancement (Kneipp et al., 2002). The EM enhancement is believed to be the predominant enhancement mechanism: due to the interaction

between the incidental laser light and the surface plasmon at the nanostructure metallic surface (i.e., the substrate), a redistribution of EM field intensity occurs in the vicinity of the metal substrate, resulting in regions of hugely enhanced excitation intensity for the Raman scattering process. And the SERS signal could be further enhanced when the laser excitation wavelength matches the wavelength of the localized surface plasmon resonance (LSPR, or nano-SPR as this being a nanoscale event) of the substrate. The nanostructures of the substrate act as nano-antenna for transmitting and enhancing Raman scattered light. It has been shown that noble metals, such as silver, gold and copper, are the best substrate materials for SERS, as they generate plasmon resonance in the visible and near infrared range. The chemical enhancement is related to the increase in the transition polarizability (i.e., Raman cross section) of the analyte molecules when they are absorbed onto the nanostructures. There is an intermediate electronic charge transfer state occurring after the absorption of molecules onto metal surface. This new electronic coupling state acts as a resonant state which triggers an electronic resonance Raman enhancement. Another mechanism for chemical enhancement involves ballistic electrons and holes which are generated in the metal and coupled to the molecular orbitals (Otto et al., 1992). Chemical SERS enhancement is a process that often takes place at special adsorption places, the so called “active sites”. When both electromagnetic and chemical enhancement effects are taken into account, the enhancement level is theoretically estimated to be on the order of 10^{14} (Kneipp and Kneipp. 2006). Hence, SERS is ultrasensitive down to the single molecule level, and distinct “fingerprinting” spectra from analytes similar in structures could be

produced. Additionally, there are no expensive reagents and time-consuming sample preparation steps needed, as in other techniques such as polymerase chain reaction (PCR) or immunoassays. Furthermore, the small Raman scattering cross-section of water, which leads to minimal background signal from aqueous samples, makes it possible to use SERS to detect the environmental pollutants in aqueous solution directly.

2.1.2. SERS substrate and SERS-based molecular labeling

SERS enhancement factors (EF) ranging from 10^6 to 10^8 have been observed from a variety of substrates (McCreery. 2000; Aroca. 2006), such as metal island films, electrodes, sharp metal tips, colloidal nanoparticle solutions, or roughened metal surfaces. One of the most common types of SERS-active substrates exhibiting strong enhancement factors are clusters of colloidal silver and gold nanoparticles in the 10-100 nm size range. Colloidal silver and gold nanoparticles can be synthesized through different chemical reduction processes (Jana et al., 2001; Faulds et al., 2004) or by laser ablation from solid silver or gold (Machmudah et al., 2013) in which chemically-clean nanoparticles can be produced. Utilization of colloidal nanoparticle solution offers a special advantage as a SERS substrate. It minimizes the burning of samples due to heat dissipation through water, allowing the use of high laser power to enhance Raman signal. In addition, the presence of large number of nanoparticles in a solution permits the acquisition of a stable average-spectrum due to the Brownian motion that governs the colloidal dispersion. However, a big drawback associated with liquid state of nano-substrates exists, namely the aggregation of metallic colloids in solution during fabrication processes. In order to overcome this disadvantage, nanoscale structures can

be fabricated by drying colloidal solutions on a surface forming self-assembled monolayers (SAMs). The transference of the colloids from liquid to solid supports stabilizes them, avoiding the aggregation/flocculation processes that usually occur with time (Ahmad and Moore. 2012). As another option, metal island films are introduced into SERS-based techniques. Metal island films are self-sustained and could form portable SERS active substrates. In addition, many of these films are water insoluble, thus allowing the transfer of analytes by means of Langmuir-Blodgett technique (Aroca et al., 2005).

SERS-based technique is an excellent candidate for biosensing. The detection of biomolecules could be accomplished in two schemes, intrinsic and extrinsic (Han et al., 2012). In the intrinsic label-free SERS biosensing scheme, the molecular signature of the analyte is acquired directly. However, this protocol is only valid for some small molecules, where a well-defined Raman spectrum can be identified and used as fingerprints. In addition, label-free detection exhibits limited selectivity in complex mixtures due to the overlapping of large amount of Raman bands. In the extrinsic SERS labeling scheme, SERS detection of biomolecules is achieved by associating the analytes of interest (i.e., the targets) with a Raman-active molecule, which is called "SERS tag or Raman tag". Usually, the specific SERS tag can be selected from a large pool of spectrally non-overlapping labeling molecules due to their intense and distinguishable spectral signatures. The SERS tags could be covalently attached to metallic nanostructures, alongside with target-recognizing agents (TRAs), such as antibodies and nucleotides strands, to create labeled SERS probes that can bind

specifically to certain biological targets. The SERS spectra of the probes are used for qualitative and quantitative detection of the targets, because the Raman intensities of these probes are correlated to the concentrations of the targets. In this extrinsic scheme, the function of the SERS tags is similar to those of external chromophores (fluorescent dyes or quantum dots). However, the SERS probes are more sensitive, and support higher multiplexing capacity owing to the narrow line widths of Raman peaks that would allow more Raman tags to be used simultaneously. Furthermore, Raman tags do not photobleach, which is advantageous for analyzing biological samples.

A simple Raman spectrum with easily identifiable characteristic peaks is essential for selecting an effective SERS tag in detection. Moreover, the Raman scattering-cross section of SERS tags should be large enough in order to generate strong SERS signals, and the tags should be easy to be conjugated to the surface of the SERS substrates to produce uniform molecular layers, which is critical to assure the consistency of the Raman signals from the SERS probes. Furthermore, the bonding between tags and the SERS active substrates should be strong for effective signal enhancement. The EFs would decrease dramatically as the distance between the analyte and the surface increases. Camden et al. (2008) demonstrated that a 2.8 nm separation between the analyte and the Ag nanosphere substrates caused a 10 times reduction of SERS intensity. Thus, small molecules are preferred to large molecules as SERS tags for less tag-substrates separation distance and therefore greater enhancement effect. Typical Raman tags include nitrogen-containing cationic dyes, sulfur-containing dyes, and thiol-small molecules.

Even though the high level of sensitivity with spectroscopic precision makes SERS a valuable tool for biological and medical sensing and detection studies, there are some real limitations, too. For example, it is still likely that the SERS signals are masked by the elastic scattering, non-specific binding, and fluorescence events simultaneously occurring along with SERS. It is not easy to produce SERS substrates with large and reproducible EFs. A slight change in the size and shape of the nanostructures could cause a significant change in LSPR, which therefore would change the EFs (Harper et al., 2013; Bantz et al., 2011; Driscoll et al., 2013). A new branch of SERS, Tip-enhanced Raman spectroscopy (TERS), is emerging as a promising *in situ* detection technique with single molecule sensitivity (Stadler et al., 2010). It utilizes nanoscale tip to serve as SERS substrate, which can overcome some of the above-mentioned limitations.

2.2. Nanoparticle

Nanoparticles (1-100 nm in diameter) display unique properties over bulk-sized materials and thus has been widely used in various area. The small size of nanoparticles correspond high surface-to-volume ratios. In addition, their physical properties can be customized since they are directly related to size, composition, and shape. Incorporating the nanoparticles into nanosensors provides advantages of rapid and high-throughput detecting ability on a portable device in environmental monitoring and diagnostics. The various modified nanoparticles, including gold nanoparticles, magnetic nanoparticles, quantum dots, and carbon nanotubes, exhibit different and specific target binding properties in building up the novel waterborne pathogen detection methods (Jain et al.,

2008; Gao et al., 2009; Peng et al., 2009). Common biorecognition elements include oligonucleotide probes, antibodies, enzymes, aptamers, cell-surface molecules, and phages (Rider et al., 2003; Arya et al., 2011). Among those, The immunological assays has advantages in terms of format simplicity, speediness, and stability over a wide range of conditions, allowing for on-site testing by untrained users. However, some artifacts, such as nonspecific binding and aggregation, exist in the step of nanoparticle conjugation with proteins. Those artifacts will definitely interference the target cells binding efficiency; hence the significant effort in this research is put into the protein conjugation theoretical study and experimental testing.

2.3. Protein immobilization

Proteins adsorb spontaneously onto solid surfaces when coming into contact via intermolecular forces, mainly ionic bonds or hydrophobic polar interactions. The non-specific adsorption of proteins is not such desirable in design and preparation of surface coatings that require high reliability and reproducibility. The immobilization of proteins in biosensors is challenging due to the fragile and varied nature of proteins. The requirement for suitable protein immobilization are: 1) efficient coupling of the detection techniques with the substrate; 2) low nonspecific protein interaction with the surface; 3) stable, yet reversible tethering of the protein while maintaining their functionality on the surface homogeneously. There are plenty of strategies for to immobilize proteins on sensor surfaces. The method can be classified into three groups: physical immobilization, covalent immobilization and bio-affinity immobilization. Physical methods include adsorption, retention into a membrane or entrapment within

a polymeric network. Adsorption is based on the establishment of low energy interactions between the functional groups of the bio-receptor and of the substrate surface. This type of immobilization offers the advantage of preserving bioreceptor properties but results in the formation of weak bonding that favors it's desorption. To avoid leakage processes, biological elements can be covered by a thin polymer membrane that allows diffusion of the target molecule or entrapped in a chemical or biological polymeric matrix. Sol-gel silica or hydrogels are typically used for that purpose. These polymers can efficiently protect the bioreceptor from external aggressions but may form a diffusion barrier that restricts the accessibility to the substrate and/or decrease light and electronic transfers to the transducer. Covalent immobilization utilizes surface bound functional groups that can react with exposed amino acid side chains on the protein surface. Amine coupling and thiol coupling are commonly used. Photochemical methods involve photolabile agents forming covalent bonds upon UV light activation. Another example is click chemistry, involving cycloaddition of an azide and an alkyne. Bioaffinity immobilization methods rely on recombinant affinity tags, the naturally occurring biotin-avidin system. Antibody immobilization can be mediated by protein A/G and glycoproteins can be immobilized via their carbohydrate moieties to surface bound lectins (sugar-binding proteins). To ensure the formation of bindings with the transducer, conducting polymers (polypyrrole, polythiophene, polyaniline) are deposited on metal electrodes (Teles and Fouseca., 2008). In recent years, particular attention has been also paid to the use of nanotechnology/nanomaterials, typically gold nanoparticles, magnetic beads, carbon

nanotubes (CNTs) or quantum dots (QDs) for the elaboration of biosensors (Xu et al., 2006; X. Zhang et al., 2009). Their particular chemical and physical properties make them very attractive to improve the efficiency of bioanalytical Microfluidics.

2.4. Microfluidic devices

Microfluidics is becoming increasingly attractive in bioanalysis because microfluidic devices require only small amounts of sample, but offer highly precise-controlled manipulation of biological samples within microscale channels (Whitesides. 2006). The small size of these devices provides the potential of creating portable lab-on-a-chip devices that facilitate low detection limits required in biological targets identification (Godin et al., 2008). The field of microfluidics emerged in the early 1950s (Haeberle and Zengerle. 2007) with the development of ink-jet technology (Le. 1998). Later, silicon wafers and Si-Pyrex technology were successfully used for the miniaturization of gas chromatograph (GC) and high-pressure liquid chromatography (HPLC) (Terry et al., 1979; Manz et al., 1990) with considering the advantage of the fluid propulsion inside microchannels. Nowadays, the field of microfluidics has evolved from simple micro-structures into complex devices applying various technologies simultaneously, such as mixing fluids (Chen and Meiners. 2004), pumping liquids (Beebe et al., 2002), and individually culture cells (Inoue et al., 2001). However, in practical cases, some limitations still exist in the variety of micro-scale components, such as the slow processing operation and expensive manufacturing costs. An alternative way is evolving microfluidics by combining with other technologies to create a new technology platform embracing hybrid advantages.

Microfluidic platforms that integrate optical and spectroscopic analysis, exploiting both absorption and scattering techniques, have been extensively reported, and the functionality of microfluidics are significantly expanded when they are combined with those optical techniques. Recently, Huang et al. (2014) presented an excellent review for optofluidics-based techniques focusing on single cell manipulation, treatment, and detection, respectively. Among them, SERS has become an emerging technology of choice for the detection of analytes at the cellular and molecular levels. The integration of microfluidics with SERS provides not only a new technology platform but also a transformation to a new paradigm of bio-sys-on-a-chip (Ewing and Abdel-Aty-Zohdy. 2003).

Even though SERS can be utilized for highly specific and sensitive biosensing, it has always been a challenge to obtain repeatable and reproducible SERS spectroscopic results at complicated experimental conditions. The degree of metallic particles aggregation, the different size of metal colloids, and the inhomogeneous distributions of molecules on the metal surface all affect the SERS signal reproducibility. Lately it has been found that the combination of SERS and microfluidics could overcome these major drawbacks for SERS-based techniques. More reproducible SERS signals can be obtained in a microfluidic channel, because of the more consistent geometries and the favorable heat dissipation inside microfluidic devices. Furthermore, the integration of microfluidic devices and SERS minimizes the sample volumes, the recording time, and damage to the biological analytes. In addition, the microfluidic-SERS systems consolidate sample preparation, target manipulation and separation, and *in situ*

detection into one working unit, and can significantly improve the effectiveness of these sensing platforms (Kniepp et al., 2002; Wlater et al., 2011; Chen and Choo. 2008).

The most common microfluidic devices are made from polydimethylsiloxane (PDMS) and other polymers. They can be made at low manufacturing costs by molding techniques, such as photolithography (Chen et al., 2012), and soft lithography (Xia and Whitesides. 1998) with the same layout prototype master. However, PDMS is a Raman active material, which has its own Raman signal. To overcome this problem, confocal Raman microscopy is used. In confocal Raman microscopy, a confocal slit is designed to collect only the laser-induced signal from a distinct focal volume within the diffraction limit (Yasui et al., 2012). With confocal Raman microscopy, the Raman signals from the PDMS channel itself are effectively removed, and then the target spectra from a small volume inside the microfluidic channel can be obtained (Sarrazin and Salmon. 2008). Alternatively, glass windows can be put on top of the detection areas, but the high cost and complicated manufacturing processes associated with manipulating glass materials limit the application of this approach. Recently, Luecha et al. (2011) demonstrated a green microfluidic device made of corn zein using standard soft lithography and stereo lithography techniques, which opened the door for using zein and other biorenewable polymers for microfluidic devices.

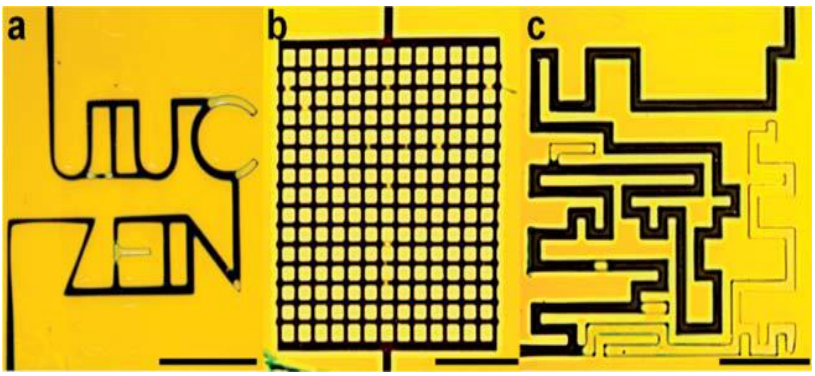

Fig. 2.1 Visualization of zein-glass microfluidic devices with complex fluidic pathways: (a) Interconnected letters composed of continuous microfluidic channels, (b) A microfluidic network with channels and chambers, (c) A solved microfluidic maize maze with multiple false paths. Blue food dye was used for visual aid. All scale bars are 5 mm (Luecha et al., 2011). Copyright Royal Society of Chemistry and reproduced with permission.

2.5. Key factors that affect the performance of Microfluidic-SERS detection

A successful system design to integrate SERS with microfluidics platform needs to take into account three important factors: 1. mixing of analyte and SERS active nanostructures; 2. synthesis or implementation of SERS-active substrate inside microfluidic devices; and 3. target trapping in microfluidic channels for better SERS detection.

2.5.1. Complete mixing in SERS applications integrated with microfluidics

A reproducible mixing performance is a critical need for a successful microfluidic-SERS platform. Microfluidic devices are usually designed to work with liquid samples. Hence, most of microfluidic-SERS systems utilize colloidal nanoparticles as SERS-active substrates. Generally, the nano-probes are injected through the microfluidic channels where they encounter analytes at a certain location for SERS detection. However, the *in situ* mixing efficiency of nano-probes and the analytes is difficult to control. Reynolds number (Re) in microfluidic systems is usually low due to the absence of turbulence and the dominance of laminar flow within the systems (Schulte

et al., 2002). Therefore the intermixing performance in the microfluidic device is poor. It is found in literatures that the intermixing efficiency relies solely on molecular inter-diffusion, which is heavily dependent on diffusion coefficient, interfacial surface area, and the gradient of species concentration (Li et al., 2013; Graveson et al., 1993). Researchers have developed various mixing optimized solutions by maximizing these factors. Current mixing techniques include two approaches, active mixing and passive mixing. Active mixing techniques require high external energy supply as well as costly extra components to be added to the microfluidic systems. The energy supply can be provided by bubble-induced vibration (Liu et al., 2003), magnetic stirring (West et al., 2002), ultrasonic wave generators (Yang et al., 2001), and electrowetting-induced merging of droplets (Palk et al., 2003). In contrast, passive mixing only utilizes the flow: thin lamellae can be created in special feed arrangements; multi-lamellae are created by Split-and Recombine (SAR) flow guidance; and eddy-based flow patterns producing high interfaces can be created by chaotic mixing (Hessel et al., 2005).

From the microfluidic-SERS standpoint, passive mixing is more widely used than active mixing. Yasui et al. (2012) fabricated a microfluidic baker's transformation (MBT) mixer as a three-dimensional passive-mixer for the efficient mixing of solutions based on chaotic mixing, which is theoretically one of the most efficient mixing mechanisms. They also quantitatively evaluated the mixing performance of the 3D microfluidic mixer with a confocal microscopic method. It is demonstrated that the mixing efficiency increased as the number of cycles increased. And compared with the straight channel design, the MBT mixer could improve the mixing efficiency by 20%

after 2 cycles. The schematics of the MBT design and the results are shown in Fig. 2.2 a and 2.2 b. Wilson et al. (2010) integrated fiber-coupled optical SERS sensors with passive micro-mixers for both the in situ synthesis of nanocolloids and their subsequent mixing with the analytes. In Fig. 2.3 a, silver nitrate and hydroxylamine hydrochloride/sodium hydroxide were introduced from channel 1 and 2 into the first mixer for nanocolloids synthesis. The analyte was introduced from channel 3 and mixed with the synthesized nanocolloids in the second mixer. Optical fibers were held in an orthogonal position to the channel for SERS signal collection. The mixing efficiency was tested by comparing the spectra of R6G conjugated with silver colloids from on-chip dynamic synthesis and quiescent bulk synthesis conditions. The on-chip SERS substrates produced ten times higher enhancement to R6G analytes (as shown in Fig. 2.3 b). Chon et al. (2010) presented a SERS-based optofluidic immunoassay system. Complicated groove-structured gradient microfluidic channels were designed and fabricated for producing serial dilutions, and homogeneous mixing conditions were maintained in their design. Walter employed a PDMS chip that integrates loops within the microfluidic channels to achieve high mixing efficiency (Walter et al., 2011). The schematic is shown in Fig. 2.4. The segmented flow was produced in the microfluidic device where the analyte and nanocolloids formed droplets in an immiscible separation and transport fluid. The so called “segmented flow” was applied to avoid memory effect, which was caused by the adhesion of nanocolloids and analytes conjugated to the optical windows (Strehle et al., 2007). By using the segmented flow, the deposition inside micro-channels could be prevented and highly reproducible SERS measurements

would be achieved. Park et al. (2005) designed an alligator teeth-shaped PDMS microfluidic channel for the efficient mixing between DNA oligomers and aggregated silver nanocolloids (Fig. 2.5). They then used confocal SERS technique for the analysis of duplex-dye labelled or label-free DNA oligonucleotides.

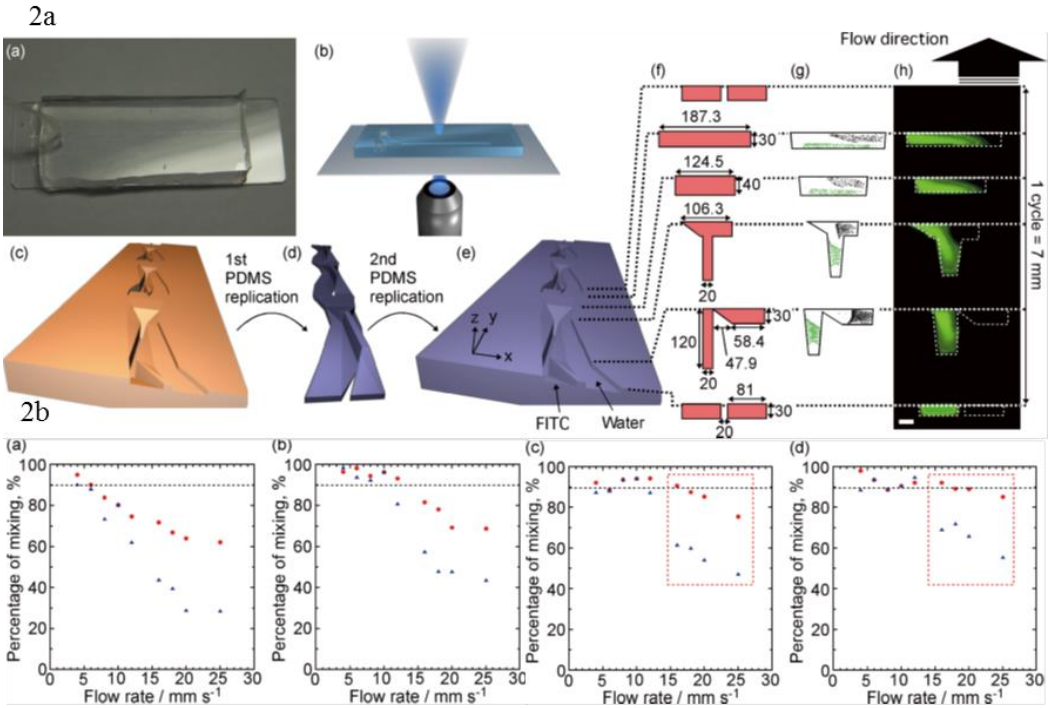

Fig. 2.2 a. (a) Photograph of the MBT mixer. (b) Schematic illustration of confocal scanning. (c) Schematic 3D diagram of the mold for the MBT mixer. (d) 1st PDMS replication from the mold. (e) 2nd PDMS replication from the 1st mold. (f) Schematic illustrations of vertical cross sections of the MBT mixer. (g) Schematics of microfluidic distributions derived from a numerical simulation of the MBT mixer. (h) Confocal micrographs of vertical cross sections of a microchannel at the 1st cycle. The scale bar is 40 um. One cycle of the MBT mixer was 7 mm. the dotted lines indicate the replication positions at the PDMS. The flow rate was 20 mm/s. the fluid direction was from bottom to up. 2.2 b. Mixing ratio of the FITC solution and water vs. flow rate at Δy = (a) 14, (b) 21, (c) 28, and (d) 35 mm (i.e. after 2, 3, 4, and 5 mixing cycles), respectively. Red circles and blue triangles show the mixing in the MBT mixer and that in a straight channel, respectively. The black dashed line indicates the 90% mixing ratio (Yasui et al., 2012). Copyright The Japan Society for Analytical Chemistry and reproduced with permission.

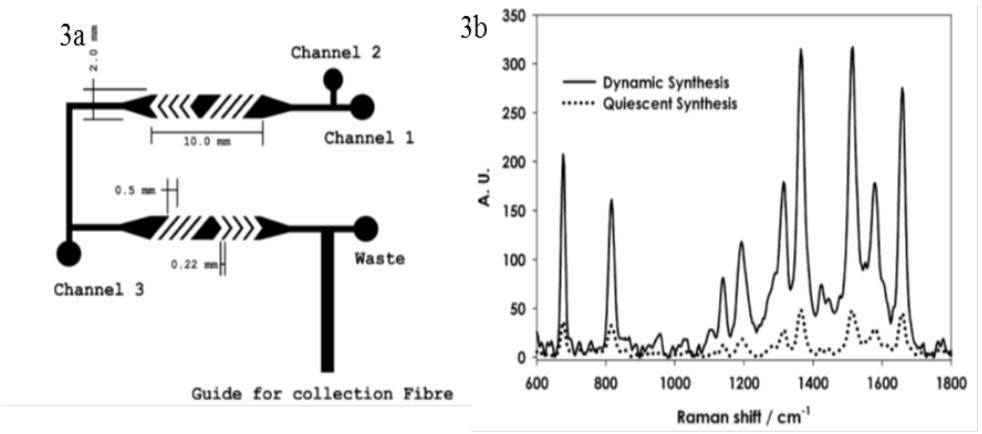

Fig. 2.3 a. Schematic illustration of the device. 2.3 b. Comparison of spectra of 10nM R6G premixed with quiescent bulk synthesized colloid and flowed through device (100 μL min-1) and 10 nM R6G infused (10 μL min^{-1}) tinto the in situ synthesized colloidal stream (200 μL min-1) to give approximately 475 pM concentration (Wilson et al., 2010). Copyright American Chemical Society and reproduced with permission.

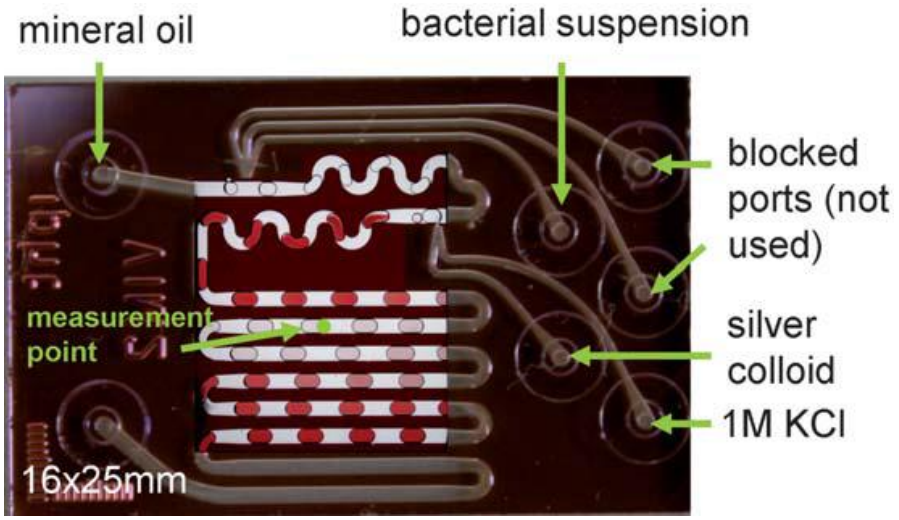

Fig. 2.4 Applied microfluidic chip with 6 injection ports; application of two phase liquid/liquid segmented flow, which is constantly flowing during the measurements; detection of Raman spectra of the separation medium oil and SERS spectra within the droplets at the measurement point in the second channel (Walter et al., 2011). Copyright Royal Society of Chemistry and reproduced with permission.

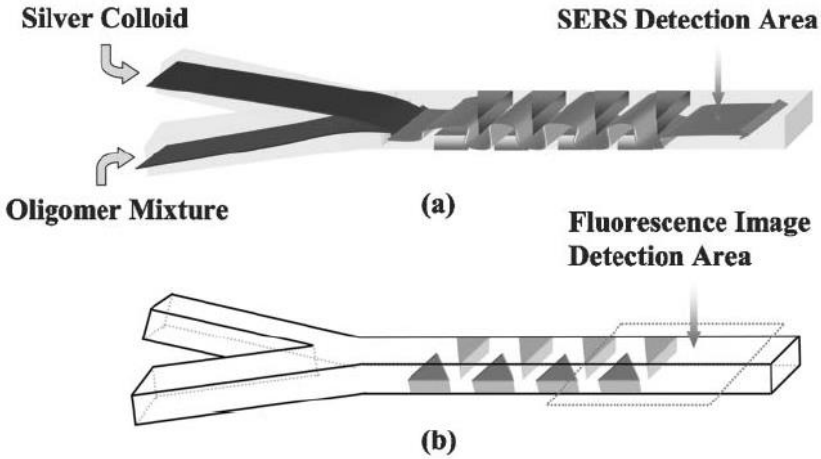

Fig. 2.5 Schematics of alligator teeth-shaped micromixer (a) confluent liquid streams travel the microchannel, the transversal and vertical dispersions of fluid occur simultaneously through the upper and lower teeth. (b) Within a rectangular duct, the triangular structures are located on upper and lower surfaces of the channel in a zigzag way (Park et al., 2005). Copyright Royal Society of Chemistry and reproduced with permission.

Other approaches to improve the efficiency of mixing inside microfluidic systems also include electrokinetical microwell mixers (Huh et al., 2009), hydrodynamic driven stage (Lee et al., 2010), but these techniques have not been implemented for microfluidic-SERS applications.

2.5.2. Integration of SERS active substrates in microfluidic devices

Even though much work has been done to improve the mixing performance, and a significant progress has been achieved from this perspective, the introduction of many reagents into the micro-scale devices seems a tedious process, and it is probably not the most effective strategy for microfluidic-SERS applications. In addition, controlling nanoparticle aggregation due to the interaction between nanostructures and channel surfaces has always been a primary challenge to obtain high and consistent SERS enhancement signals from within a microfluidic device. Recently, an alternative strategy has emerged in which, instead of injecting nanocolloids into devices, SERS-

active substrates are fabricated, aligned, and bound to microfluidic devices directly (Huang et al., 2013; Im et al., 2010). Nowadays, more and more on-chip SERS applications integrating SERS active substrate inside microchannels are being reported. Connatser et al. (2008) integrated nanostructures in microfluidic devices by applying electron beam lithography on a polymer layer. Another approach for integrated substrates in microfluidics is presented by Banerjee et al. (2010) by introducing a nanoporous anodic aluminum oxide (AAO) layer of hexagonally packed holes on top of an aluminum substrate (Fig. 2.6). A microfluidic channel was placed on the substrate to provide the analyte solution and then achieve a high throughput. The choice of AAO as substrate matrix is due to its high biocompatibility as this platform is used to monitor protein binding to a lipid bilayer.

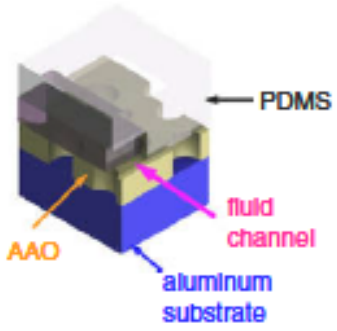

Fig. 2.6. The schematics of the microfluidic channel on AAO (yellow). The latter is resting on Al support (blue). Arrow points to the fluid channel and the direction of the flow (Banerjee et al., 2010). Copyright Elsevier and reproduced with permission.

Despite the fact that SERS substrates have been successfully integrated to microfluidic systems, there are still a lot of problems in compatibility and controllability in their implementation. In order to further improve the flexibility and stability of the integrated SERS substrates in the microfluidics, a number of novel techniques have been implemented for *in situ* functionalization of lab-on-a-chip platforms. Xu et al.

(2011) applied femtosecond laser technique to produce silver SERS substrates at desired position of the microchannel and obtained the signal enhancement of ~10^8 for p-aminothiophenol (p-ATP) and flavin adenine dinucleotide (FAD) (Fig. 2.7 a). After preparing well the silver precursor and injecting into microchannels, the femtosecond laser pulse (central wavelength: 800 nm; pulse width: 120 fs; and repetition rate: 80 MHz) was tightly focused into the precursor solution by 100× oil immersion objective lens with a high numerical aperture (NA=1.40). By using femtosecond laser technique for silver SERS substrates, the sizes and shapes of the substrates could be precisely and flexibly controlled. They also fabricated silver microflower arrays as both catalytic-active sites for the reduction of 4-nitrophenol to 4-aminophenol and SERS active substrate in microfluidic devices (Xu et al., 2012), as shown in Fig. 2.7 b.

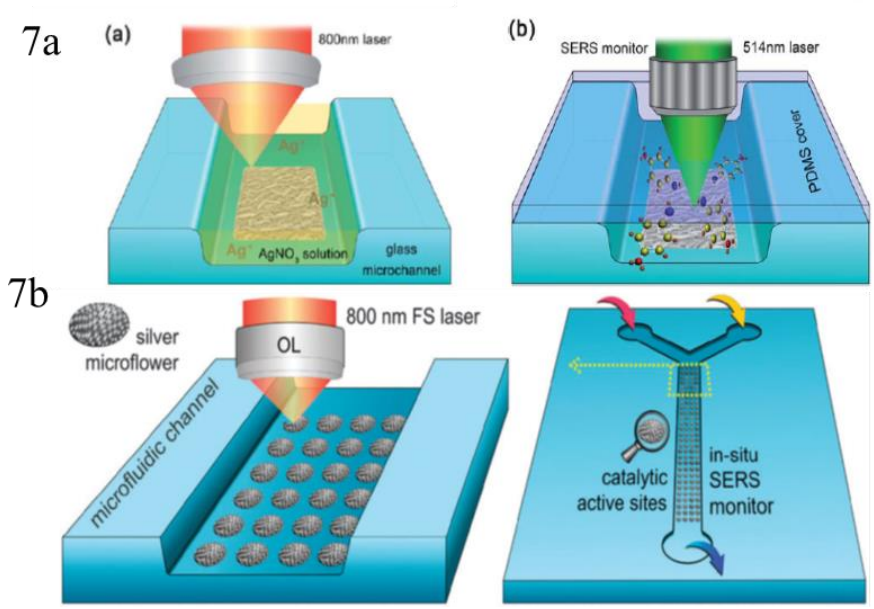

Fig. 2.7 a. Sketch of femtosecond laser fabrication of the silver SERS substrate inside a microfluidic channel (a), and the application of this SERS monitor for target molecule detection at visible light (514.5 nm) excitation (b) (Xu et al., 2011). 2.7 b. Scheme for laser fabrication of SMAs inside a microfluidic channel (Xu et al., 2012). Copyright Royal Society of Chemistry and reproduced with permission.

Oh and Jeong (2014) patterned plasmonic nanoprobes with rich electromagnetic hot spots as SERS active substrates in microfluidic channels. The silver film substrate with an initial thickness of 30 nm was etched into patterned nanotips and nanodots with oxygen plasma treatment, resulting in excellent SERS performance (shown in Fig. 2.8). This integrated optofluidic device enables the label free and solution phase SERS detection of small molecules with low Raman activity such as dopamine at micromolar level.

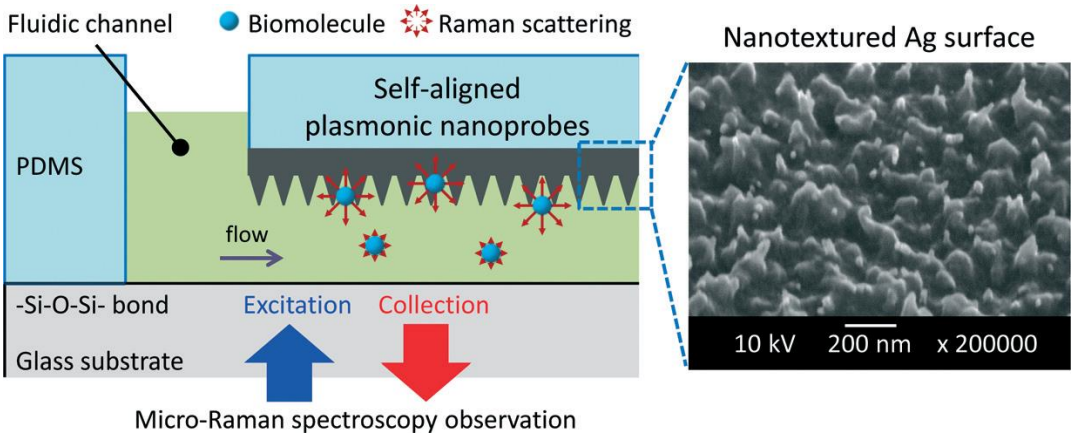

Fig. 2.8 A schematic illustration of the optofluidic SERS chip with plasmonic nanoprobes self-aligned along microfluidic channels. The perspective scanning electron microscope (SEM) image shows the plasmonic nanoprobes with nanotips and nanodots (Oh and Jeong. 2014). Copyright Royal Society of Chemistry and reproduced with permission.

There are several other research groups implementing SERS active substrates within microfluidic devices based on other mechanisms. For example, microdroplet reactors are one of the most widely used techniques for nanocomposite beads production with high uniformity in shape and size, and densely loaded with metal ions for SERS optical detection (Abalde-Cela et al., 2010; Hwang et al. 2011).

2.5.3. Target trapping & sorting

One outstanding advantage of integrating microfluidic systems with SERS analysis is that a high reproducibility of SERS signal measurement could be obtained in continuous flows instead of static conditions. Such platforms allow for the analysis of small volumes by positioning the sample into the SERS detection area. However, for certain targets, long integration time is needed to obtain a strong SERS signal and the targets are required to remain in the focal area for the duration of the signal acquisition. Furthermore, in the ultrasensitive detection procedures, where the concentrations of targets are extremely low, it is also necessary to hold samples in the SERS detection area for certain duration to achieve effective signal collection. Hence, an effective trapping and sorting method is needed for classification of samples containing multiple targets. Recently, various methods have been developed to trap targets at the laser spot for effective SERS signal acquisition. Various optical, electrical, and mechanical mechanisms have been explored for trapping and sorting applications (Fig. 2.9 (a)-(f)) (Chrimes et al., 2013).

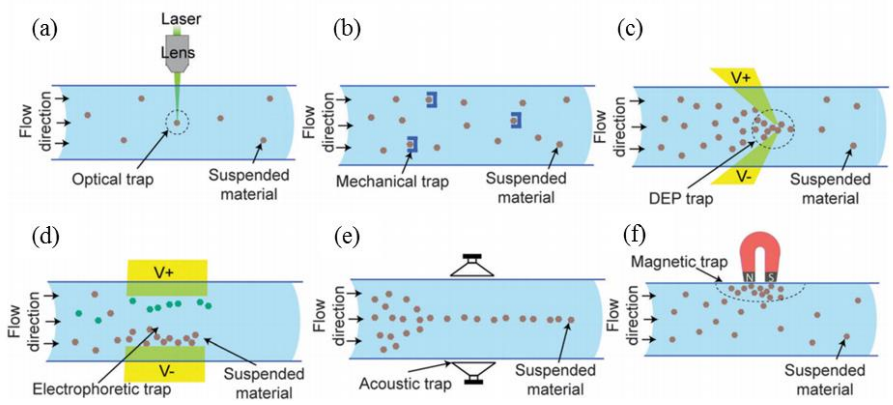

Fig. 2.9 Schematic of microfluidic traps with different kinds of forces: (a) optical (b) mechanical (c) dielectrophoretic (d) electrophoretic (e) acoustic and (f) magnetic forces (Chrimes et al., 2013). Copyright Royal Society of Chemistry and reproduced with permission.

2.5.3.1. Optical trapping

Light beams are commonly used in order to trap suspended objects. Optical cell trapping and sorting methods are non-invasive in nature, and they provide high-precision controllability of micro-scale and nano-scale particles. When a light beam is projected onto a photoconductive layer, the induced current goes through only the partially illuminated area, forming a non-uniform electric field in the liquid chamber for molecular trapping (Moffitt et al., 2008). Optical cell trapping employs either gradient or scattering forces (Huang et al., 2014). Scattering forces push objects along the direction of propagation of the light, while gradient forces pull objects along the spatial gradient of light intensity. When gradient forces exceed those from scattering forces, an object is attracted to the point of highest intensity formed by focused light and can be stably trapped at this position in all three dimensions (Ashkin et al., 1986). Gradient force-based manipulation techniques are also called “optical tweezers” due to the ability to precisely control force for a large dynamic range. Recently, Werner et al. (2011) demonstrated contact-free immobilization of more than 200 yeast cells into a high-density array of optical traps in a microfluidic chip (see Fig. 2.10 a). Then the cells of interest were optically guided into the sorting channel by the same steerable tweezers. However, this sorting strategy needs long laser irradiation time which might cause the cell damage. Werner et al. also studied influences of the trapping laser on yeast viability by monitoring the evolution of pH of optically trapped cells in a low-pH environmental (see Fig. 2.10 b). It was demonstrated that cells assays should not be exposed to the trapping laser longer than 15 min to avoid experimental artifacts caused by laser-

induced cell stress and death. Wang et al. (2014) demonstrated the first microfluidic flow cytometer capable of optically switching the flow direction of cells at high throughput based on gradient force optical trapping mechanism. Scattering force and gradient force are both proportional to the intensity of light. However, scattering force is weaker and repulsive force along the propagation direction that introduces less damage to live cells. One example of scattering force is the use of cross-type optical particle separation (COPS) technique, which employs a slightly focused laser beam to push single cells or particles. Compared with conventional optical tweezers, COPS uses the optical scattering force under a loosely focused beam so that the energy density on the spot is much smaller than that of the tightly focused beam of optical tweezers. Bragheri et al. (2012) demonstrated a COPS type optofluidics performed using a femtosecond laser for cell separation. The integrated design made the device compact and potentially suitable for multifunctional operations with less cellular damage. This kind of optifluidic device has been used as a micro fluorescence-activated cell sorter (microFACS) on polystyrene beads (Lee et al., 2013). A novel active SERS platform was demonstrated in an optoelectrofluidic device (Hwang et al., 2011). Instead of integrating SERS active substrates inside the microfluidic devices, Hwang et al. concentrated the gold nanoparticles to form SERS active "hot spot" by introducing a laser source into the sample solution without causing any change of the concentration distribution of target molecules (Fig. 2.11 a and 2.11 b). The SERS detection limit of target molecule (adenine) was improved to 250 μM (Fig. 2.11 c and 2.11 d).

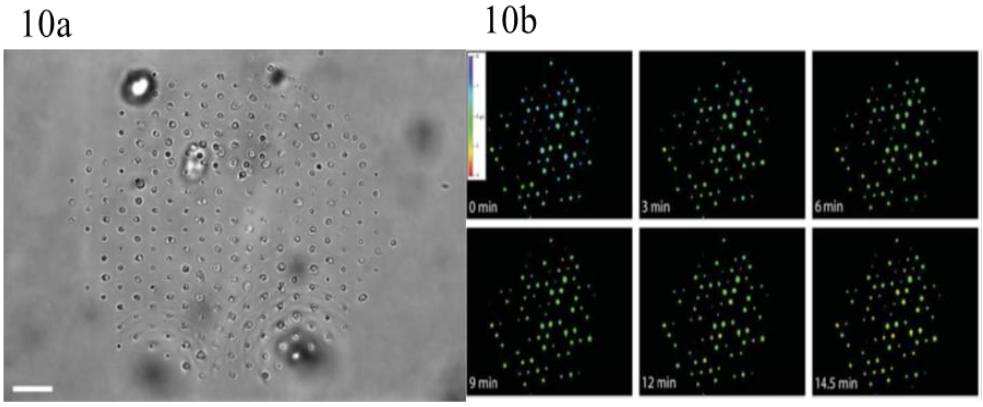

Fig. 2.10 a. Transmission micrograph of more than 200 optically trapped yeast cells; scale bar: 30 mm. 2.10 b. Sequence of fluorescence micrographs showing the temporal decrease of intercellular pH of optically trapped yeast cells induced by the trapping laser. Cells were glucose-deprived and trapped at pH 4. Intracellular pH was determined from the ratio of fluorescence intensities measured at 570 nm and 670 nm (Werner et al., 2011). Copyright Royal Society of Chemistry and reproduced with permission.

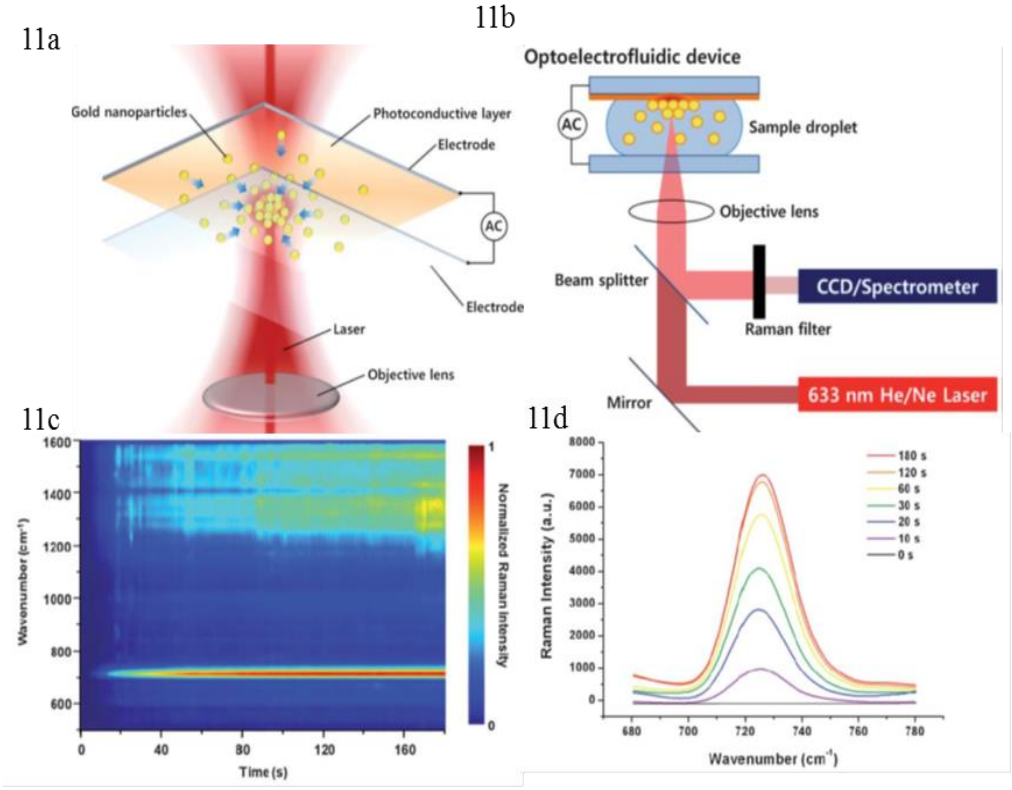

Fig. 2.11 a. Schematic diagram of optoeletrofluidic SERS spectroscopy. 2.11 b. Experimental set up for optoelectrofluidic SERS spectroscopy. 2.11 c. Optoeletrofluidic enhancement intensity map. 2.11 d. The SERS spectra of adenine according to the time of application of an ac voltage of 20 V_{pp} at 100 KHz (Hwang et al., 2011). Copyright Royal Society of Chemistry and reproduced with permission.

Optical trapping methods integrated with other forces, such as mechanical and electrical force, have also been investigated. Weinert et al. (2011) utilized thermal gradient forces from laser heating to transport and trap biomolecules in optical microfluidic structures. Chen et al. (2013) combined optical force with electrical and mechanical force for single cell sorting. It was realized by exciting laser-induced cavitation bubbles in a 3D PDMS microfluidic channel to generate high-speed liquid jets that deflect detected fluorescent cells and particles focused by 3D sheath flows. Huang et al. (2013) integrated single-wall carbon nanotube (SWNT) electrode into multilayer PDMS channels to realize the optoelectronic tweezers platform for single-cell sample preparation. The implementation of SWNT into microfluidic devices made the device simpler and more flexible. Although the optical technique can provide high spatial resolution, its penetration depth and trapping force are limited and the apparatus used is quite complicated, which makes it very difficult to miniaturize the devices.

2.5.3.2. Electrical trapping

Conventionally, the most widely used methods for cells trapping and separation are based on electrokinetic phenomena. One of the most studied methods utilizes the mechanism of dielectrophoresis (DEP), which is strong to achieve accurate classification of cells at high throughput flow rate. DEP force is a force exerted on a suspended dielectric particle in the presence of a non-uniform electric field. The magnitude and direction of the force are related to the electric field intensity, particle radius, permittivity of the particle and suspending fluid, as well as the conductivity the particle and suspending fluid. DEP offers the controllable, selective and accurate

manipulation of target bioparticles (Lapizco-Encinas et al., 2005; Wlodkowic and Cooper, 2010; Zhang et al., 2010). Unlike electrophoresis, which relies on the charge-to-size ratio of particles, the dielectrophoresis relies on the dielectric properties of particles (Pysher and Hayes, 2007). The DEP systems can be operated either in a droplet-based manner by simply injecting a droplet of the sample containing target particles onto the surface of the DEP platform, or in a flow-through manner by providing a stream of medium containing the target particles through a microchannel that is integrated with the DEP platform. In either approach, the DEP systems are expected to produce sufficient DEP forces to overcome the influential forces such as hydrodynamic drag, gravity, electrothermal, intra-particle and surface-particle adhesive forces to effectively guide the micro/nano particles within the system (Khoshmanesh et al., 2011). DEP can be used to trap and sort multiple suspended materials, such as nanoparticles (Zhang et al., 2009), and cells (Khoshmanesh et al., 2012). With a conventional Raman detection system, Chrimes et al. (2011) analyzed the concentration of suspended nanoparticles (tungsten trioxide nanoparticles and polystyrene, in Fig. 2.12 a and 2.12 b) in microfluidic devices by DEP manipulation. In the study of Miccio et al., DEP chips fabricated in PDMS microfluidic devices were integrated with photorefractive crystal substrates. By projection of laser through a holographic Spatial-Light-Modulator (SLM), the reconfigurable DEP trapping of flowing carbon nanotubes (CNTs) was possible through the optical writing/erasing of various light intensity patterns (Miccio et al., 2012). Khoshmanesh et al. combined DEP and hydrodynamic drag forces to separate Lactobacillus bacteria from a background of yeasts

(Khoshmanesh et al., 2012). With a hybrid of multiple electrokinetic isolation mechanisms, three genera of bacteria, *S. aureus*, *E. coli*, and *P. aeruginosa* were successfully identified from human blood cells in less than one minute without the use of any antibody/chemical immobilization inside an on-chip microfluidic deivce (Cheng et al., 2013). They used dielectrophoresis (DEP), electrophoresis, and electrohydrodynamics (EHD) simultaneously to achieve concentration of bacteria from diluted human blood (Fig. 2.13).

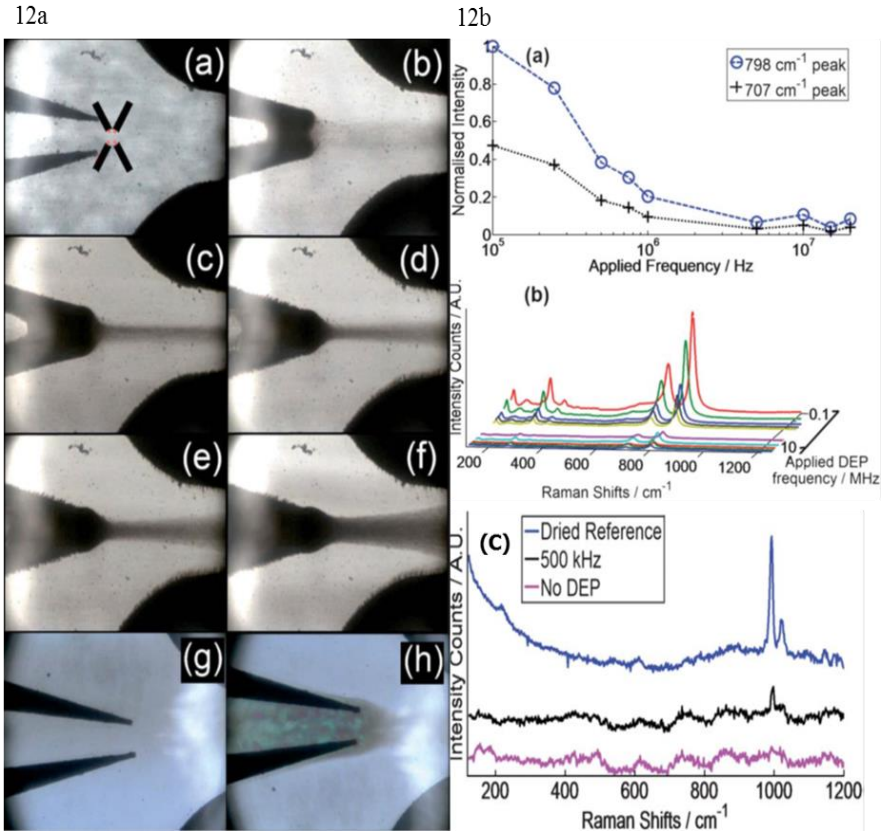

Fig. 2.12 a. Microscope images of DEP system with WO_3 nanoparticles at different frequencies: (a) no DEP voltage, (b) 20 MHz (c) 10 MHz (d) 1MHz (e) 750 kHz (f) 250 kHz, microscope images of DEP system with polystyrene nanoparticles at the following frequencies: (g) no DEP voltage (h) 500 kHz. 2.12 b. (a) plot of normalized WO_3 nanoparticles Raman peak intensity vs. the applied DEP frequency (b) plot of WO_3 nanoparticles Raman spectra at different DEP frequencies (c) plot of polystyrene Raman spectra under various conditions (Chrimes et al., 2011). Copyright Royal Society of Chemistry and reproduced with permission.

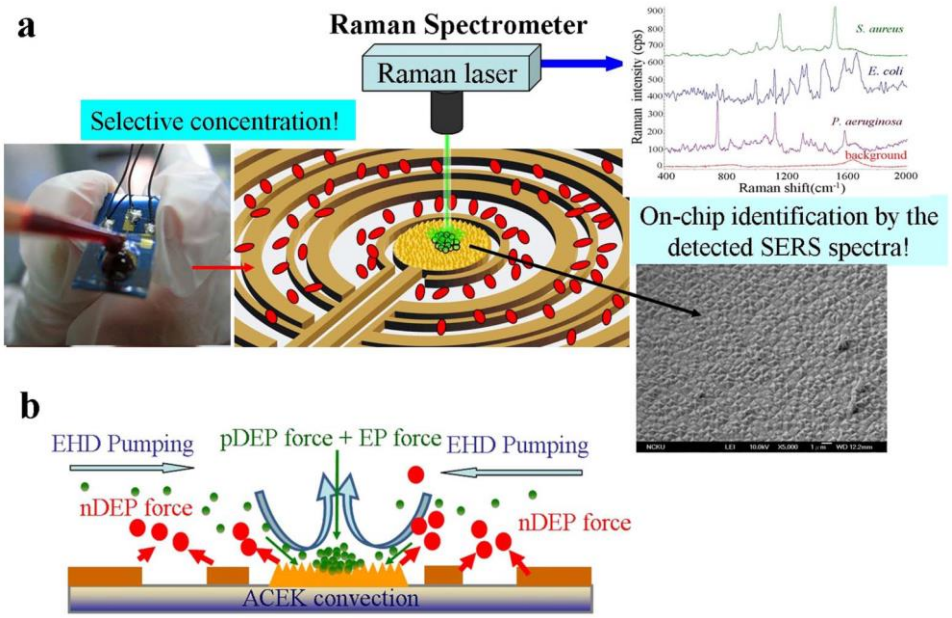

Fig. 2.13. (a) Experimental setup. The SEM image shows the roughened Au surface at the center electrode. AC electric field induced dielectrophoresis and electrohydrodynamics were used to rapid concentrate bacteria form human blood. SERS Raman spectroscopy fingerprint of the concentrated bacteria identifies the bacteria. (b) Illustration of the hybrid mechanism of selective concentration over a wide range asymmetric electrode array (Cheng et al., 2013). Copyright Nature Publishing Group and reproduced with permission.

2.5.3.3. Other mechanisms applied for trapping

Mechanical force can directly trap cells using shear stress in a liquid flow (e.g., sheath flow in flow cytometry). However, mechanical cell trapping may require precise flow channel design and several flow control components, such as valves and/or pumps. Syme et al. designed a novel microfluidic array for trapping individual cells by mechanical force (Fig. 2.14). Cells were labelled with SERS-active nanoprobes and were detected with real time SERS mapping technique (Syme et al., 2010).

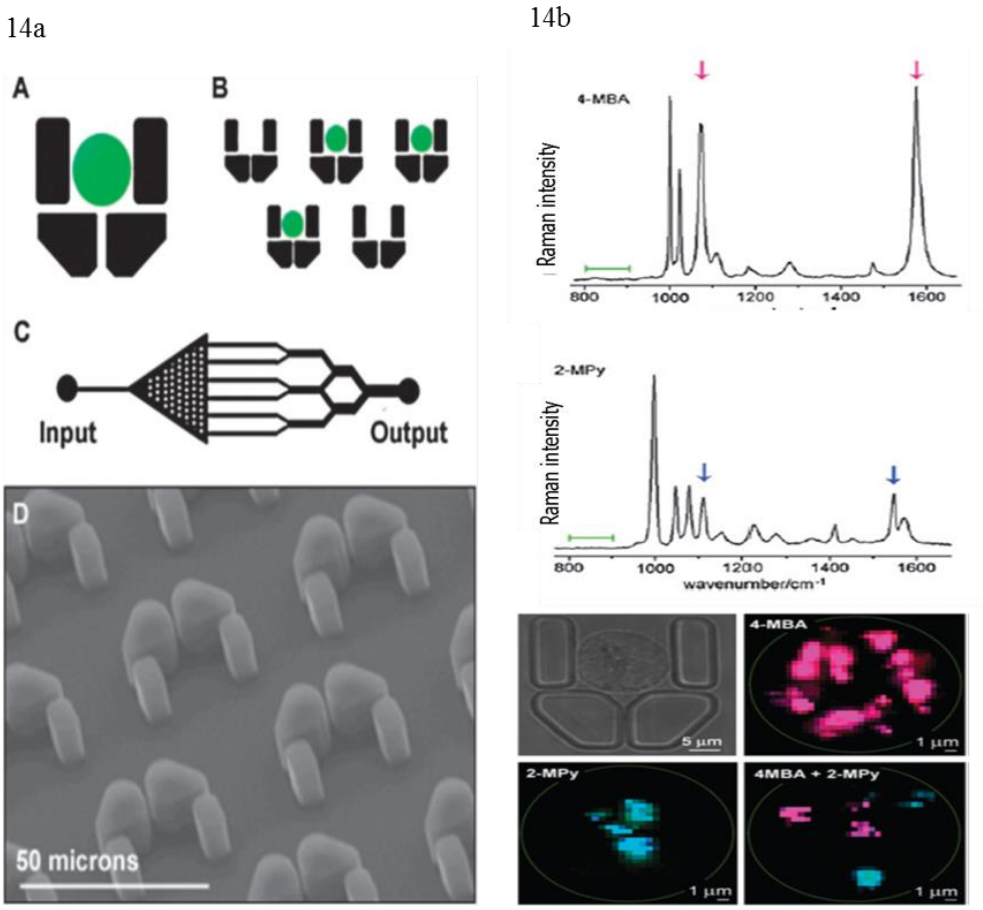

Fig. 2.14 a. Schematic diagrams of a single PDMS cell trap (A), the trapping array (B) and layout of the microfluidic device (C) with the cell trapping array represented as black triangle with white dots. (D) Scanning electron microscope image of 18 μm *18 μm * 10 μm PDMS cell traps on a device. 2.14 b. Upper: Raman spectra of 4-mercaptobenzoic acid (4-MBA) 1050-1090 and 1560-1590 cm^{-1} were used to assign 4-MBA (pink arrows); middle: Raman spectra of 2-mercaptopyridine (2-MPy). 1090-1130 and 1525-1555 cm^{-1} were used to assign 2-MPy (blue arrows); lower: SERS maps of individual CHO cells containing differently labelled Ag nanoparticles (Syme et al., 2010). Copyright Royal Society of Chemistry and reproduced with permission.

Many applications have also been explored for trapping and sorting targets in microfluidic devices, such as enhanced evaporation (Zhang et al., 2010), acoustic force (Jeong et al., 2011) and magnetic force (Chikkaveeraiah et al., 2011). The magnetic method can sort and separate magnetically labeled particles. In Chikkaveeraiah's study, the detection limit of the protein-magnetic bead conjugated into the device could be improved to sub pg per mL protein (Fig. 2.15 a, path B). Before injecting the proteins

analytes into the microfluidic device, multi enzyme and antibody modified magnetic particles were completely mixed with target proteins off-chip in order to increase the possibility of targets trapping. This method differs from the conventional strategy in which capture antibodies on the sensor surface capture protein, followed by attachment of a labeled detection antibody (Fig. 2.15 a, Path A). The microfluidic immunoarray provided accurate and sensitive detection of biomarker proteins PSA and IL-6 in prostate cancer patient serum and excellent correlation with single protein assays by standard ELISA (shown in Fig. 2.15 b).

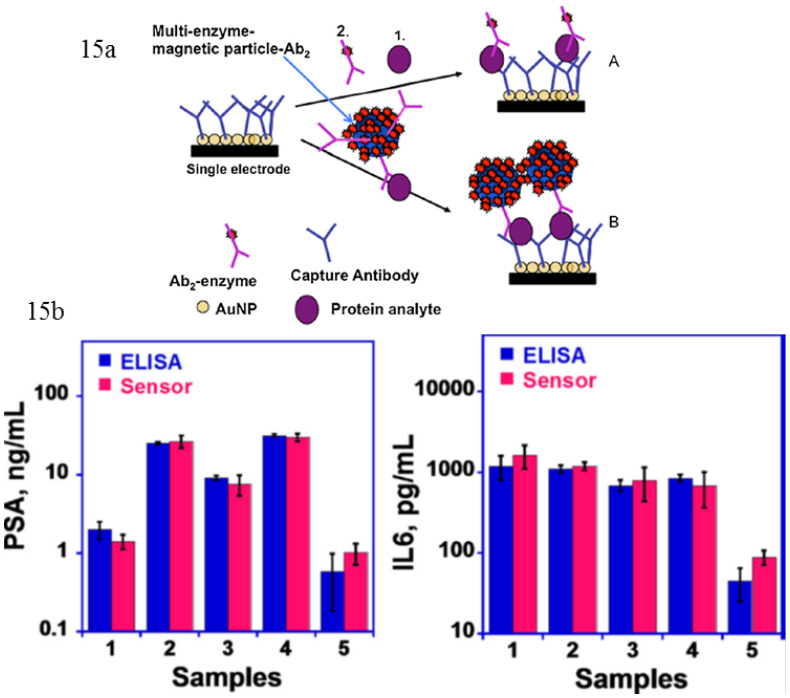

Fig. 2.15 a. Alternative strategies for electrochemical detection by amperometric immunosensors featuring AuNP surfaces with capture antibodies attached: (A) immunosensor after incubating with protein analyte (1) and flowing in a conventional single-enzyme (HRP) labeled antibody (2, Ab_2); (B) immunosensor as used in this work after analyte protein capture off-line with MP-Ab_2-HRP having many thousands of HRP labels. MP-Ab_2-HRP-analyte bioconjugates are trapped by antibodies on the electrodes, and amperometric signals are then developed by injecting a solution of mediator and hydrogen peroxide. 2.15 b. Comparison of microfluidic immunoarray assay results with standard ELISA assays for PSA and IL-6 in human serum (for both assays, n = 4) (Chikkaveeraiah et al., 2011). Copyright Elsevier and reproduced with permission.

Recently, Yang established a capillary-driven SERS-based microfluidic chip for abrin detection (Yang et al., 2014). Anti-abrin polyclonal antibodies and secondary antibodies were immobilized on different places of the micropillar array as the detection zone and control zone (Fig. 2.16 a). The external anti-abrin SERS probes were dissolved from the sample liquid and reacted within the micropillar array and then driven through by capillary action (Fig. 2.16 b). The detection signal was provided by the external SERS probes captured on the detection and control zones (Fig. 2.16 c).

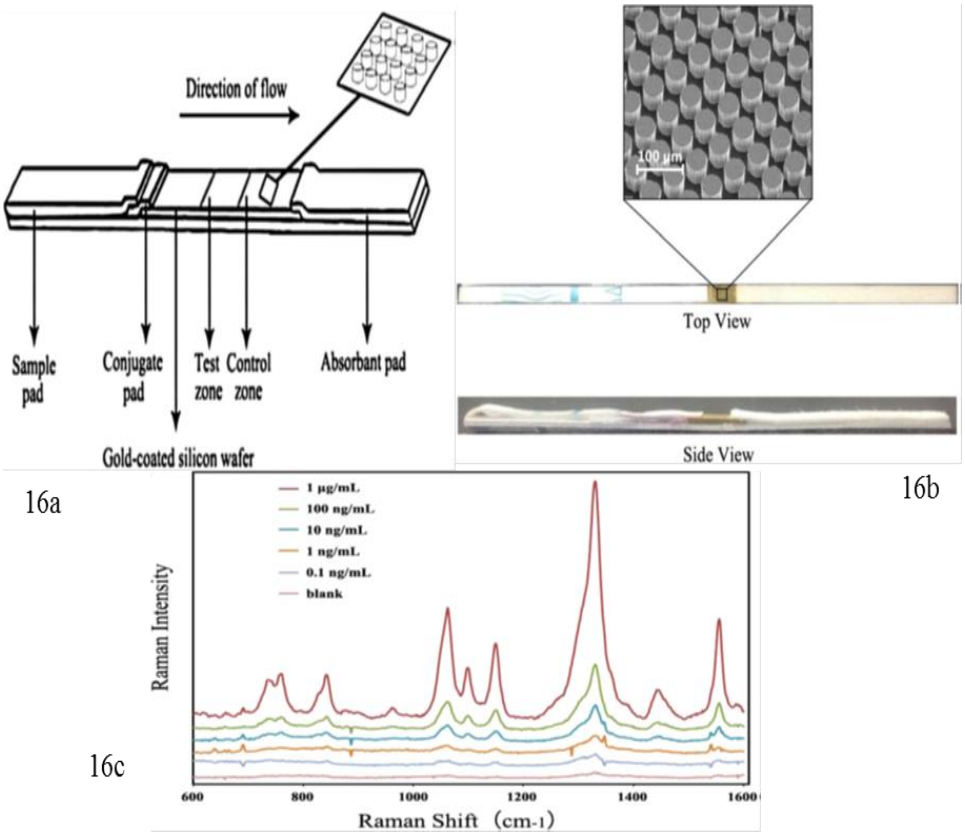

Fig. 2.16 a. Schematic of capillary-driven SERS microfluidic chip. 2.16 b. Characterization of capillary-driven SERS microfluidic chip. 2.16 c. SERS spectra of the abrin-spiked sample at different concentrations (Yang et al., 2014). Copyright SpringerOpen and reproduced with permission.

2.6. Applications of microfluidic-SERS detection

The integration of microfluidic devices and SERS has been widely investigated in different bioanalytical applications. Here some most recent work in biological/environmental analysis is reviewed in details to illustrate the impact of this novel technological development.

2.6.1. Microfluidic-SERS Immunoassays

Immunosensors are based on highly selective antibody (Ab) - antigen (Ag) reactions. The immobilized sensing element can be either an Ab or an Ag. In the first case, analyte binding is measured directly. In the second case, the method is based on the competition between immobilized Ag, the analyte (Ag) and a fixed amount of Ab. Microfluidic-SERS immunoassay improves the detection sensitivity, and reduces the time-cost as well as the reaction volume of the assay. Additionally, it is possible to selectively capture specific antigens on well-defined spot in flow. Knauer et al. (2012) demonstrated an immunoassay microarray flow-through system for online SERS detection of antibody-captured *E.Coli* bacteria. The microarray substrate coated with specific antibodies was integrated into the flow cell facing upside down (Fig. 2.17 a). As shown in Fig. 2.17 b, after passing SERS active silver nanocolloids and bacteria into the channel, the detection of single microbial cell in the flow cell could be achieved using SERS mapping. Other than the conventional bacteria detection microfluidic constructions, the bacteria were immobilized onto the antibody-functionalized surface prior to the addition of nanocolloids in this system, which diminished the need for

mixing. The silver nanoparticles then could be homogeneously surrounded the bacterial cells due to the laminar flow.

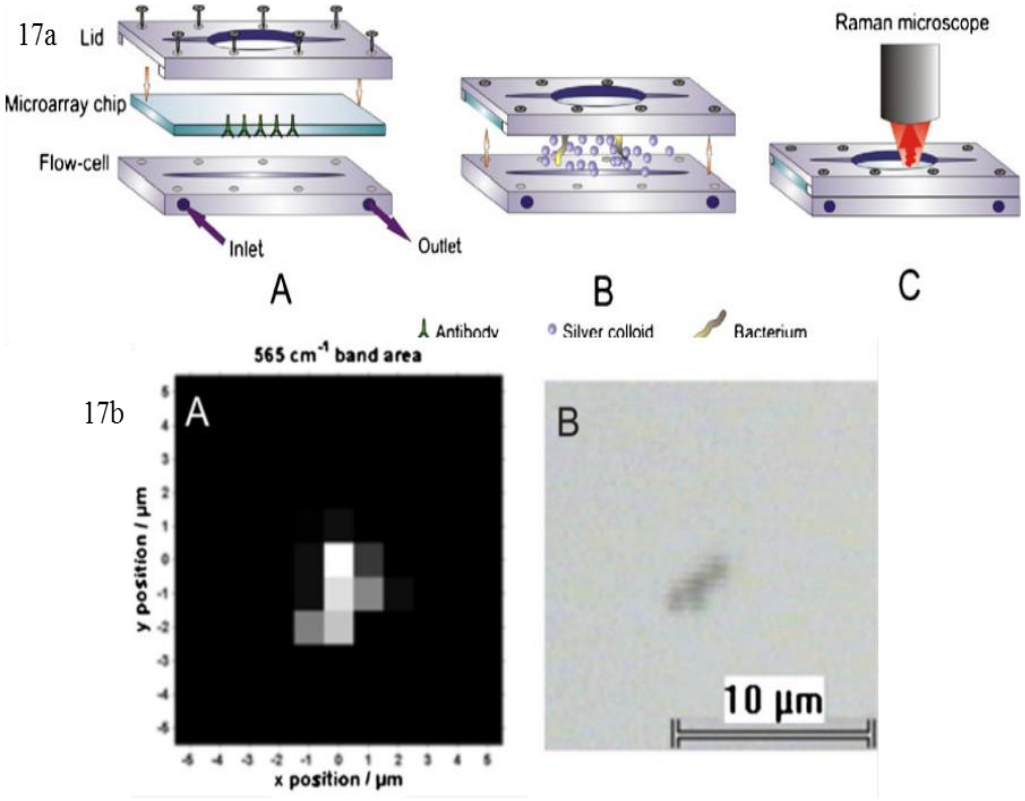

Fig. 2.17 a. Schematic set up of the flow cell. (a) Prior to antigen addition, the lid is fixed to the flow cell. The microarray is sited between them holding the antibodies facing to the flow cell. (b) The antigens are added in the flow cell bound on the antibodies. For SERS detection colloids are brought in contact to the bound bacteria. (c) A closed flow cell illustrating the SERS measurement. 2.17 b. Resulting SERS image of a single *E. Coli* cell from mapping carried out by means of the vibrational mode at 565 cm^{-1}. One spectrum is made each 1 μm (a). The complimentary light image of the *E.Coli* cell on the microarray where SERS imaging was carried out (b) (Knauer et al., 2012). Copyright Springer and reproduced with permission.

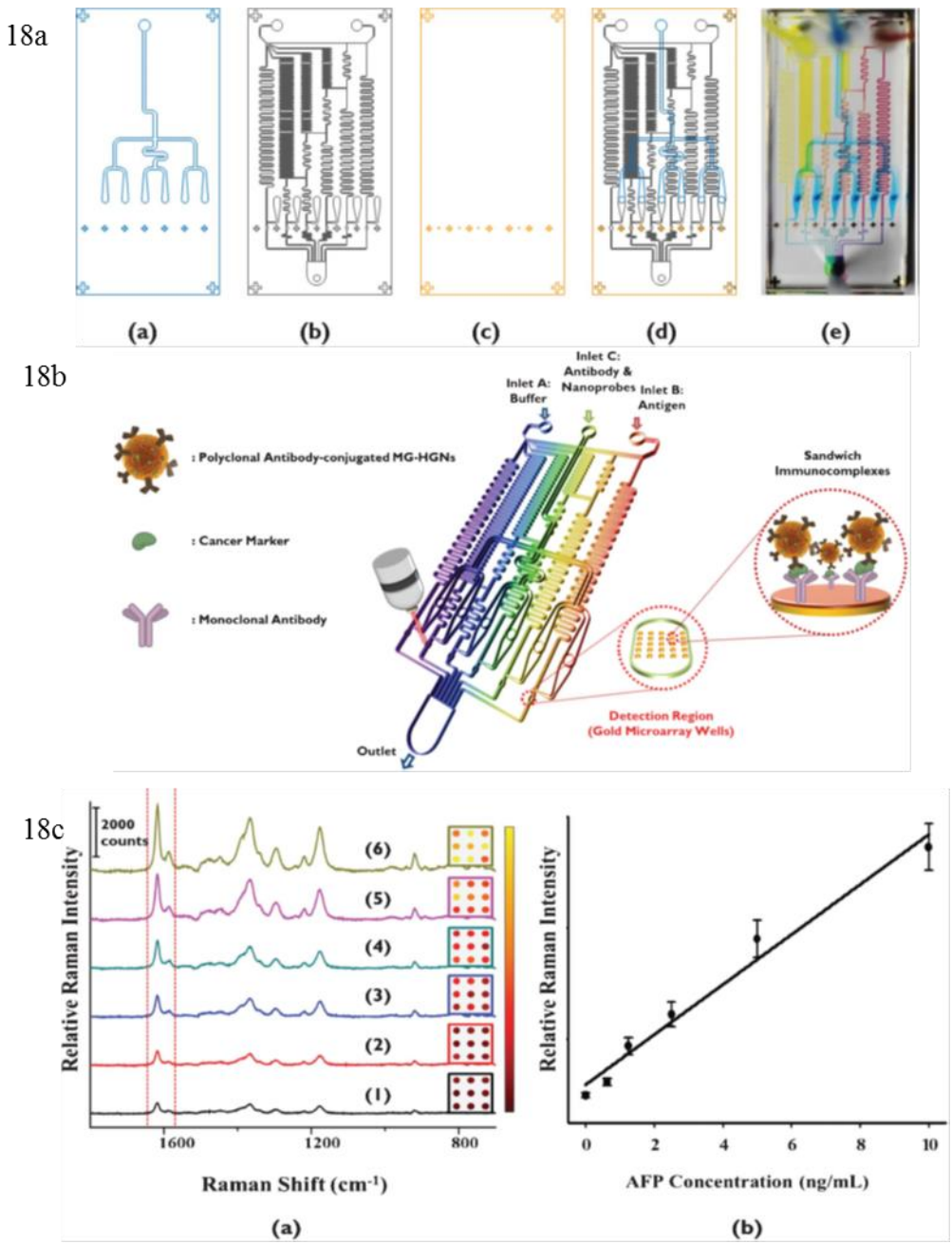

Fig. 2.18 a. Schematic illustration of a gold array-embedded gradient chip consisting of three layers. (a) Top layer: PDMS panel for the uniform distribution of antibody-conjugated HGNs; (b) middle layer: PDMA gradient panel for the generation of various concentrations of a cancer marker; and (c) bottom layer: gold array-embedded glass substrate for the immobilization of sandwich immunocomplexes. (d) Photograph of an integrated gold array embedded gradient chip, and (e) photograph of the channel filled with different ink solutions (yellow, blue and red) injected through three inlets. 2.18 b. Layout of a gold array-embedded gradient chip for the SERS-based immunoassay. The illustrations in the enlarged circles represent the formation of sandwich immunocomplexes on the surface of 5*5 round gold wells embedded in the gradient channel. 2.18 c. (a) SERS spectra for decreasing concentrations of AFP: (1) 0 ng/mL, (2) 0.625 ng/mL, (3) 1.25 ng/mL, (4) 2.5 ng/mL, (5) 5.0 ng/mL, (6) 10 ng/mL. (b) Corresponding intensity

change of the SERS signal for different concentrations of AFP antigen (Lee et al., 2012). Copyright Royal Society of Chemistry and reproduced with permission.

Lee et al. (2012) demonstrated a SERS-based optofluidic immune-sensor with a gold array-embedded gradient channel for quantitative analysis of the alpha-fetoprotein (AFP), an indicator of tumor activity in hepatocellular carcinoma (HCC) with a microfluidic chip (Fig. 2.18 a). The SERS signal was measured under the steady-state condition by moving the laser spot to each reaction chamber (Fig. 2.18 c).

2.6.2. Microfluidic-SERS DNA/RNA assay

Nowadays, Fluorescence spectroscopy is the mainstream method for DNA/RNA detection platforms. However, it is not without its own drawbacks. Microfluidic-SERS assay offers greater multiplexing capacity, and the additional information contained in the distinct Raman fingerprint signatures of different components in targets. Furthermore, the microfluidic platforms eliminate the needs of tedious washing steps to remove the unbound and not hybridized oligonucleotides. Strelau et al. (2010) developed a sequence-specific detection method for DNA with a solid chip surface to immobilize capturing DNAs, and readout based on SERS spectra of the hybridized samples. Choi et al. (2012) demonstrated a SERS-based micro-network gradient platform to detect two different types of DNA oligomer mixtures. As shown in Fig. 2.19 a, the micro-structure could produce a series of different concentration gradients for the target DNA oligomers, Cy3-labeled DNA oligomers (BRAC1-Mutation) and TAMRA labeled DNA oligomer (BRAC1-Wild). The groove-shaped mixer was incorporated into the channel to improve the mixing efficiency. The quantitative

analysis was achieved by collecting the SERS signals of mixtures of two DNA oligomers absorbed onto the surface of silver nanoparticles (Fig. 2.19 b).

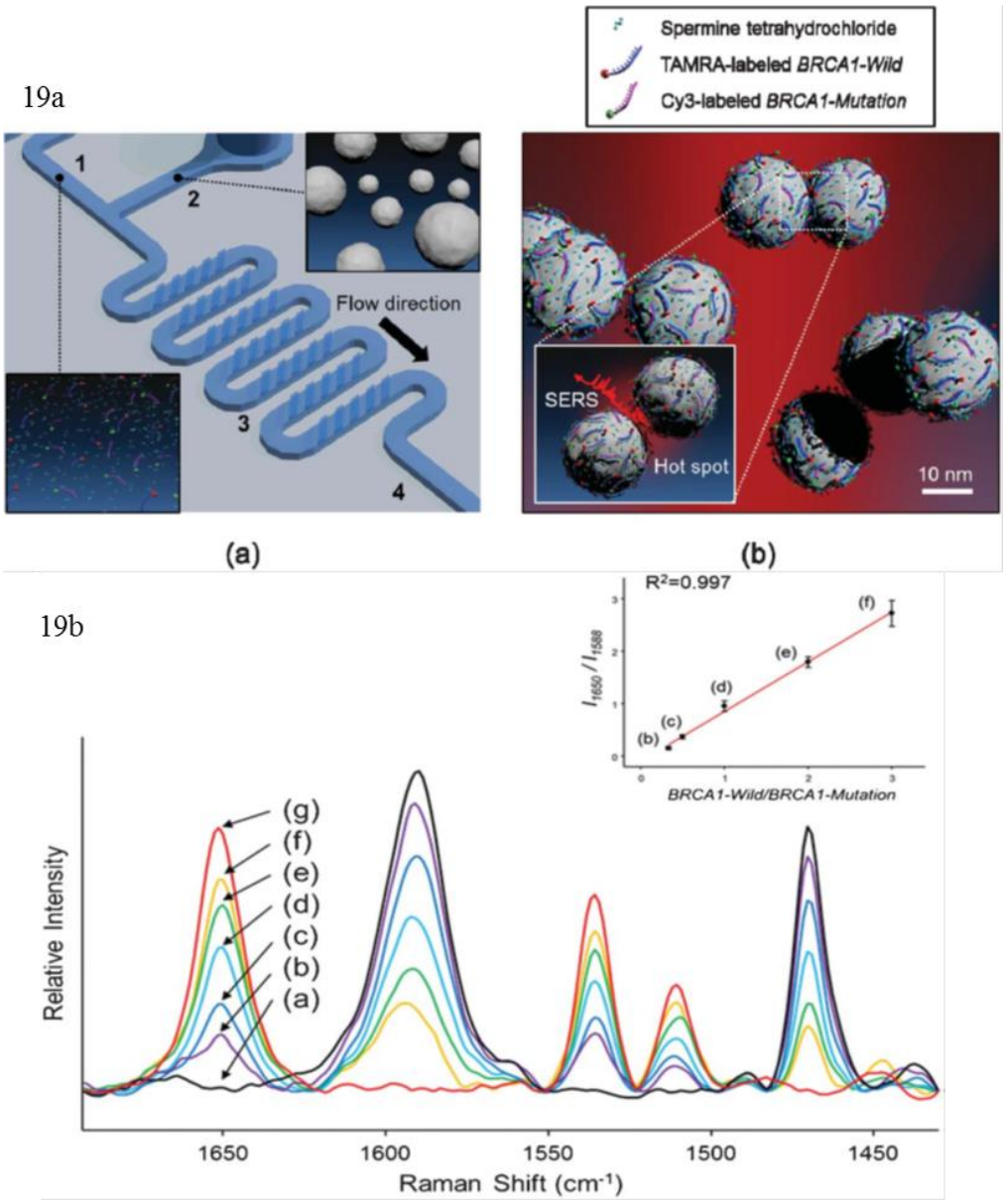

Fig. 2.19 a. (a) Groove channel structures to efficiently mix DNA oligomer mixtures and silver nanoparticles. 1: DNA oligomer mixtures, 2: silver nanoparticles, 3: groove channels, and 4: SERS detection point. (b) SERS signal coming from DNA oligomers adsorbed on silver nanoparticle aggregates in the microfluidic channel. 2.19 b. Confocal SERS spectra of different molar ratios of duplex DNA oligomer mixtures. The molar ratio between TAMRA-labeled BRCA1-Wild and Cy3-labeled BRCA1-Mutation are (a) 0 : 1, (b) 1 : 3, (c) 1 : 2, (d) 1 : 1, (e) 2 : 1, (f) 3 : 1, and (g) 1 : 0. The insert shows the variation in peak area ratio (I1650/I1588) as a function of BRCA1-Wild/BRAC1-Mutation molar ratio (Choi et al., 2012). Copyright Royal Society of Chemistry and reproduced with permission.

Recently, Qi et al. (2014) improved the ssDNA detection sensitivity to single-molecule level within 10 min detection time. They implemented molecular sentinel (MS) immobilized onto nanoporous gold (NPG) disks inside microfluidics. MS involved the design of the complementary sequence of a target ssDNA into a stem-loop "hairpin". As shown in Fig. 2.20, the probe had a thiol group for immobilization onto gold nanostructures, and a fluorophore cyanine 3 (Cy3) for SERS detection. The detection limit of target ssDNA (breast cancer marker genes ERBB2) was 20 pM and the hybridization events could be observed and quantified within 10min after injecting the target DNA molecules.

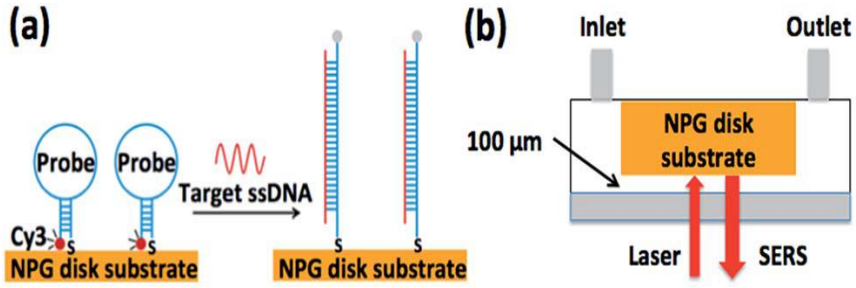

Fig. 2.20 Schematic of MS sensing mechanism in microfluidics: (a) ssDNA MS probes in a hairpin configuration are immobilized on NPG disk substrates. Intense SERS signals are observed due to the short distance between Cy3 molecules and the gold surface. Probes become straight and rigid after hybridization with target ssDNA molecules. The SERS signal disappears because Cy3 molecules now are about 10 nm away from the gold surface. (b) Microfluidic configuration for SERS data acquisition (Qi et al., 2014). Copyright Royal Society of Chemistry and reproduced with permission.

2.6.3. Microfluidic-SERS assay for environmental surveillance

Conventional environmental assays for pollutants are time-consuming, high cost, and require highly skilled personnel. Microfluidic-SERS assay can be utilized to overcome some of these problems. Microfluidic-SERS assays have been developed for ultrasensitive trace analysis of pollutants such as metal ions and pesticides for

environmental monitoring. Recently, Wang et al. (2014) reported qualitative and quantitative detection of organic pollutants and pesticides by integrating SERS optrode within microfluidic chips with *in situ* laser-induced polymerization and silver deposition. The detection limit by this SERS optrode was 1.0×10^{-8} M.

Qi et al. (2014) implemented a rapid quantitative detection of As (III) ions in a continuous flow by integrating SERS into a zigzag microfluidic chip (Fig. 2.21 a (a)). Glutathione (GSH) and 4-mercaptopyridine (4-MPY) functionalized silver nanoparticles were conjugated with As (III) ions for SERS detection under a confocal micro-Raman spectrometer. The As (III) ions could be detected by SERS of the 4-MPY reporters due to the aggregation-induced hotspots after full mixing in the zigzag channel (Fig. 2.21 a (c-e)). The characteristic peak at 1098 cm^{-1} was evaluated for quantitative analysis. Results showed an excellent selectivity of As (III) and the limit of detection was determined to be 0.67 ppb (Fig. 2.21 b).

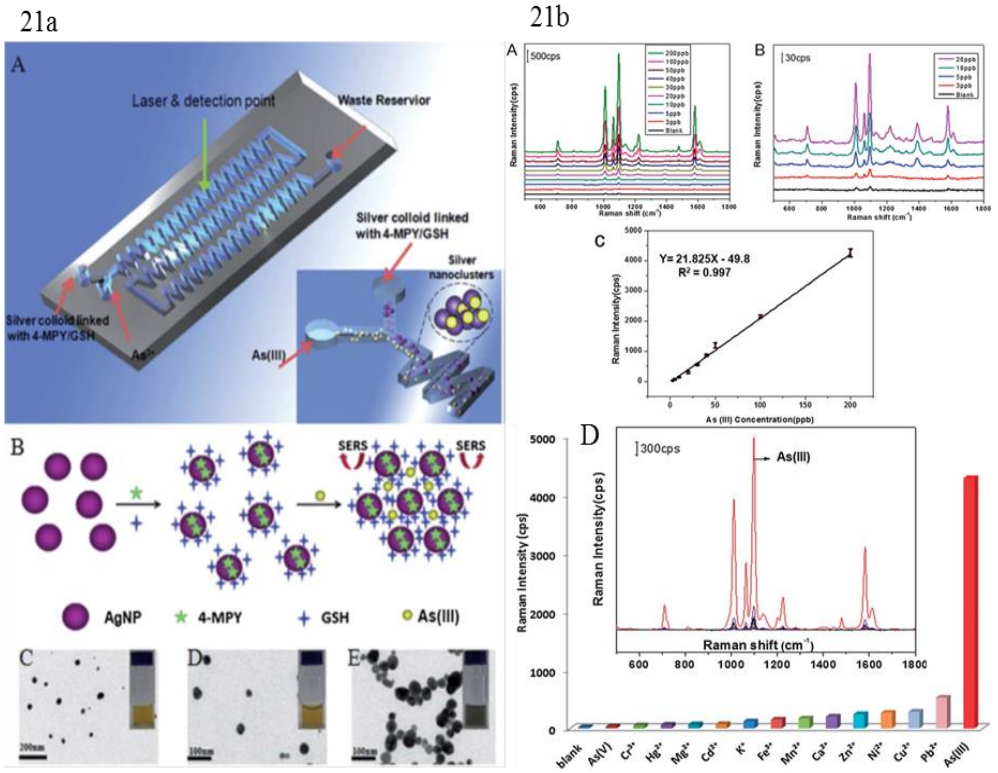

Fig. 21a. (A) Schematic diagram of the microfluidic chip used for analyzing the As (III) ions. The rapid, full mixing of the As (III) ions and GSH/4-MPY functionalized AgNPs achieved in a zigzag (75° angles) microfluidic channel (inset). (B) The analytical principle for As (III) ions. (C) Non-aggregated AgNPs, (D) Non-aggregated GSH/4-MPY functionalized AgNPs, and (E) aggregated GSH/4-MPY functionalized AgNPs in the presence of As (III) ions. The scales bars are 200 nm, 100 nm, and 100 nm respectively. 21b. (A) SERS spectra changes upon the functionalization of AgNPs by GSH/4-MPY with various As (III) ion concentrations. SERS spectra changes of GSH/4-MPY functionalized AgNPs at lower concentrations of As (III) ions. (C) Calibration curve of As(III) ions at 1098 cm^{-1} for the detection of the linear range (D) SERS intensity changes of the aggregated GSH/4-MPY functionalized AgNPs in the presence of different metal ions at 1098 cm^{-1} (Qi et al., 2014). Copyright Royal Society of Chemistry and reproduced with permission.

Yazdi and White (2013) demonstrated an optofluidic SERS device optimized for on-site multiplexing detection of three fungicides in the field. The portability was greatly improved by avoiding bulky sample loading pumps, and by integrating fiber optic cable for sample excitation and signal collection (Fig. 2.22 a). Three fungicides, 0.1 ppb malachite green, 5ppb thiram and 5 ppm methyl parathion, could be detected simultaneously in this SERS microsystem (Fig. 2.22 b).

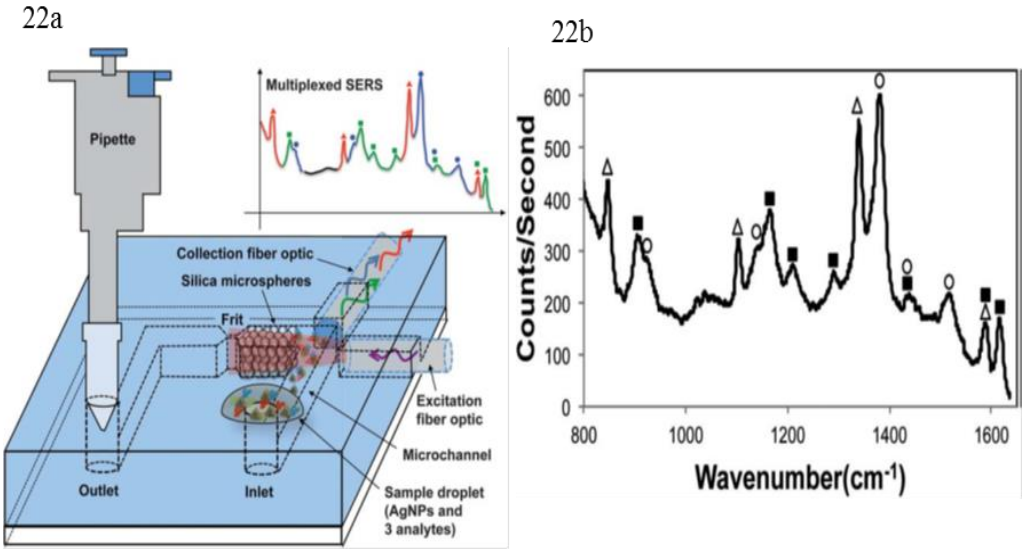

Fig. 2.22 a. Concept of the pump-free optofluidic SERS device. Negative pressure from a pipette draws the sample into the channel. Packed silica microspheres trap and concentrate AgNPs and adsorbed analytes. Integrated fiber optic cables eliminate the need for a microscope. 2.22 b. Multiplexed SERS spectrum of 0.1 ppb malachite green oxalate (■), 5 ppm methyl parathion (Δ), and 5 ppb thiram (O) (Yazdi and White. 2013). Copyright Royal Society of Chemistry and reproduced with permission.

Gao et al. (2014) reported a SERS-based microdroplet sensor for trace analysis of diquat dibromide monohydrate (DQ) in drinking water. There were two droplet generators in the microfluidic device: one for silver nanoparticle synthesized *in situ* and the other for target (Fig. 2.23 a-c). Then each nanoparticle droplet was synchronously merged with another droplet containing DQ for SERS detection. A LOD of 5 nM was reported using this SERS-based microdroplet sensor (Fig. 2.23 d), which meets the controlled level for the contaminant defined by USEPA.

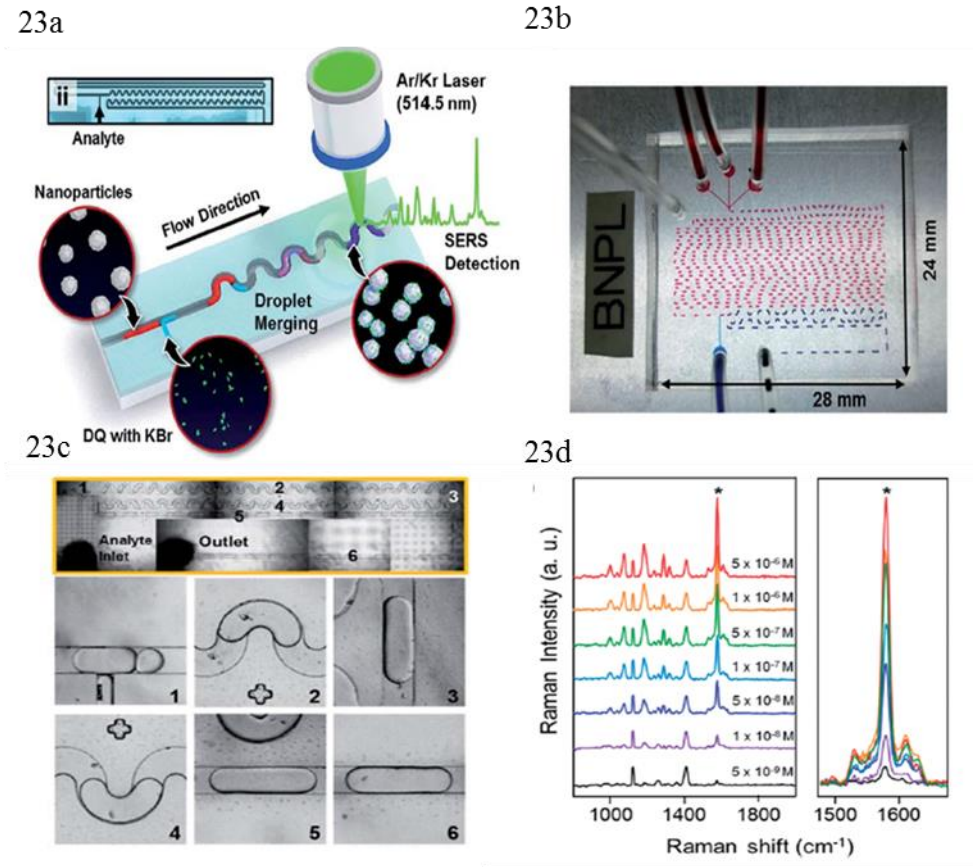

Fig. 2.23 a. Schematic illustration of an integrated microdroplet channel for SERS detection of DQ. 2.23 b.The channel is composed of two compartments. The first is the synthetic section for AgNP synthesis (red ink) and the second is for droplet merging and SERS analysis (blue ink). 2.23 c. Sequential merging process between two droplets and six different channel positions for SERS measurements. 2.23 d. concentration-dependent SERS spectra of DQ in the integrate microdroplet channel (Gao et al., 2014). Copyright Royal Society of Chemistry and reproduced with permission.

Microfluidic-SERS assays were also developed for other environmentally-important pollutants, such as malachite green in fishpond water (Xie et al., 2014), mercury (II) ions (Chung et al., 2013), thiocyanate (Wu et al., 2014), as well as Methotrexate, an antifolate antibiotic (Hidi et al., 2014).

2.6.4. Microfluidic-SERS assay of living cells

The structure of a cell is complex due to the various biological constituents in and on the surface of the cell, such as proteins, DNA, lipids, and carbohydrates. SERS is perfectly suited to selectively analyze targets with complex components, while microfluidic systems can be used to keep cells stable in solution.

Zhang et al. (2008) demonstrated the characterization of a Chinese hamster ovary (CHO) cell in a microfluidic device by the means of SERS. Popp et al. analyzed the enzymatic activity of thiopurine S-methyltransferase (TPMT) identified in lysed red blood cells inside a lab-on-a-chip SERS unit (März et al., 2011). Zhou et al. reported a highly sensitive detection method of bovine serum albumin (BSA) on a PDMS microfluidic chip using SERS analysis. Yang et al. (2011) reported the detections of the proteins lysozyme and cytochrome c as well as the bacterial species *S. oneidensis* MR-1 in aqueous solutions with high sensitivity using SERS and optical fibers. Lu et al. differentiated 21 methicillin-sensitive *S. aureus* (MSSA) and 37 MRSA using clinical isolates within SERS coupled microfluidic chips (Lu et al., 2013). In this optofluidic platform, segmented flow was created by using mineral oil as the segregation medium to remove the memory effects; designed winding channels was used to enhance the mixing efficiency; and PDMS background spectra was minimized by implementing confocal micro-Raman spectrometer (Fig. 2.24 a). A global supervised DFA dendrogram statistical model was developed in this study for classification of the 58 *S.aureus* isolates. In order to improve the accuracy of the

analysis, 300 spectra were collected for each isolate. As shown in Fig. 2.24 b, the discrimination between MRSA and MSSA was excellent.

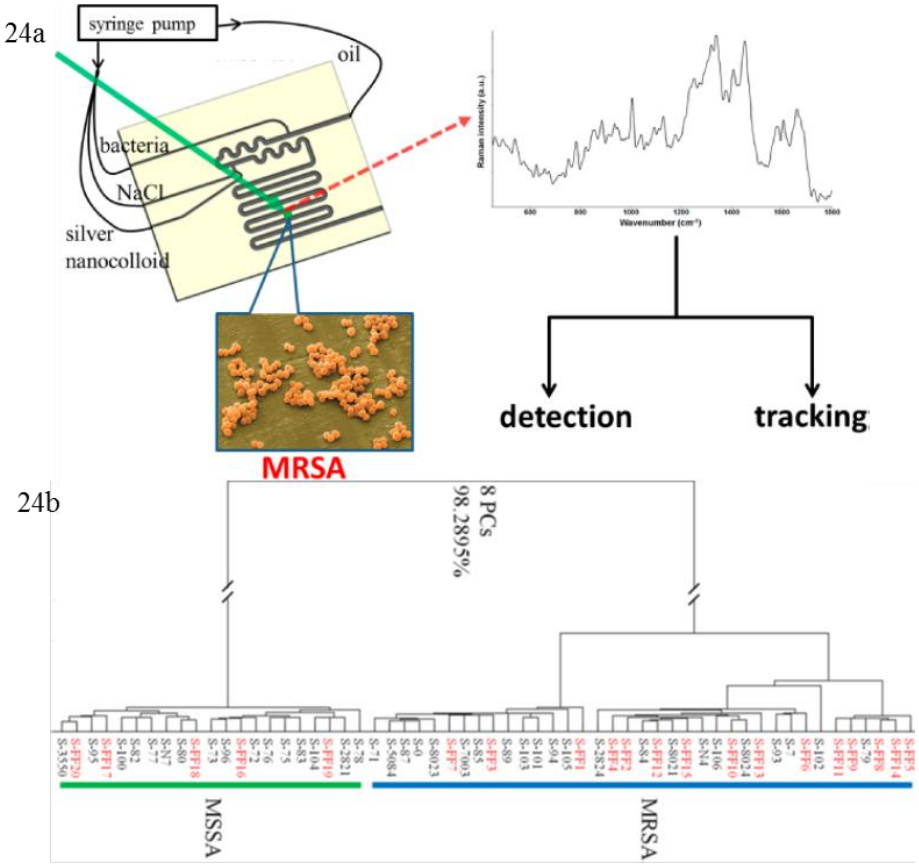

Fig. 2.24 a. (a)Scheme of the optofluidic platform (b) Composite dendrogram representing the global chemometric model to identify MRSA and MSSA. 2.24 b. Entries in black represent the training data using MRSA and MSSA samples from China, and those in red denote the validation data using MRSA and MSSA samples from the United States (Lu et al., 2013). Copyright American Chemical Society and reproduced with permission.

2.7. Data analysis

SERS spectroscopic data obtained in microfluidic devices for biological samples are usually complex and information-rich due to the complex fingerprinting signatures of the target biomolecules. The number of SERS peaks of bioanalytes is always large because of the complex organic components of these analytes. Furthermore, the simultaneous presence of multiple nanoparticles, SERS reporter molecules, and targets

generates highly overlapping spectra in many measurements. Thus, it is often necessary to utilize multivariate statistical analysis to discriminate and classify complex samples.

Deconvolution is a qualitative technique commonly used to decompose overlapping spectral bands to known peaks based on different band signatures. Lorentzian and Gaussian fitting are the two main techniques used in deconvolution of SERS spectra (Paquet-Mercier et al., 2013). Hierarchical cluster analysis (HCA) is a method of structuring a complex set of observations into unique, mutually exclusive clusters of subjects similar to each other with respect to certain characteristics, which has become a popular tool for the unsupervised qualitative analysis of complex experimental data, especially for biological and medical samples (Kniggendorf et al., 2011; Hundson and Chumanov. 2009).

It is common to use regression modeling to quantitatively assess concentrations of chemical ingredients of samples, which are proportional to the intensity of given SERS peaks. Quantitative concentration determination has been developed for chemical compounds such as dipicolinic acid (Quang et al., 2008), glucose (Yang et al., 2012) based on microfluidic-SERS data and subsequent statistical modeling. Xia et al. (2014) improved the quantitative SERS signal accuracy of Rhodamine 6G and malachite green with an average relative prediction error less than 10% within a SERS-microfluidics system.

To better analyze SERS spectra both quantitatively and qualitatively, sometimes it is necessary to combine different statistical techniques in spectral data analysis. In the SERS-microfluidics study of thiopurine S-methyltransferase (TPMT) activity in lysed

red blood cells, multiple statistical analysis methods were carried out for data processing (Fig. 25). The conversion of 6-mercaptopurine to 6-methylmercaptopurine catalyzed by TPMT is observed as it gives evidence for the enzyme activity (März et al., 2011). Multiple statistical analysis methods were also utilized in discrimination of bacteria on strain level within a SERS-microfluidics platform (Walter et al., 2011). A sum of 11 200 spectra were recorded with an integration time of 1 s for each spectrum for classification of an E. coli model system consisting of nine different species. Practically speaking, 5600 spectra were used to train the Support Vectors Machine (SVM) model and the other 5600 spectra were applied for the evaluation to validate the established SVM. As shown in Table 2.1. The validation of the bacteria on strain level is achieved accomplishing SVM accuracies of 92%.

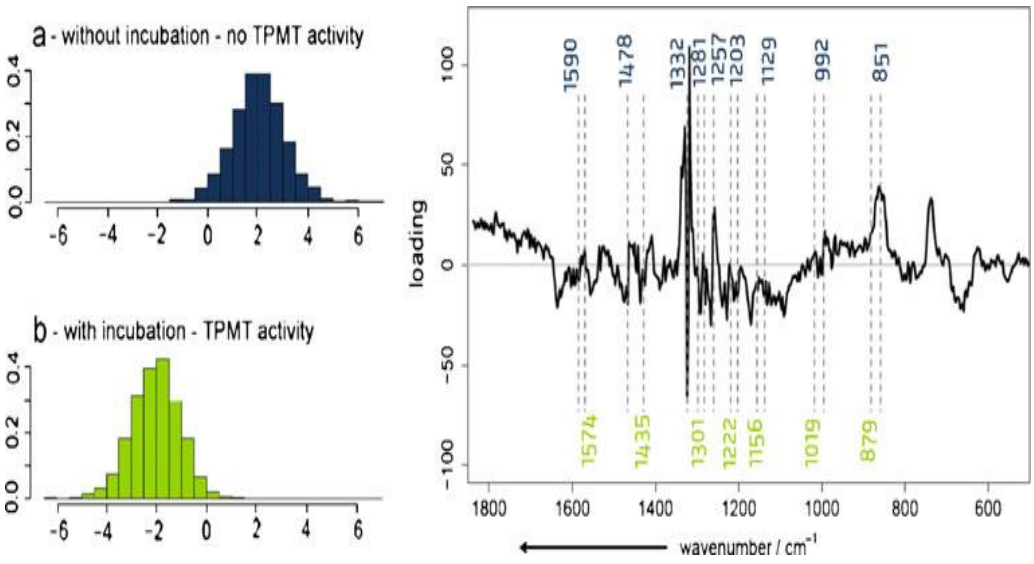

Fig. 2.25 LDA model of incubated test blood sample and test blood samples without incubation. a&b .Histograms of LDA values of spectra from each group. c. LDA loading with assignment of bands appearing in SERS spectrum of TMPT absent (blue) and present (green) (März et al., 2011). Copyright Springer and reproduced with permission.

Table 2.1 Results of E.coli validation on strain level including only the fingerprint region. A SVM model is trained with the first dataset (5600 spectra) in the PCA space (using the first 25 principle components only) and tested with the second dataset (5600 spectra) transferred to the same PCA space (Walter et al., 2011) Copyright Royal Society of Chemistry and reproduced with permission.

	E. coli DSM1508	E. coli DSM2769	E. coli DSM423	E. coli DSM479	E. coli DSM498	E. coli DSM499	E. coli DSM501	E. coli DSM5208	E. coli DSM613
(a) A linear SVM is applied resulting in an overall accuracy of 90.1%									
E. coli DSM1508	431	1	11	2	15	8	4	7	10
E. coli DSM2769	0	634	2	2	45	0	0	8	11
E. coli DSM423	9	1	289	4	17	26	15	2	4
E. coli DSM479	4	2	0	298	10	1	0	0	1
E. coli DSM498	11	62	11	13	581	7	4	2	36
E. coli DSM499	2	0	24	0	5	625	15	0	7
E. coli	2	0	4	0	5	6	249	20	0

DSM501									
E. coli DSM5208	0	6	1	0	1	0	24	643	0
E. coli DSM613	7	8	1	0	43	6	0	0	1297
# of spectra	466	714	343	319	719	679	311	682	1366
(b) A radial basis SVM is applied resulting in an overall accuracy of 91.0%									
E. coli DSM1508	449	0	6	1	14	6	6	0	4
E. coli DSM2769	0	644	4	2	45	1	0	3	8
E. coli DSM423	4	0	288	4	9	17	14	3	4
E. coli DSM479	0	2	1	298	5	0	0	0	1
E. coli DSM498	3	55	13	12	587	7	7	1	21
E. coli	2	0	24	0	7	633	17	0	10

DSM499									
E. coli DSM501	1	0	2	0	2	5	233	24	1
E. coli DSM5208	0	3	0	0	1	1	31	649	0
E. coli DSM613	7	1	5	2	49	9	3	2	1317
# of spectra	466	714	343	319	719	679	311	682	1366

2.8. Future perspective

The integration of microfluidic devices with SERS detection has yielded simple and miniaturized instrumentation that is suitable for the detection and characterization of small volume of chemical and biological analytes with high sensitivity and specificity. Despite its rapid progress in the past few years, a few challenges remain to be addressed before this approach can truly become an alternative to the existing techniques. Although some quantitative work has been reported, due to the nature of the SERS, which is dependent on nanoscale, localized phenomenon, enhancement factors measured for the same sample can vary quite a bit from measurement to measurement, and hence render the quantitative results inconsistent. How to assure the consistency in SERS measurements is still a work in progress. In addition, a complete database of standard SERS spectra of compounds, or biological samples of interests (e.g., pathogenic microorganisms, biological toxins, pollutants), which is needed for classification and discrimination analysis, still does not exist. Furthermore, the cost for

nanomaterials and instrumentation needs to further go down before microfluidic SERS platforms can really impact applications of rapid detection in fields.

2.9. Reference

Abalde-Cela S, Auguie B, Fischlechner M, Huck W, Alvarez-Puebla R, Liz-Marzan L, Abell C 2010 Microdroplet fabrication of silver-agarose nanocomposite beads for SERS optical accumulation *Soft Matter* 7 1321-1325

Ahmad A, Moore E 2012 Electrochemical immunosensor modified with self-assembled monolayer of 11-mercaptoundecanoic acid on gold electrodes for detection of benzo[a]pyrene in water *Analyst*. 137 5839-5844

Aroca R 2006 Surface-Enhanced Vib. Spectrosc., *John Wiley & Sons Ltd*, West Sussex

Aroca R, Alvarez-Puebla R, Pieczonka N, Sanchez-Cortez S, Garcia-Ramos J 2005 Surface-enhanced Raman scattering on colloidal nanostructures Advances in Colloid and Interface Science 116 45-61

Ashkin A, Dziedzic J, Bjorkholm J, Chu S 1986 Observation of a single-beam gradient force optical trap for dielectric particles *Opt Lett.* 11 288-290

Arya SK, Singh A, Naidoo R, Wu P, McDermott MT, Evoy S. 2011 Chemically immobilized T4-bacteriophage for specific *Escherichia coli* detection using surface plasmon resonance. *Analyst.* 136 486-492

Banerjee A, Perez-Castillejos R, Hahn D, Smirnov A, Grebel H 2010 Micro-fluidic channels on nanopatterned substrates: Monitoring protein binding to lipid bilayers with surface-enhanced Raman spectroscopy *Chemical Physics Letters*. 489 121-126

Bantz K, Meyer A, Wittenberg N, Im H et al. 2011 Recent Progress in SERS biosensing *Phys. Chem. Chem. Phys*. 13 11551-11567

Beebe D, Mensing G, Walker G 2002 Physics and Applications of microfluidics in biology *Annual Review of Biomedical Engineering.* 4 261-286

Chikkaveeraiah B, Mani V, Patel V, Gutkind J, Rusling J 2011 Microfluidic Electrochemical Immunoarray for Ultrasensitive Detection of Two Cancer Biomarker Proteins in Serum Biosens Bioelectron. 26 4477-4483

Bragheri F, Minzioni P, Martinez Vazquez R, Bellini N, Paie P, Mondello C, Ramponi R, Cristiani I, Osellame R 2012 Optofluidic integrated cell sorter fabricated by femtosecond lasers *Lab Chip*. 12 3779-3784

Camden J, Dieringer J, Zhao J, Van Duyne R 2008 Controlled Plasmonic Nanostructures for Surface-Enhanced Spectroscopy and Sensing *Acc. Chem. Res*. 41 1653-1661

Campion A and Kambhampati P 1998 Surface-enhanced Raman scattering *Chem. Soc. Rev.* 27 241-250

Chen LX, Choo J 2008 Recent advances in surface-enhanced Raman scattering detection technology for microfluidic chips Electrophoresis. 29(9) 1815-1828

Chen W, Lam R, Fu J 2012 Photolithographic surface micromachining of polydimethylsiloxane (PDMS) *Lab Chip*. 12 391-395

Chen H and Meiners J 2004 Topologic mixing on a microfluidic chip *Appl. Phys. Lett*. 84 2193-2195

Chen Y, Wu T, Kung Y, Teitell M, Chiou P 2013 3D pulsed laser-triggered high-speed microfluidic fluorescence-activated cell sorter *Analyst*. 138 7308-7315

Cheng I, Chang H, Chen T, Hu C, Yang F 2013 Rapid (<5 min) Identification of Pathogen in Human Blood by Electrokinetic Concentration and Surface-Enhanced Raman Spectroscopy *Scientific reports*. 3 1-8

Choi N, Lee K, Lim D, Lee E, Chang S, Oh K, Choo J 2012 Simultaneous detection of duplex DNA oligonucleotides using a SERS-based micro-network gradient chip *Lab Chip*. 12 5160-5167

Chon H, Lim C, Ha S, Ahn Y, Lee E, Chang S, Seong G, Choo J 2010 On-Chip Immunoassay Using Surface-Enhanced Raman Scattering of Hollow Gold Nanospheres *Anal Chem*. 82 5290-5295

Chrimes A, Khoshmanesh K, Stoddart P, Mitchell A, Kalantar-zadeh K 2013 Microfluidics and Raman microscopy: current applications and future challenges *Chem Soc Rev*. 42 5880-5906

Chrimes A, Kayani A, Khoshmanesh K, Stoddart P, Mulvaney P, Mitchell A, Kalantar-zadeh K 2011 Dielectrophoresis–Raman spectroscopy system for analysing suspended nanoparticles *Lab Chip*. 11 921-928

Chung E, Gao R, Ko J, Choi N, Lim D, Lee E, Chang S, Choo J 2013 Trace analysis of mercury(II) ions using aptamermodified Au/Ag core–shell nanoparticles and SERS spectroscopy in a microdroplet channel *Lab Chip*.13 260-266

Connatser R, Cochran M, Harrion R, Sepaniak M 2008 Analytical optimization of nanocomposite surface-enhanced Raman spectroscopy/scattering detection in microfluidic separation devices *Electrophoresis*. 29 1441-1450

Driscoll AJ, Harpster MH, Johnson PA 2013 The development of surface-enhanced Raman scattering as a detection modality for portable in vitro diagnostics: progress and challenges *Phys Chem Chem Phys*. 15(47) 20415-33

Ewing R and Abdel-Aty-Zohdy H 2003 Proceedings of the 2003 International Conference on Microelectronics Systems Education

Faulds K, Littleford R, Graham D, Dent G, Smith W 2004 Comparison of Surface-Enhanced Resonance Raman Scattering from Unaggregated and Aggregated Nanoparticles *Anal Chem*. 76 592-598

Fleischmann M, Hendtra P, McQuillan A 1974 Raman Spectra of Pyridine adsorbed at a silver electrode *Chemical Physics Letters*. 26 163-166

Gao J, Gu H, Xu B. 2009 Multifunctional magnetic nanoparticles: design, synthesis, and biomedical applications. *Accounts of Chemcial Research*. 42 1097-1107

Gao R, Choi N, Chang S, Lee E, Choo J 2014 Real-time analysis of diaquat dibromide monohydrate in water with a SERS-based integrated microdroplet sensor *Nanoscale*. 6 8781-8786

Godin J, Chen C, Cho S, Qiao W, Tsai F, Lo Y 2008 Microfluidics and photonics for Bio-System-on-a-Chip: A review of advancements in technology towards a microfluidic flow cytometry chip *J. Biophotonics*. 1 355-376

Graveson P, Branjeberg J, Jensen O 1993 Microfluidics-a review *J. Micromechanics. Microengineering.* 3 168-182

Haeberle S, Zengerle R 2007 Microfluidic platforms for lab-on-chip applications *Lab Chip*. 7 1094-1110

Han X, Zhao B, Ozaki Y 2012 Label-free detection in biological applications of surface-enhanced Raman scattering *Trends in Analytical Chemistry*. 38 67-78

Harper MM, McKeating KS, Faulds K 2013 Recent developments and future directions in SERS for bioanalysis *Phys. Chem. Chem. Phys*. 15 5312

Hessel V, Lowe H, Schonfeld F 2005 Micromixers-areview on passive and active mixing principles *Chem. Engineering Sci.* 60 2479-2501

Hidi I, Muhlig A, Jahn M, Liebold F, Cialla D, Weber K, Popp J 2014 LOC-SERS: towards point-of-care diagnostic of methotrexate *Anal Methods*. 6 3943-3947

Parisi J, Su L, Lei Y 2013 In situ synthesis of silver nanoparticle decorated vertical nanowalls in a microfluidic device for ultrasensitive in channel SERS sensing *Lab Chip*. 13 1501-1508

Huang K, Wu Y, Lee J, Chiou P 2013 Microfluidic integrated optoelectronic tweezers for single-cell preparation and analysis *Lab Chip*. 13 3721-3727

Huang N, Zhang H, Chung M, Seo J, Kurabayashi K 2014 Recent advancements in optofluidics-based signel-cell analysis: optical on-chip cellular manipulation, treatment, and property detection *Lab Chip*. 14 12301245

Huang J, Zhao A, Zhang X, He L, Wang T, Chui Y 2013 Ordered Ag/Si Nanowires Array: Wide-Range Surface-Enhanced Raman Spectroscopy for Reproducible Biomolecule Detection *Nano Lett*. 13 5039-5045

Huh Y, Chung A, Cordovez B, Erickson D 2009 Enhanced on-chip SERS based biomolecular detection using electrokinetically active microwells *Lab Chip*. 9 433-439

Hundson SD, Chumanov G 2009 Bioanalytical applications of SERS (surface-enhanced Raman spectroscopy) *Anal. Bioanal. Chem*. 394 679-86

Hwang H, Han D, Oh Y, Cho Y, Jeong K, Park J 2011 In situ dynamic measurements of the enhanced SERS signal using an optoelectrofluidic SERS platform *Lab Chip* 11 2518-2525

Hwang H, Kim S, Yang S 2011 Microfluidic fabrication of SERS-active microspheres for molecular detection *Lab Chip*. 11 87-92

Im H, Bantz K, Lindquist N, Haynes C, Oh S 2010 Vertically Oriented Sub-10-nm Plasmonic Nanogap Arrays *Nano Lett*. 10 2231-2236

Inoue I, Wkamoto Y, Moriguchi H, Okano K, Yasuda K 2001 On-chip culture system for observation of isolated individual cells *Lab Chip*. 1 50-55

Jana, N, Gearheart L, Murphy C 2001 Wet Chemical Synthesis of High Aspect Ratio Cylindrical Gold Nanorods *J Phys Chem B*. 105 4065-4067

Jain PK, Huang X, El-Sayed IH, El-Sayed MA. 2008 Noble metals on the nanoscale: optical and photothermal properties and some applications in imaging, sensing, biology and medicine. *Accounts of Chemcial Research*. 41 1578-1586

Jeanmaire D, Van Duyne R 1977 Surface raman spectroeletrochemistry: Part1. Heterocyclic, aromatic, and aliphatic amines adsorbed on the anodized silver electrode *J. Electroanal. Chem*. 84 1

Jeong J, Lee J, Lee C, Yeh S, Lee A, Shung K 2011 Particle manipulation in a microfluidic channel using acoustic trap *Biomed Microdevices*. 13 779-788

Khoshmanesh K, Nahavandi S, Baratchi S, Metchell A, Kalantar-zadeh K 2011 Dielectrophoretic platforms for bio-microfluidic systems *Biosensors and Bioelectronics*. 26 1800-1814

Khoshmanesh K, Baratchi S, Tovar-Lopez F, Nahavandi S, Wlodkowic D, Mitchell A, Kalantar-zadeh K 2012 On-chip separation of *Lactobacillus* bacteria from yeasts using dielectrophoresis *Microfluid Nanofluid*. 12 597-606

Kim D, Campos A, Datt A, Gao Z, Rycenga M, Burrows N, Greeneltch N, Mirkin C, Murphy C, Van Duyne R, Haynes C 2014 Microfluidic-SERS devices for one shot limit-of-detection *Analyst*. 139 3227-3234

Knauer M, Ivleva N, Niessner R, Haisch C 2012 A flow-through microarray cell for the online SERS detection of antibody-captured E coli bacteria *Anal Bioanal Chem*. 402 2663-2667

Kneipp K, Kneipp H 2006 Single Molecule Raman Scattering *Appl Spectrosc*. 60 322A-334A

Kneipp K, Kneipp H, Itzkan I, Dasari R, Feld M 2002 Surface-enhanced Raman scattering and biophysics *J. Phys. Condens. Matter*. 14 R597-R624

Kneipp J, Kneipp H, Kneipp K 2008 SERS—a single-molecule and nanoscale tool for bioanalytics *Chem Soc Rev*. 37 1052-1060

Kniggendorf A, Gaul T, Wollweber M 2011 Hierarchical Cluster Analysis (HCA) of Microorganisms: An Assessment of Algorithms for Resonance Raman Spectra *Applied Spectroscopy*. 65 165-173

Kudelski A 2008 Analytical application of Raman spectroscopy *Talanta* 76 1-8

Lai C, Chen L, Chen G, Xu Y, Wang C 2013 Microchannel-Based Surface-Enhanced Raman Spectroscopy for Integrated Microfluidic *Analysis Applied Spectroscopy*. 68 124-127

Lapizco-Encinas BH, Davalos RV, Simmons BA, Cummings EB, Fintschenko Y 2005 An insulator-based (electrodeless) dielectrophoretic concentrator for microbes in water *J. Microbio. Meth*. 62 317-326

Le H 1998 Progress and Trends in Ink-jet Printing Technology *J. Imaging Sci. Technol*.42 49-62

Lee K, Lee K, Jung J, Chang C, Sung H 2013 Optical mobility of blood cells for label-free cell separation applications *Applied Physics Letters*. 102 141911

Lee M, Lee K, Kim K, Oh Kwang, Choo J 2012 SERS-based immunoassay using a gold array-embedded gradient microfluidic chip *Lab Chip*. 12 3720-3727

Lee S, Joo S, Park S, Kim S, Kim H, Chung T 2010 SERS decoding of micro gold shells moving in microfluidic systems *Electrophoresis*. 31 1623-1629

Li Q, Li B, Wang Y 2013 Surface-enhanced Raman scattering microfluidic sensor *Rsc Adv*. 3 13015-13026

Li Y, Syed L, Liu J, Hua D, Li J 2012 Label-free electrochemical impedance detection of kinase and phosphatase activities using carbon nanofiber nanoelectrode arrays *Analytica Chimica Acta*. 744 45-53

Liao P, Bergman J, Chemla D, Wokaun A, Melngailis J, Hawryluk A, Economou N 1981 Surface-enhanced raman scattering from microlithographic silver particle surface *Chem. Phys. Lett.* 82 355-359

Liu R, Yang J, Pindera M, Athavale M, Grodzinski P 2002 Bubble-induced acoustic micromixing *Lab Chip.* 2 151-157

Lu X, Samuelson D, Xu Y, Zhang H, Wang S, Rasco B, Xu J, Konkel M 2013 Detecting and Tracking Nosocomial Methicillin-Resistant *Staphylococcus aureus* Using a Microfluidic SERS Biosensor *Anal Chem*. 85 2320-2327

Luecha J, Hsiao A, Brodsky S, Liu G, Kokini J 2011 Green microfluidic devices made of corn proteins *Lab Chip*. 11 3419-3425

Machmudah S, Wahyudiono, Takada N, Kanda H, Sasaki K, Goto M 2013 Fabrication of gold and silver nanoparticles with pulsed laser ablation under pressurized CO_2 *Adv. Nat. Sci. Nanosci. Nanotechnol*. 4 045011

Manz A, Miyahara Y, Miura J, Watanabe Y, Miyagi H, Sato K 1990 Design of an open-tubular column liquid chromatograph using silicon chip technology *Sens. Actuators, B.* 1 249-255

März A, Monch B, Rosch P, Kiehntopf M, Henkel T, Popp J 2011 Detection of thiopurine methyltransferase activity in lysed red blood cells by means of lab-on-a-chip

surface enhanced Raman spectroscopy (LOC-SERS) *Anal Bioanal Chem*. 400 2755-2761

McCreery R 2000 Raman Spectroscopy for Chemical Analysis *Wiley-Interscience*

McQuillan A, Hentra P, Fleischmann M 1975 Raman spectroscopic investigation of silver electrodes *J. Electroanal. Chem*. 933-944

Miccio L, Memmolo P, Grilli S, Ferraro P 2012 All-optical microfluidic chips for reconfigurable dielectrophoretic trapping through SLM light induced patterning *Lab Chip*. 12 4449-4454

Moffitt J, Chemla Y, Smith S, Bustamante C 2008 Recent advances in optical tweezers *Annu. Rev. Biochem.* 77 205-228

Moskovits M 1985 Surface-enhanced spectroscopy *Rev. Mod. Phys*. 57 783

Oh Y, Jeong K 2014 Optofluidic SERS chip with plasmonic nanoprobes self-aligned along microfluidic channels *Lab Chip*. 14 865-868

Otto A, Mrozek I, Grabhorn H, Akemann W 1992 Surface-enhanced Raman scattering *J. Phys. Condens. Matter*. 4 1143-1212

Palk P, Pamula V, Fair R 2003 Rapid droplet mixers for digital microfluidic systems *Lab Chip*. 3 253-259

Paquet-Mercier F, Aznaveh NB, Safdar M, Greener J 2013 A microfluidic bioreactor with in situ SERS imaging for the study of controlled flow patterns of biofilm precursor materials *Sensors (Basel).* 13 14714-27

Park T, Lee S, Seong G, Choo J, Lee E, Kim Y, Ji W, Hwang S, Gweon D, Lee S 2005 Highly sensitive signal detection of duplex dye-labelled DNA oligonucleotides in a

PDMS microfluidic chip: confocal surface-enhanced Raman spectroscopic study *Lab Chip*. 5 437-442

Paul R, McQuillan A, Hendra P, Fleischmann M 1975 Laser Raman spectroscopy at the surface of a copper electrode *J. Electroanal. Chem*. 66 248-249

Peng C, Li Z, Zhu et al., 2009 Simultaneous and sensitive determination of multiplex chemical residues based on multicolor quantum dot probes. *Biosensors and Bioelectronics.* 24 3657-3662

Piorek B, Lee S, Santiago J, Moskovits M, Banerjee S, Meinhar C 2007 Free-surface microfluidic control of surface-enhanced Raman spectroscopy for the optimized detection of airborne molecules *PNAS* 104 18898-18901

Plieth W, Dietz H, Anders A, Sandmann G, Meixner A, Weber M, Kneppe H 2005 Electrochemical preparation of silver and gold nanoparticles: Characterization by confocal and surface enhanced Raman microscopy *Surface Science*. 597 119-126

Pysher MD, Hayes MA 2007 Electrophoretic and dielectrophoretic field gradient technique for separating bioparticles *Anal. Chem*. 79 4552-7

Qi N, Li B, You H, Zhang W, Fu L, Wang Y, Chen L 2014 Surface-enhanced Raman scattering on a zigzag microfluidic chip: towards high-sensitivity detection of As(III) ions *Anal Methods*. 6 4077-4082

Qi J, Zeng J, Zhao F, Lin S, Raja B, Strych U, Willson R, Shih W 2014 Label-free, in situ SERS monitoring of individual DNA hybridization in microfluidics *Nanoscale*. 6 8521-8526

Quang L, Lim C, Seong G, Choo J, Do K, Yoo S 2008 A portable surface-enhanced Raman scattering sensor integrated with a lab-on-a-chip for field analysis *Lab Chip*. 8 2214-2219

Rider TH, Petrovick MS, Nargi FE, et al. 2003 A B cell-based sensor for rapid identification of pathogens. *Science.* 301 213-215

Sarrazin F, Salmon J 2008 Chemical Reaction Imaging within Microfluidic Devices Using Confocal Raman Spectroscopy: The Case of Water and Deuterium Oxide as a Model System *Anal. Chem*. 80 1689-1695

Schulte T, Bardell R, Weigl B 2002 Microfluidic technologies in clinical diagnostics *Clin. Chim. Acta.* 321 1-10

Soga T 2000 The resonance Raman effect of uranyl chloride in dimethyl sulfoxide *Spectrochim. Acta, Part A.* 56 79-89

Stadler J, Schmid T, Zenobi R 2010 Nanoscale Chemical Imaging Using Top-illumination Tip-Enhanced Raman Spectroscopy *Nano Lett*. 10 4514-4520

Strehle K, Cialla D, Rosch Petra, Henkel T, Kohler M, Popp J 2007 A Reproducible Surface-Enhanced Raman Spectroscopy Approach Online SERS Measurements in a Segmented Microfluidic System *Anal Chem*. 79 1542-1547

Strelau K, Kretschmer R, Moller R, Fritzsche W, Popp J 2010 SERS as tool for the analysis of DNA-chips in a microfluidic platform *Anal Bioanal Chem*. 396 1381-1384

Syme C, Sirimuthu N, Faley S, Cooper J 2010 SERS mapping of nanoparticle labels in single cells using a microfluidic chip *Chem Commun*. 46 7921-7923

Terry S, Jerman J, Angell J 1979 A gas chromatographic air analyzer fabricated on a silicon wafer *IEEE Trans. Electron Devices.* 26 1880-1886

Walter A, Marz A, Schumacher W, Rosch P, Popp J 2011 Towards a fast, high specific and reliable discrimination of bacteria on strain level by means of SERS in a microfluidic device *Lab Chip*. 11 1013-1021

Wang S, Liu C, Wang H, Chen G, Cong M, Song W, Jia Q, Xu S, Xu W 2014 A SERS optrode prepared by in situ photo-induced reactions and its application for highly sensitive on-chip detections *ACS Applied Materials & Interfaces*. 6 11706–11713

Wang Y, Yan B, Chen L 2013 SERS Tags: Novel Optical Nanoprobes for Bioanalysis *Chem Rev.* 113 1391-1428

Weinert F, Mast C, Braun D 2011 Optical fluid and biomolecule transport with thermal fields *Phys. Chem. Chem. Phys*. 13 9918-9928

Werner M, Merenda F, Piguet J, Salathe R, Vogel H 2011 Microfluidic array cytometer based on refractive optical tweezers for parallel trapping, imaging and sorting of individual cells *Lab Chip*. 11 2432-2439

West J, Karamata B, Lillis B, Gleeson J, Alderman J, Collins J, Lane W, Mathewson A, Berney H Application of magnetophydrodynamic actuation to continuous flow chemistry *Lab Chip*. 2 224-230

Wilson R, Bowden S, Parnell J, Cooper J 2010 Signal Enhancement of Surface Enhanced Raman Scattering and Surface Enhanced Resonance Raman Scattering Using in Situ Colloidal Synthesis in Microfluidics *Anal Chem*. 82 2119-2123

Whitesides G 2006 The origins and the future of microfluidics *Nature*. 442 368-373

Wlodkowic D, Cooper JM 2010 Microfabricated analytical systems for integrated cancer cytomics *Anal. Bioanal. Chem*. 398(1) 193-209

Wu L, Wang Z, Zong S, Cui Y 2014 Rapid and reproducible analysis of thiocyanate in real human serum and saliva using a droplet SER-microfluidic chip *Biosensors and Bioelectronics*. 62 13-18

Xia T, Chen Z, Chen Y, Jin J, Yu R 2014 Improving the quantitative accuracy of surfaceenhanced Raman spectroscopy by the combination of microfluidics with a multiplicative effects model *Anal Methods*. 6 2363-2370

Xia Y and Whitesides G 1998 Soft Lithography *Annu. Rev. Mat. Sci*. 28 153-184

Xu B, Ma Z, Wang L, Zhang R, Niu L, Yang Z, Zhang Y, Zheng W, Zhao B, Xu Y, Chen Q, Xia H, Sun H 2011 Localized flexible integration of high-efficiency surface enhanced Raman scattering (SERS) monitors into microfluidic channels *Lab Chip*. 11 3347-3351

Xu B, Zhang R, Liu X, Wang H, Zhang Y, Jiang H, Wang L, Ma Z, Ku J, Xiao F, Sun H 2012 On-chip fabrication of silver microflower arrays as a catalytic microreactor for allowing in situ SERS monitoring *Chem Commun*. 48 1680-1682

Yang Z, Matsumoto S, Goto H, Matsumoto M, Maeda R 2001 Ultrasonic micromixer for microfluidic systems *Sensors and Actuators* A. 93 266-272

Yang X, Gu C, Qian F, Li Y, Zhang J 2011 Highly Sensitive Detection of Proteins and Bacteria in Aqueous Solution Using Surface-Enhanced Raman Scattering and Optical Fibers *Anal Chem*. 83 5888-5894

Yang X, Zhang A, Wheeler D, Bond T, Gu C, Li Y 2012 Direct molecule-specific glucose detection by Raman spectroscopy based on photonic crystal fiber *Anal Bioanal Chem*. 402 687-691

Yang H, Deng M, Ga S, Chen S, Kang L, Wang J, Xin W, Zhang T, You Z, An Y, Wang J, Cui D 2014 Capillary-driven surface-enhanced Raman scattering (SERS)-based microfluidic chip for abrin detection *Nanoscale Research Letters*. 9 138

Yasui T, Omoto Y, Osato K, Kaji N, Suzuki N, Naito T, Okamoto Y, Tokeshi M, Shamoto E, Baba Y 2012 Confocal Microscopic Evaluation of Mixing Performance for Three-Dimensional Microfluidic Mixer *Analytical Sciences* 28 57-59

Yazdi S, White M 2013 Multiplexed detection of aquaculture fungicides using a pump-free optofluidic SERS microsystem *Analyst*. 138 100-103

Zhang J, Do J, Premasiri W, Ziegler L, Klapperich C 2010 Rapid point-of-care concentration of bacteria in a disposable microfluidic device using meniscus dragging effect *Lab Chip*. 10 3265-3270

Zhang C, Khoshmanesh K, Tovar-Lopez F, Mitchell A, Wlodarski W, Klantar-zadeh K 2009 Dielectrophoretic separation of carbon nanotubes and polystyrene microparticles *Microfluid. Nanofluid.* 7 633-645

Zhang W, Lin CY, Han LL, Li LQ, Gao P, Lin H, Gong XH, Huang F, Tang YQ, Ma JX, Zhang HY, Wang C, Yang P, Li H, Sun MP, He X, Pang XH 2010 Study on the immuno-effects and influencing factors of Chinese hamster ovary (CHO) cell hepatitis B vaccine among adults, under different dosages *Zhonghua Liu Xing Bing Xue Za Zhi*. 31(7)767-70

Zhang C, Xing D 2010 Single-Molecule DNA Amplification and Analysis Using Microfluidics Chem Rev. 110 4910-4947

Zhou J, Ren K, Zhao Y, Dai W, Wu H 2012 Convenient formation of nanoparticle aggregates on microfluidic chips for highly sensitive SERS detection of biomolecules *Anal Bioanal Chem*. 402 1601-1609

CHAPTER 3. GNERAL METHOD: BACTERIAL RAMAN IDENTIFICATION AND NANOPROBE FABRICATION

3.1. Bacterial s ample preparation for Raman spectroscopic analysis

Different bacterial strains were cultured in petri dishes of 60 mm× 15 mm that have a layer of agar-based Luria Broth medium. After 18 hours 37 ℃ incubation, the desired bacteria colonies were inoculated in liquid Luria Broth medium for liquid culture. After 18 hours incubation at 37℃, bacterial solution was transferred to 15 mL centrifuge tubes and concentrated under 3000 RPM speed for 3 min. After removing the supernatant, the dense pellets of bacteria were obtained for subsequent Raman identification tests. DXR Raman microscope (Thermo Scientific, Waltham, MA, USA) was used for Raman spectra acquisition with 780 nm excitation at 10 mW, 10× objective, and 25 μm slit. The laser exposure time was 60 s and spectral resolution was 2.4–4.4 cm^{-1}. The OMNIC™ suite (Thermo Scientific, Waltham, MA, USA) was used for data processing. The spectra were baseline-corrected and smoothed (11 smooth points). An iterative polynomial background removal algorithm was implemented to remove background fluorescence from the Raman spectral data (Zhang et al., 2010). 15-20 spectra were acquired from each sample, and the average spectrum was calculated.

3.2. High concentration and pure bacterial culture fingerprinting using Raman spectroscopy

Fig. 3.1 shows the average of all preprocessed Raman spectra of *E. coli* O157:H7. Bacterial Raman spectra consist of bands representing the chemical makeup of the cell,

primarily proteins, lipids, carbohydrates and nucleic acids. Peak assignment is shown in Fig. 3.2.

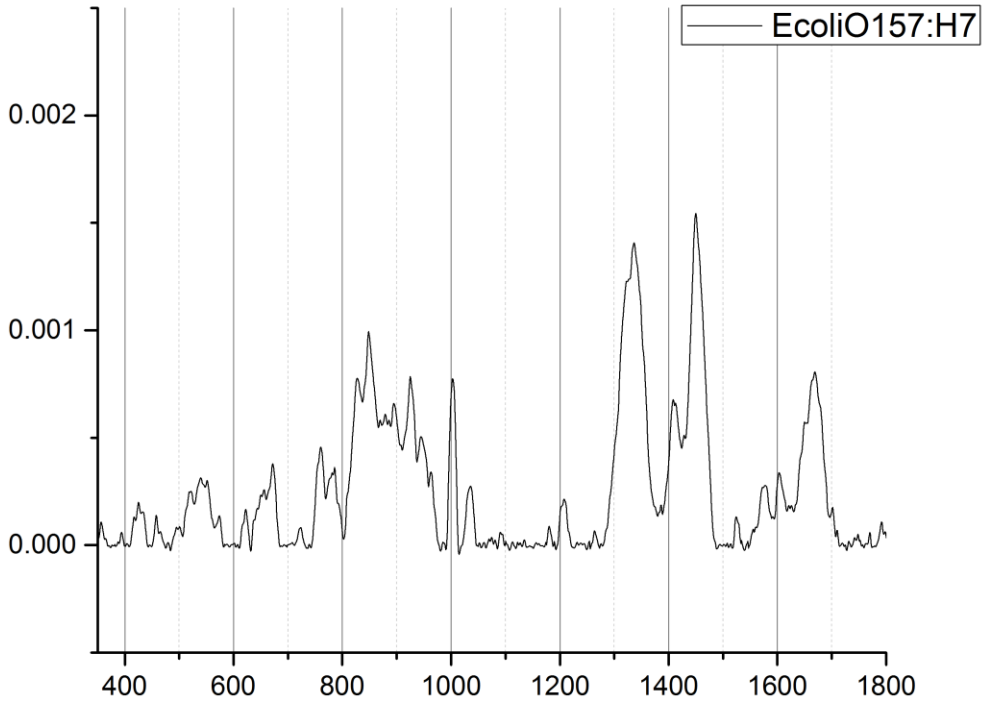

Fig. 3.1 The average Raman spectrum of *E.Coli* O157:H7 strain studied in this work.

Proteins are polymers of amino acids that are linked by peptide bounds. The precise position of bands in Raman spectrum depend on inter and intra molecular effects, including peptide-bond angles and hydrogen-bonding patterns (De Gelder. 2008). Amide, disulphide bridges, and aromatic amino acids are essential spectral features in Raman proteins spectra. Amide I bands, located in 1650 cm^{-1}, are assigned to C=O stretching; bands near 1550 cm^{-1} are assigned to N-H and C-N stretching, representing Amide II; and the peak at 1300 cm^{-1} can be arranged to C-N stretching and N-H bending. The S-S Raman bands are located in the spectral range of 500-550 cm^{-1}. The common aromatic residues existed in living cells are phenylalanine (Phe), tyrosine (Tyr), and

tryptophan (Trp). Theirs band positions may vary up to 5 cm^{-1} in the Raman spectra of proteins.

Lipids represent the main structure of the cell membrane, lipopolysaccharide and the storage depot of carbon inside the cell. Lipids include simple lipids, such as triglycerides, which consist of three fatty acids and glycerol; and complex lipids, such as phospholiqids, which consist of triglycerides and other elements like nitrogen or phosphorous. In Raman spectra analysis, the main bands are: 1200-1300 cm^{-1} assigned to CH_2 stretching and twisting vibration; 1050-1160 cm^{-1} assigned to C-C stretching vibration; 1400-1500 cm^{-1} assigned to CH_2 or CH_3 bending; and 1650 cm^{-1} stretching vibration (Bendinger et al., 1992; Lin-Vien et al., 1991).

Carbohydrates are important components in the cell capsule structure, which means they can be used for bacterial identification, too. The bands located at 400-700 cm^{-1} is assigned to endocyclic and exocyclic deformations (Brade et al., 1988). The bands located in 800-950 cm^{-1} are assigned to COC and CC deformation vibration. Those located in the region 1000-1200 cm^{-1} are assigned to C-O stretching vibrations.

Nucleic acids are polymers of nucleotides, where the nucleotides are composed of a base attached to a sugar by a glycosidic linkage and phosphate. The special sequence of the nucleotides in the nucleic acids represents the genetic information of the cell. The bands around 600-800 cm^{-1} are critical and strong which represented adenine, guanine, cytosine, and thymine. The bands located 1485 and 1576 cm^{-1} could be assigned to

adenine and ring stretching, respectively.

(a)

amide 1	
a-helix	1650-1657
antiparallel B sheet	1612-1640
parallel B sheet	1626-1640
turn	1655-1675
	1680-1696
unordered	1640-1651
amide 2	1550
ammide 3	
a-helix	1270-1300
random coli	1243-1253
B sheet	1229-1235

(b)

aromatic aminoacid	
Phe	620
Tyr	640
Trp	750
Tyr	830,850
	1000,
Phe	1030
Trp	1011
	1170-
Tyr,Phe	1200
	1340-
Trp	1360

(c)

S-S bonding stretching	
In lysozyme	577
	545
	528
	509
	489
	466

(d)

DNA	
Guanine	678
Adenine	729
Thymin, Cytosine	785
backbone (PO-2 stretching)	1098
Adenine	1336
A,T,C	1485
A (ring stretch, N6H2 deformation)	1576

(e)

Lipids*	
C4N+ and O-C-C-N synnetric stretch	865
Alkyl CC trans and gauche stretches	1056, 1116
Alkyl CC gauche stretch	1075
Alkyl=C-H cis stretch	1260
Alkyl C-H2 twist	1300
Alkyl C-H2 bend	1440
Alkyl C=C stretch	1650
Ester C=O stretches	1736
Alkyl=C-H stretches	3023

(f)

Carbohydrate*	
C-C-C deformation	479
H-C-O stretches and chlorophyll a N-C-C deformation	744
Hemiacetal stretches and methylene deformation	854
a-helix C-C backbone stretch, COC stretch	945
Carbohydrate C-O-H bending	1082
COH deformation, CO and CC stretch	1120
carotene CH stretch	1160
CH2 deformation and COH bending, chlorophyll a C-N stretch	1340
C=C stretch	1537

*Lipids and carbohydrate are tested in algal cell

Fig. 3.2 Raman peaks assignments of different bacteria cell contents from reference. (a) amide, (b) amino acid, (c) S-S content, (d) nucleic acids (Barhoumi et al., 2008), (e) lipids, (f) carbohydrates.

The featured Raman peaks of *E.coli* O157:H7 could be only obtained by using high concentration and pure bacterial sample. In addition, long laser exposure time and

strong laser powder are needed for spectral collection. However, the concentration of target pathogen is extremely low in real water samples. One of merits in our multiplex self-referencing SERS detection strategy is to rapidly obtain the target pathogen fingerprinting Raman peaks at very low concentration water solution (10 CFU/mL). In our lab-scale testing results, not all the featured Raman peaks of target pathogen (*E.coli* O157:H7) are shown, which is mainly due to the variation of nanoprobe conjugation location and density on the surface of the bacterial cells. Furthermore, some of the strong Raman signals from nanoprobe overlap with the relatively weaker bacterial fingerprinting signals, which also prevents the observation of all featured peaks come from target bacteria. However, the part of measurable bacterial signals is still able to validate the existence of the specific pathogen in prepared samples. Table 3.1 exhibits the featured peaks of *E.coli* O157:H7 observed in our multiplex self-referencing SERS detection testing (the details could be found in Chapter 5).

Table. 3.1 Band assignment of E.coli O157:H7 featured peaks shown in multiple self-referencing SERS measurement

Wavenumber (cm^{-1})	Band assignment
1660	Amide 1 vibration
1603	Phenylalanine in protein
1578	Adenine ring stretching
1336	$\gamma(NH_2)$ adenine, polyadenine, Phenylalanine in protein
1035	Phenylalanine in protein
1002	Phenylalanine in protein
925	CN stretching

830/850	Tyrosine
761	Aromatic aminoacids/Tryptophan
731	adenine, glycosidic ring mode, DNA
539	S-S bond stretching

3.3. Gold nanoparticles fabrication

Gold nanorods (GNRs) have generated a lot of interests in research community in the last decade, due to their unique property of interacting strongly with light at the plasmon frequency (light absorption, scattering and an enhanced localized electromagnetic field at the particles surface). GNRs have two distinct plasmon resonance absorption bands, a longitudinal band and a transverse band, that are related to electron motion along the longitudinal and transverse directions, respectively. Compared to gold nanospheres, GNRs give better field enhancement at the tips/edges due to the appearance of a surface plasmon band at lower energies because of a much weaker plasmon damping than that in spherical particles, which could specifically improve the performance in the application of surface-enhanced Raman scattering (SERS) technique (Ding et al. 2007). In addition, the singularity at the sharp locations is also the reason of local electromagnetic enhancement due to the quasi-static lightning-rod effect. Because Maxwell's equations are second-order differential equations, the fields can become singular when the first or second derivative is not defined. However, real metals have finite conductivity, and the radius of curvature at the tip is finite. Consequently, there is no real field singularity, but the field at the tip can be strongly enhanced (Neacsu et al., 2005). However, controlling the size and the aspect ratio (length/width) of each rod is not easy. GNRs can be synthesized through

seed-mediated growth with aspect ratios ranging from 1.5-4.5 by using hexadecyltrimethylammonium bromide (CTAB)-capped seeds. (Nikoobakht and El-Sayed, 2003). After some modification to the synthesis process, we obtained GNRs with a stable aspect ratio of 3.6 (with longitudinal wavelength at ~780 nm).

The synthesis of Au nanocages was based on the galvanic replacement between silver nanocubes (acted as sacrificial templates) and $HAuCl_4$ solution. The different electrochemical potential between Ag+/Ag (0.80 V) and AuCl4-/Au (1.00 V) contributed to the success of the replacement reaction (Xia et al. 2011):

$$3Ag(s) + AuCl_4^-(aq) \rightarrow Au(s) + 3Ag^+(aq) + 4Cl^-(aq)$$

Specifically, the added Au can grow on and adopt the morphology of the Ag cubes. After oxidizing the interior Ag, a hollow structure is generated. As more $HAuCl_4$ solution is added, a nanobox structure with a uniform smooth and homogeneous wall composed of Au/Ag alloy is formed. Continuous addition of Au solution led to dealloying and corner reconstruction of nanobox to generate porous Au nanocage. Along with these series reactions, the solution color changes and surface plasmon resonance peak red-shifts. The details are described below.

3.3.1. Gold nanorod-based probe synthesis

Materials and methods

Reagent

Hexadecyltrimethylammoniumbromide (CTAB), ≥99%; Gold(III) chloride trihydrate ($HAuCl_4.3H_2O$), 99.9+%; Sodium borohydride ($NaBH_4$), ≥99%; Silver nitrate ($AgNO_3$) more than 99%; L-Ascorbic acid (AA), ≥99.0%; 4-Aminothiophenol

(4-ATP), 97%; Phosphate-buffered saline (PBS), 10× concentrate. All reagents are purchased from Sigma-Aldrich. 18.2 MΩ.cm E-pure water is used for all regents' preparation.

Equipment

New Brunswich Scientific Excella E24 Incubator; Disposable scintillation vials with paper-lined plastic caps (VWR); Poly(propylene) micro-centrifuge tubes, capacity 1.7 ml (Costar); Hot plate (Corning, PC-4200).

GNR Seed solution

Hexadecyltrimethyl ammonium bromide (99%) (CTAB) solution (7.5 mL, 0.1 M) was mixed with 0.25 mL of 0.01 M $HAuCl_4$. 0.60 mL of ice-cold 0.01 M $NaBH_4$ was added into the mixed solution. 2 min vigorous stirring was needed for the seed solution. After the color became brownish yellow, the seed solution was successfully synthesized. The seed solution should be used for GNRs synthesis within 3 hours.

Synthesis of GNRs

95 mL 0.1 M CTAB was added to 0.6 mL 0.01 M $AgNO_3$ and 4 mL 0.01 M $HAuCl_4$. Then, 0.64 mL 0.1 M L-Ascorbic acid was added into the system. After mixing, the color of the solution changed to colorless. Then, 0.72 mL seed solution was added into the solution and then the GNRs growth solution was incubated at 27℃ for 2 hrs. Then, GNRs solution was washed by centrifugation (6000×g for 20 min). After removing the supernatant, the washed product was transferred into a scintillation vial and diluted to 3 mL with pure water (O.D. =44 A.U., assumed concentration: 5.809×10^{13} unit/mL, 0.0134 M Au, based on the rod size from TEM image and mass calculation).

Functionalization GNRs with 4-ATP and ATT

Chemical surface modification method was developed to functionalize GNRs via ligand exchange followed by conjugation of target specific antibodies via covalent bonding, forming the nanoprobes for pathogen SERS detection. Two highly effective Raman tag molecules (4-ATP and 3ATT) are identified in my work because of the distinguishable Raman spectral signatures. Furthermore, I optimize the conjugation protocols to link antibody molecules to the two linkers through diazo-histine binding, which is more effective and efficient than the EDC-NHS conjugation pathway.

3 mL of 10 mM 4-ATP and ATT (pH=2) was added into 24 mL GNR-CTAB with LSPR OD (optical density) =6. The mixture solution was kept in disposable scintillation vials at 60℃ oil bath with 180 rpm stirring speed for around 19 hrs. Then, functionlized GNRs solution was washed twice by centrifugation (6000×g for 10 min) with 20mM CTAB and pH=4 pure water. Finally suspend the products in 0.25 mL water (O.D.=74 A.U., the assumed concentration: 7.696×10^{14} units/mL, 0.178 M Au).

Conjugating antibodies to functionalized GNRs

Gold nanoparticles show large extinction cross section (estimated to be 10^{-10}~10^{-11} cm^2), which is specifically dependent on the particles' shape and size. The relationship between the intensity of the SPR peak and the concentration follows the Beer-Lambert law, knowing the extinction cross section. Roughly, when the GNR O.D. equals to 1 A.U., the concentration of the particles could be estimated as 0.1 nM, namely 6×10^{10} units/mL. For antibody conjugation, 0.75 μg anti-E.coli O157:H7 mouse monoclonal antibodies (P3C6, ab75244 from Abcam) were incubated with 500 μL GNR-4ATP

(O.D.=11.2, ≈1.12 nM); 0.75 μg another anti-E.coli O157:H7 mouse monoclonal antibodies (3011, ab20976 from Abcam) were incubated with 500 μL GNR-ATT (O.D.=48, ≈4.8 nM).

3.3.2. Gold nanocages-based probe synthesis

Materials and methods

Reagent

Gold(III) chloride trihydrate ($HAuCl_4.3H_2O$), 99.9+%; Silver nitrate ($AgNO_3$) more than 99%; Ethylene glycol (99%), sodium sulfide (Na_2S, 99%); Polyvinylpyrrolidone (PVP, 99%); silver nitrate (>99%); 3-Mercaptopropionic acid (≥99%); Phosphate-buffered saline (PBS), 10× concentrate. All reagents are purchased from Sigma-Aldrich. 18.2 MΩ.cm E-pure water is used for all regents' preparation.

Equipment

New Brunswich Scientific Excella E24 Incubator; Disposable scintillation vials with paper-lined plastic caps (VWR); Poly(propylene) micro-centrifuge tubes, capacity 1.7 ml (Costar); Hot plate (Corning, PC-4200); Ultrasonic cleaning bath.

Synthesis of Gold Nanocube

The synthesis of Au nanocages was based on the galvanic replacement between silver nanocubes (acted as sacrificial templates) and HAuCl4 solution. Heating oil bath to 160 C and set the spin rate of the stir bar to 200 rpm. Pipette 6 ml of ethylene glycol (EG) into a 20 mL reaction vial and add a clean stir bar. Place a cap loosely on the top of the vial to allow water vapor to escape. Put the vial into the hot oil bath for 1 hr. Remove the vial cap and pipette 70 or 80 ul 3mM Na_2S solution in EG into the vial and

put the cap back. Wait for 8 min, pipette 1.5 mL of 0.02 g/mL PVP in EG and 0.5 mL of 0.048 g/mL $AgNO_3$ in EG into the vial. After 15-18 min, the solution changed color from transparent to dark ruddy-red and green-ochre. Cool down the vial in ice-cold water. Then wash them with one time acetone and 2 times DI water. The re-dispersed solution is eventually stored in 1 mL DI water. Edge length of 90 nm Nanocubes (480 nm) can be synthesized by polyol processing.

Gold nanocage synthesis

Prepare a minimum of 10 mL of 9 mM PVP (MW= 55,000) in DI water. The concentration is calculated in terms of the repeating unit (1 mg PVP/1 ml water). 5 mL of this solution is required per titration. Pipette 5 mL of the 9 mM PVP solution into a 50-mL flask to which a clean stir bar has been added. Then pipette 100 mL of the as-stored Ag nanocubes into the PVP solution. Cover the flask with a rubber septum. Heat the suspension to a mild boil for approximately 10 min. Remove the rubber septum from the flask. Add the 10 mM $HAuCl_4$ solution to the reaction flask drop by drop (7.5μL per minute). As the $HAuCl_4$ solution is added to the reaction flask, a series of color changes will be observed and can be used to estimate the position of the SPR peak for the Au nanocages. Stop adding $HAuCl_4$ solution when the appropriate color is observed. Allow the reaction to reflux for an additional 10 min until its color becomes stable and then cool the system to room temperature. Vigorous magnetic stirring should be maintained during the entire process. Transfer the reaction(s) to a 50-mL centrifuge tube. Rinse the reaction flask with deionized water and add the washings to the centrifuge tube. During the galvanic replacement reaction, AgCl is generated, which

upon cooling of the reaction media precipitates out of the solution. This AgCl can be dissolved and removed with a saturated solution of NaCl. To do this, add NaCl crystals to the aqueous dispersion until saturation is reached. Centrifuge the mixture at 2,000g for a minimum of 30 min. A pellet of Au nanocages should be obtained on top of the precipitated NaCl and a blue tinge will color the wall of the centrifuge tube. Using a pipette, remove and discard the supernatant containing the dissolved AgCl.

Functionalization of Cage with 3-MPA

The 3-MPA-gold nanocages were prepared by ligand-exchange reaction between 3-MPA and the citrate-stabilized gold nanocages. The cages solution were diluted to 100 mL with O.D.=1.0. Ligand-exchange reaction was performed at room temperature by mixing the prepared cage solution with a 100 μL of aqueous solution of 20 mM 3-MPA under shaking treatment. The mixed solution was treated overnight under the room temperature.

Linking antibodies to Cages-3MPA matrix

After centrifuging the functionalized nanocages at 6000G for 10 min, supernatant were removed. The pellet was washed with DI water for 1 time. For antibody conjugation, 0.75 μg anti-E.coli O157:H7 rabbit polyclonal antibodies (HRP ab68450 from Abcam) were incubated with 500 μL Cage-3MPA (O.D.=10).

3.4. Methodology development for nanoprobe characterization

3.4.1. Surface plasmon band measurement

In GNRs-4ATP complex, extinction spectra (Fig.3.3) show around 60 nm blue shift of the longitudinal peak of the 4-ATP-GNRs as compared to GNRs; and then show 30

nm red-shift after conjugating multi-histidine proteins (ODx3) on 4-ATP-GNRs with no peak broadening. The observed spectral shifts can be attributed to changes in the refractive index of the local environment surrounding the GNRs, and also can be used as a simple and quick way to monitor the functionalization/conjugation events.

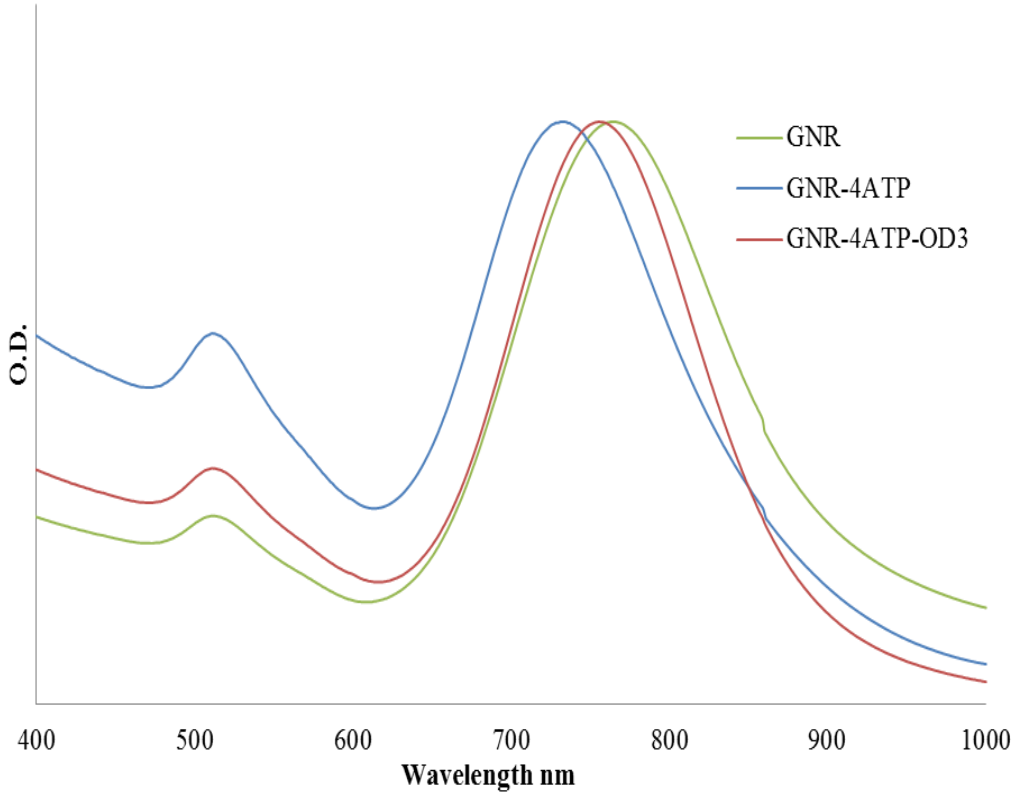

Fig. 3.3 Extinction spectra of GNR, GNR-4ATP, and GNR-4ATP-protien

The spectral characterization also provides an important and simple way to monitor possible aggregation of plasmonic nanoparticles during a conjugation process. Nanorod aggregation includes three major features: significant broadening, strong red shift of the longitudinal peak, and increase in transverse to longitudinal (T-to-L) peak ratio. The final nanoprobes (i.e., after antibody conjugation) show mean value of T-to-L peak ratio change of less than 40% (Table 3.2). In addition, the full-width at half maximum of the longitudinal peak does not increase with the 4-ATP functionalization or antibody

conjugation, as shown in Figure 3.4 and Table 3. These spectroscopic data confirm that nanorods started to aggregate when the antibodies amount is increased to 7.5µg.

Table 3.2 Spectral Characteristics of Gold Nanorods and Gold Nanorod Conjugates

	FW at HM (nm)	% increase in transverse to longitudinal peak ratio
CTAB-GNR	129	-
4-ATP-GNR	132	32
5µg Ab-4-ATP-GNR	170	36
7.5µg Ab-4-ATP-GNR	264	66
10µg Ab-4-ATP-GNR	307	63

The change in surface plasmon resonance of gold NPs, before and after conjugating of linkers and proteins, was monitored by UV/Vis spectroscopy measurement. Equipment: UV/Vis spectrometer (PerkinElmer Life and Analytical Sciences. Shelton, CT, USA).

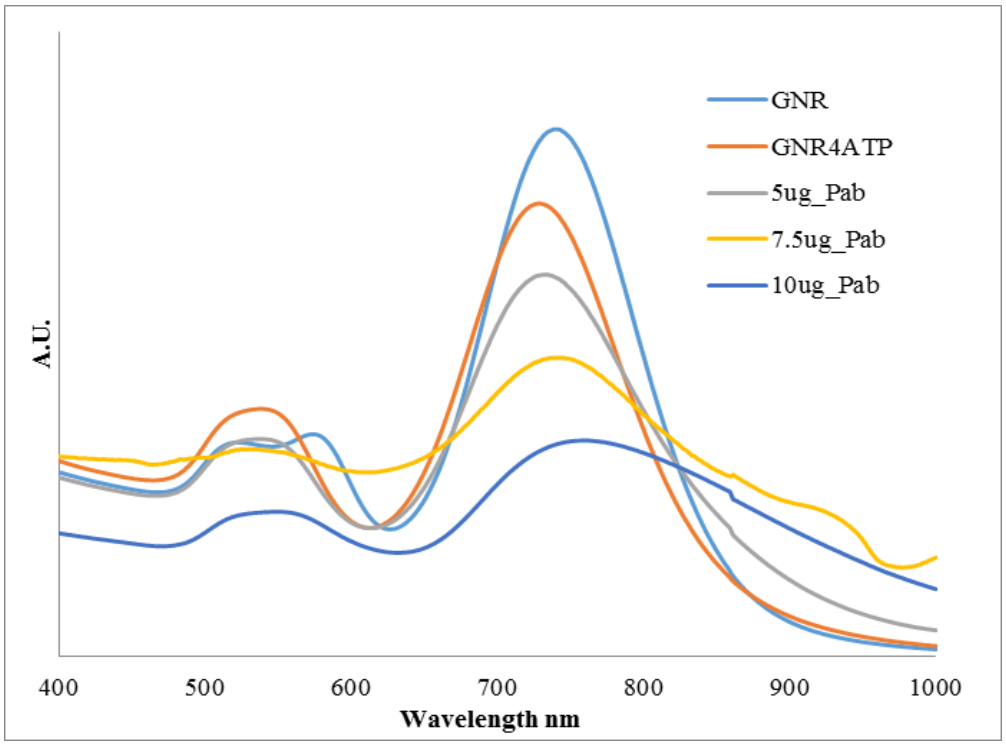

Fig. 3.4 Extinction spectra of GNR-4ATP conjugated with different amount of polyclonal antibody

3.4.2. Zeta potential and particle size measurement

Fabricated gold GNRs have high positive surface charge due to the presence of cationic surfactant. After functionalization with 4-ATP, the surface potential decreases from 45 mV to approximately 13 mV (Fig.3.5). Then, conjugation of tested proteins with functionalized GNR results in decrease in zeta potential to -9 mV. This observed negative zeta potential provides another evidence for successful antibody conjugation. Furthermore, the particles sizes measurement (Fig.3.6) results demonstrated 3 or 4 GNR particles were connected together due to the dimerization between two 4-ATP molecules from different GNR particle surface. Covalent attachment of functional linkers can provide a steric barrier against aggregation and improve the colloidal stability at increased ionic strength. As a result, we can conclude that the GNR-4ATP

fabrication process prevents huge aggregation and colloidal instability from the Dynamic Light Scattering results.

The particle size and zeta potential analysis was carried out using Malvern Nano ZS Zetasizer, equipped with a HeNe laser operating at 633 nm (Malvern Instruments Ltd, Worcestershire, UK). Analysis (n=11) was carried out at room temperature by keeping angle of detection at 173°. Particle size and zeta potential of the samples were measured as original concentration without dilution.

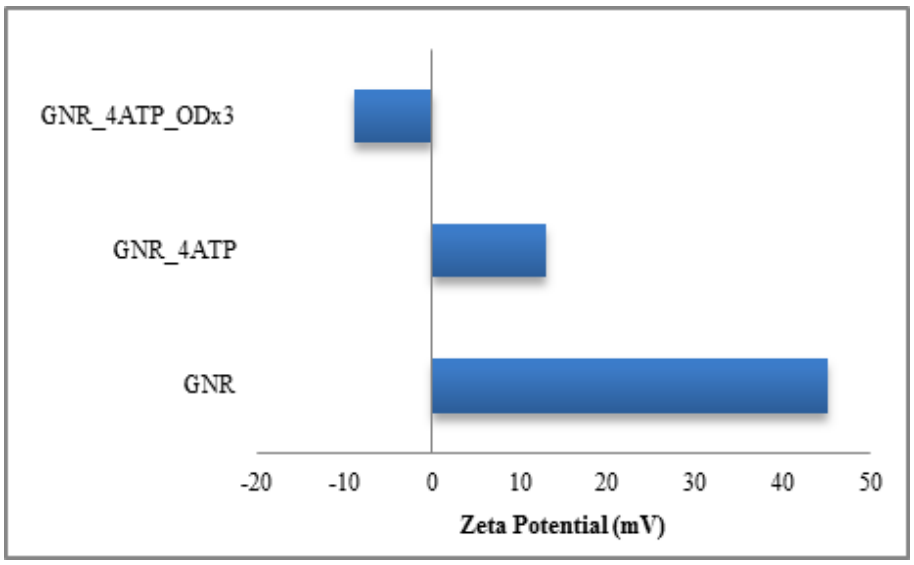

Fig. 3.5 Zeta potential measurement results of GNR, GNR-4ATP, and GNR-4ATP-protein

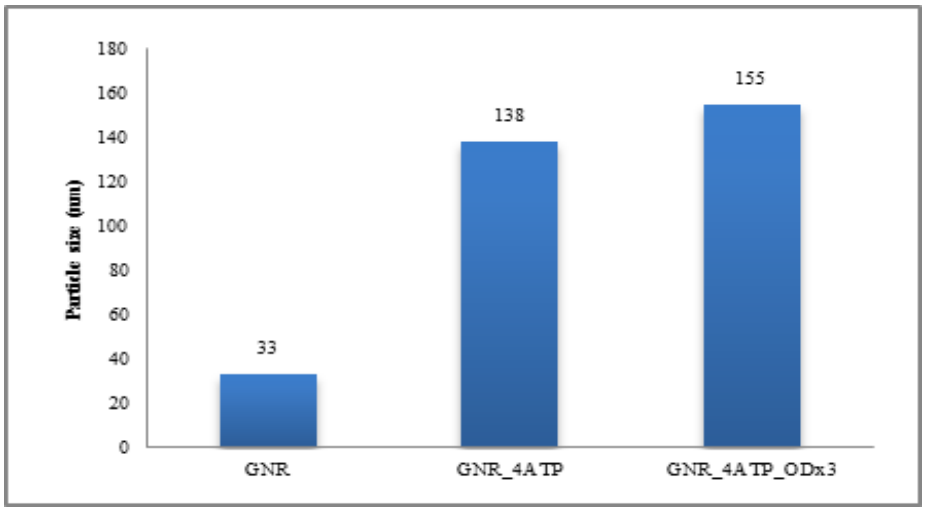

Fig. 3.6 Particle size measurement results of GNR, GNR-4ATP, and GNR-4ATP-protein

3.4.3. SERS measurement

4-ATP, as a strong Raman tag molecule, shows certain amount of Raman featured peaks in SERS measurement. Featured peaks include C-C and C-S vibrational a_1 and b_2 modes (in-plane, in-phase modes) located at 1590, 1078, 1435 and 1143 cm^{-1}.

The SERS spectra of GNR-4ATP conjugated with vaccine in Fig. 3.7, shows further enhancement at diazo bonds (1390/1432 cm^{-1}) which is contributed from the covalently bonding events between his-tags in antibody protein and the free diazonium moieties on the GNR surface.

DXR Raman microscope (Thermo Scientific, Waltham, MA, USA) was used for Raman spectra acquisition with 780 nm excitation at 10 mW, 10× objective, and 50 μm slit. The laser exposure time was 5 s and spectral resolution was 2.5–4.6 cm^{-1}. The OMNIC™ suite (Thermo Scientific, Waltham, MA, USA) was used for data processing. The spectra were baseline-corrected and smoothed. An iterative polynomial background removal algorithm was implemented to remove background fluorescence from the Raman spectral data. Ten spectra were acquired from each sample, and the average spectrum was calculated.

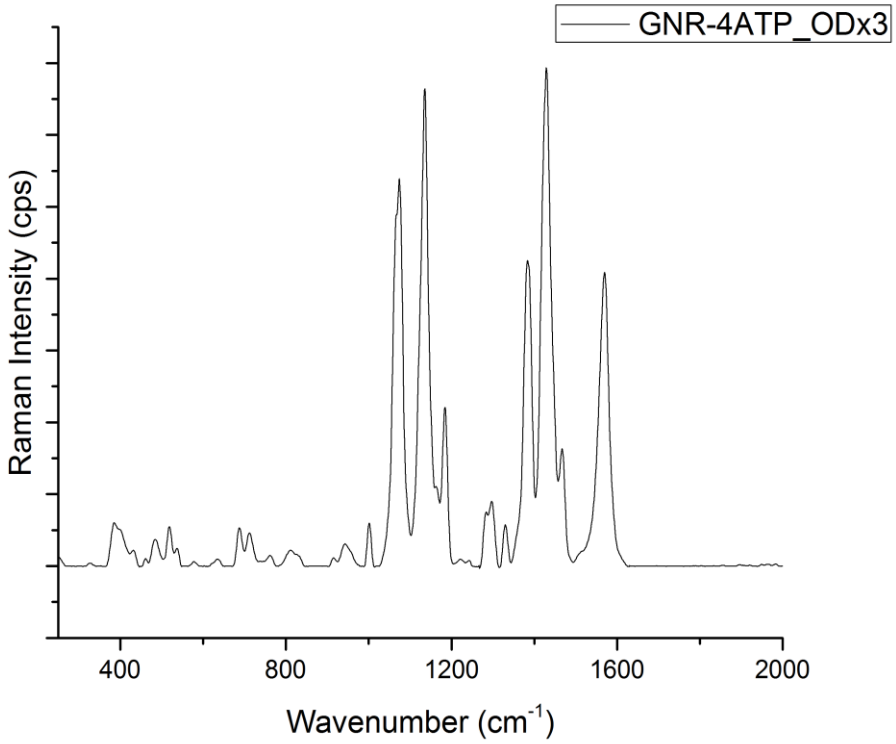

Fig.3.7 SERS spectra of GNR-4ATP conjugated with protein

3.4.4. Numerical simulation of the electromagnetic field around the nanoprobes

Nobel nanoscale metal particles possess unique optical characteristics because of their surface plasmon resonance, which is the collective coherent oscillation of the conduction band electrons on the nanoparticle surface in resonance with an electromagnetic wave from any external laser source. The plasmon resonance results in a significant enhancement of the electromagnetic field around the nanostructures at the plasmon resonance frequency. The enhancement from plasmon resonance from metallic nanoparticle is the core of surface enhanced Raman scattering theory. Nevertheless, there exists various parameters, such as shape, size and polarization of the incident light, would define the enhancement efficiency. In addition, complex instrumentation is needed for the measurement of scattering cross section to calculate

the relative enhancement factor. Therefore, in order to estimate the enhancement factors to theoretically predict the optical properties of fabricated nanaoparticles in our study and indicate the experiments' performance, it is critical to develop the electromagnetic fields simulation models in SERS technique applications.

After Mie's work (Barber and Hill. 1990; Mishchenko et al., 2002), analytical solutions to Maxwell's equations were found for a sphere in an absorbing medium or for nanoparticles presenting a simple shape, such as spheroids or infinite cylinders. However, when more complex shapes as well as surface conjugation events on certain spots of nanostructures are involved, for example, nanorod mainly used in our study, advanced numerical approaches are required. Some methods, such as T-matrix or multiple multipole methods have been available to describe the fields inside and outside of the nanoparticle at a given wavelength. Volume discretization is the starting point of the discrete dipole approximation (DDA), the finite difference time domain (FDTD), and the finite element method (FEM). In DDA, a nanoparticle is described as a spherical or cubic array of coupled point dipoles whose polarizability is linked to the wavelength dependent dielectric function of the metal. In FDTD, a time dependent electromagnetic field is descripted rather than wavelength dependent. FDTD is a direct method to solve Maxwell's curl equations in differential form, which is one of the simplest methods to implement. Similar to DDA, the FDTE method employs "staircase" meshing grid. Compared with these two methods, FEM is considered to bring out a more accurate electromagnetic fields simulation of complicated shape particles because FEM utilizes adaptive meshes rather than cubic grids subsequently improving near-field accuracy as

well as significantly decreasing computation time. It is a numerical technique that finds an approximate solution of the partial differential equations by discretization of the computational domain into smaller finite triangular elements to produce a system of ordinary differential equations. In FEM, the nanoparticle and its surroundings are divided into elements in which the fields are written as a linear combination of base functions. Boundary conditions between neighbor elements lead to a system of equations that has to be solved for determining the weighting coefficients. Furthermore, FEM can use unstructured meshes therefore produces higher resolution for arbitrary shaped objects (Asano and Yamamoto. 1975; Ghosh and Pal. 2007; Mischenko et al., 1999; Draine and Flatau. 1994; Grosges et al., 2005; Yee. 1996). Figure 3.8 shows the meshing grids for these three simulation methods.

In our study, FEM electromagnetic computations were performed using a commercial software package (COMSOL Multiphysics 4.4). It is worth noting that the position of SPR peak of nanoparticles depends on the dielectric constant of environment, thus, various solvent may result in variation for the SPR peak position. In our study, the nanoparticles were fabricated with different wet-chemistry based methods in which the main solvent could be considered as water. The dielectric constants of gold (see figure 3.9) were cited from the literature (Johnson and Christy. 1972). The computational domain consists of a 3D scatterer embedded within a dielectric media (water, n=1.33) surrounded by a swept perfectly matched layer (PML) and a rectangular scattering boundary condition. All meshes consist of tetrahedral elements with varying degree of

spacing depending on geometric considerations. Adjustments to mesh density were applied until convergent solutions were obtained.

In Figure 3.10 and 3.11, we compute the electromagnetic enhancement of two shapes using ideal geometries to validate the experimental results we obtained for these two specific dimensions nanoparticles. We simulated the extinction cross section, absorption cross section, and scattering cross section for one rod model (diameter 30 nm, length 90 nm) and one sphere model (50 diameter). As we discussed earlier, rod-shaped particles have two SPRs (transverse and longitudinal). Compared with spherical particles, the additional longitudinal SPR peak shows higher sensitivity in SERS applications. Hence, in order to investigate the scattering efficiency of the longitudinal SPR, it is critical to set the polarization of incident light is parallel to the axial direction of the nanorod in simulation. The corresponding plasmon resonance wavelengths for the rod (longitudinal SPR) and the 50 nm sphere were generally consistent to those in the UV/Vis/NIR extinction measurement results in figure 3.12 and figure 3.13. It is worth noting that the gold nanorods have much larger absorption and scattering cross-sections than the gold nanospheres. Such high absorption and scattering cross sections should make gold nanorods better candidate than nanosphere for photothermal therapy and SERS applications in our study.

Theoretically, the extinction cross section is equal to the total of the absorption cross section and the scattering cross section. The scattering cross-section is usually weak compared with the abs cross section. Nevertheless, the characteristics of the scattering cross section are mainly due to the size of the particle. Therefore, different sizes of

nanospheres modes were established to briefly investigate the relationship between the particle size and the scattering cross-section intensities. For nanosphere of different sizes, their SPR peaks are basically falling into the range of 520-540 nm with slight peak shifts and broadening. The broadening can be attributed to enhanced radiation damping for large particles. As shown in figure 3.14 the scattering cross-sections of a smaller size gold sphere is smaller than that in the 50 nm sphere model.

Since these models reply on modal or spatial discretization, they do not yield the exact values of the electromagnetic field or absorption and scattering cross section. The error relative to exact calculations is tightly linked to the way the discretization is performed.

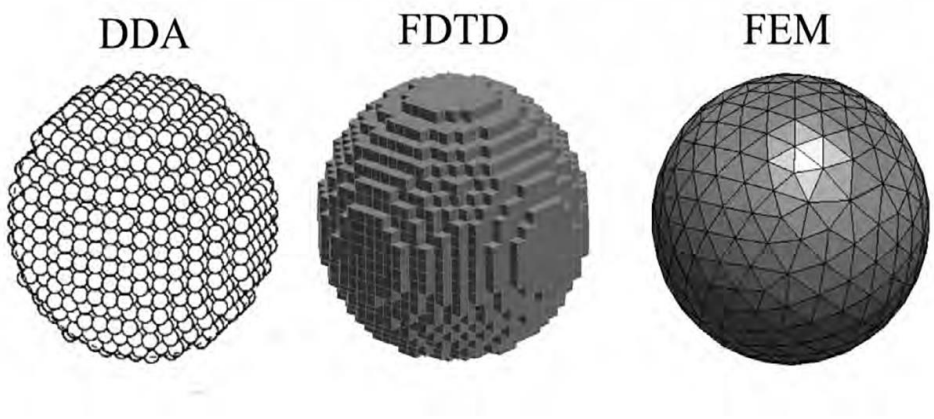

Fig. 3.8 Examples of mesh generation with DDA, FDTD and FEM methods

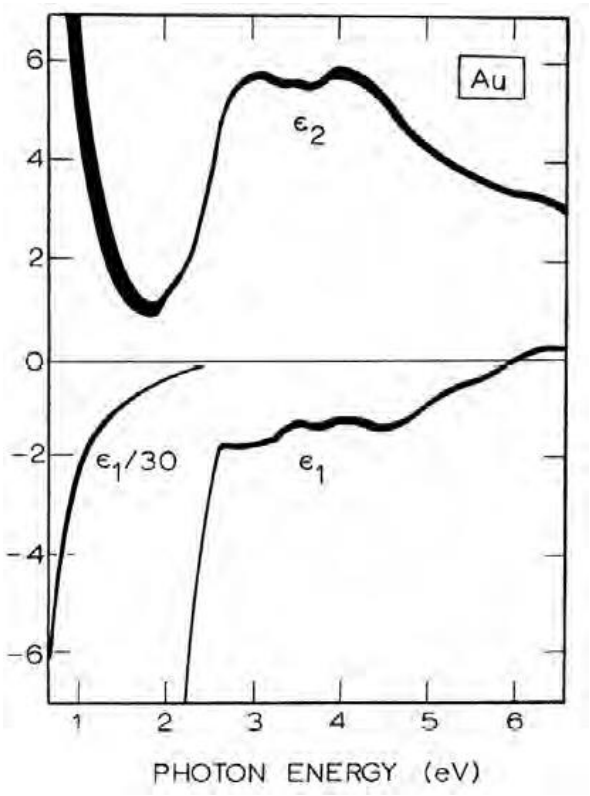

Fig. 3.9 Dielectric constants for gold as a function of photon energy. The width of the curves is representative of the instrumental error (Johnson and Christy. 1972)

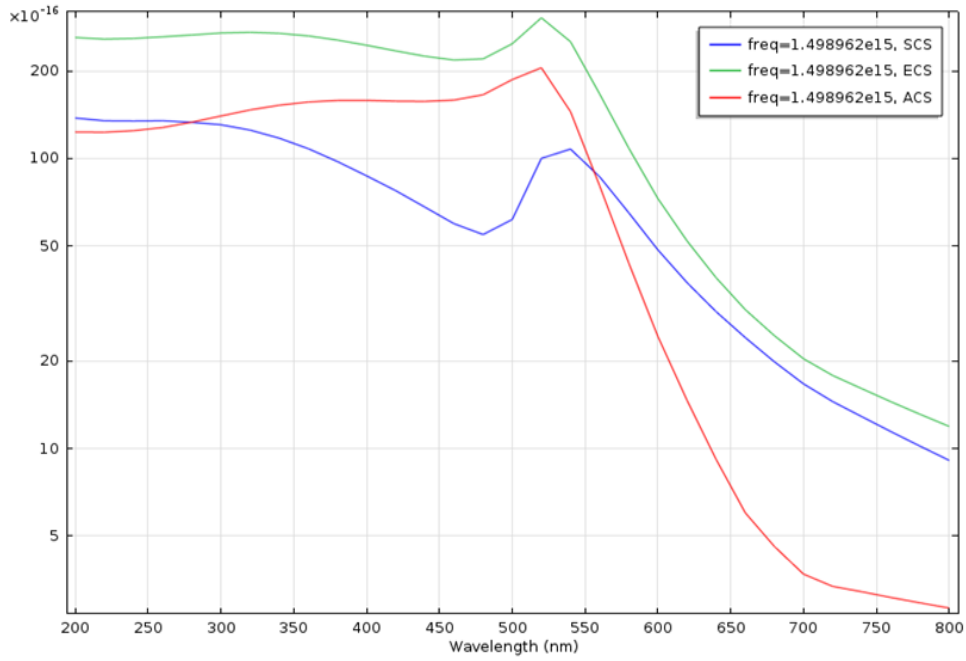

Fig. 3.10 Numerical cross-section simulation of a single gold sphere with 50 nm diameter using FEM model. ACS: absorption cross section (m^2); SCS: scattering cross section (m^2); ECS=ACS+SCS, extinction cross section (m^2)

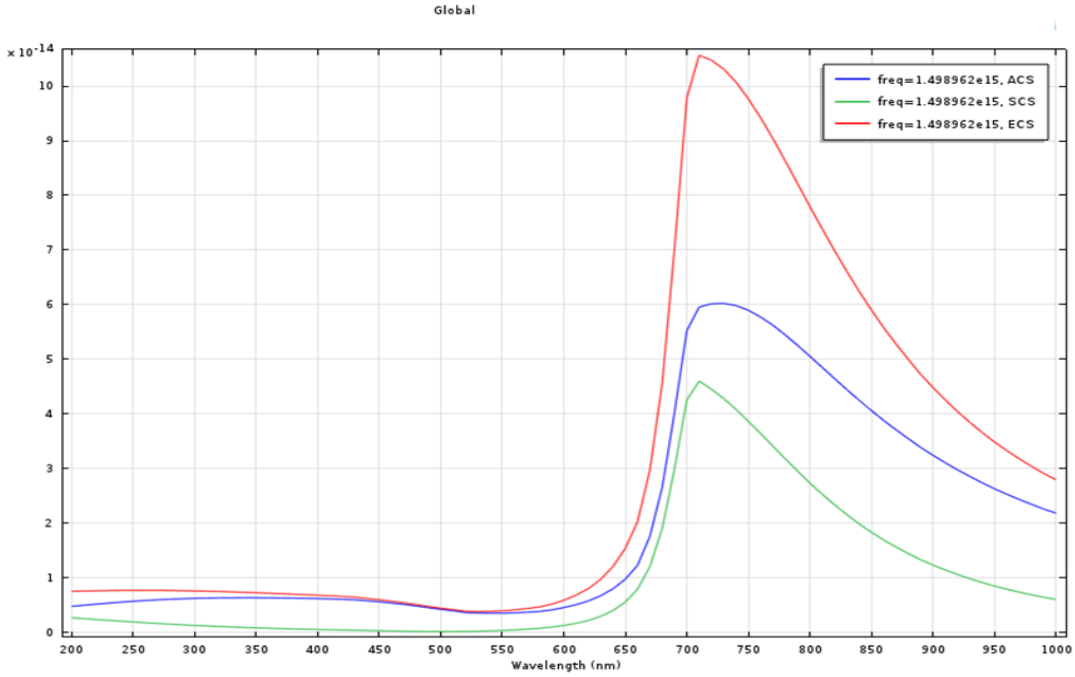

Fig. 3.11 Numerical cross-section simulation of a single gold rod (30 nm diameter, 90 nm length) using FEM model. ACS: absorption cross section (m^2); SCS: scattering cross section (m^2); ECS=ACS+SCS, extinction cross section (m^2)

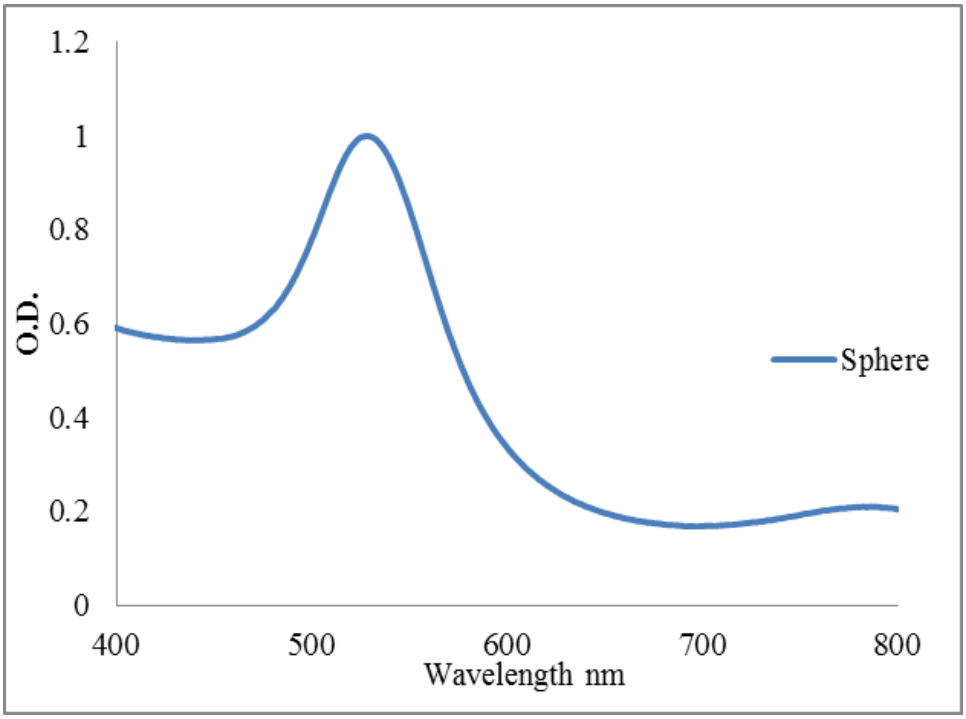

Fig. 3.12 Experimental extinction spectra of a colloid solution of gold sphere

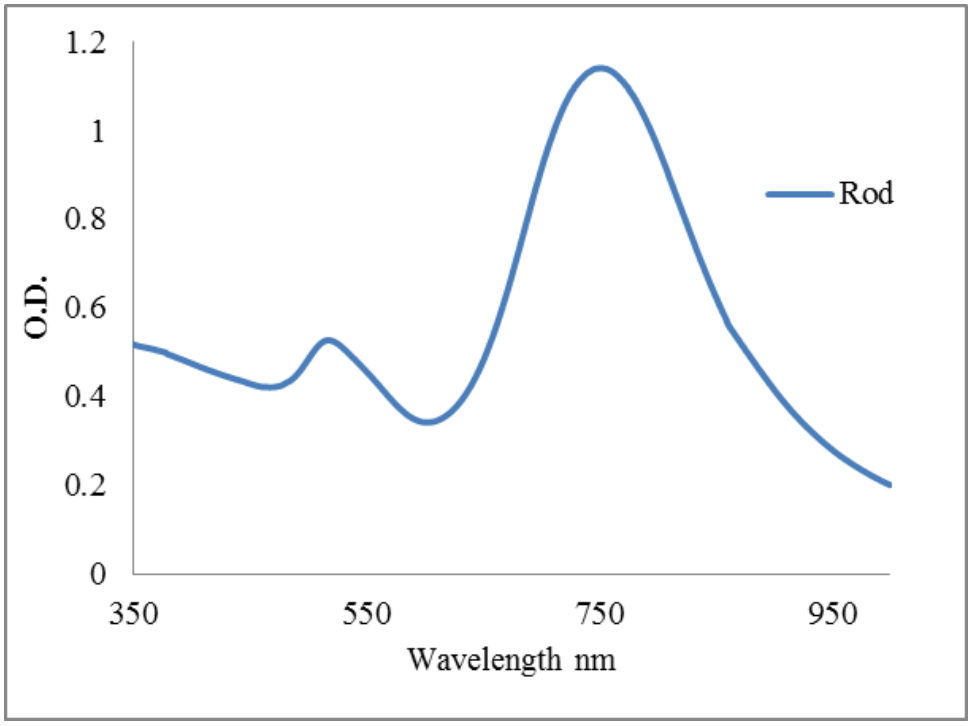

Fig. 3.13 Experimental extinction spectra of a colloid solution of gold gold rod

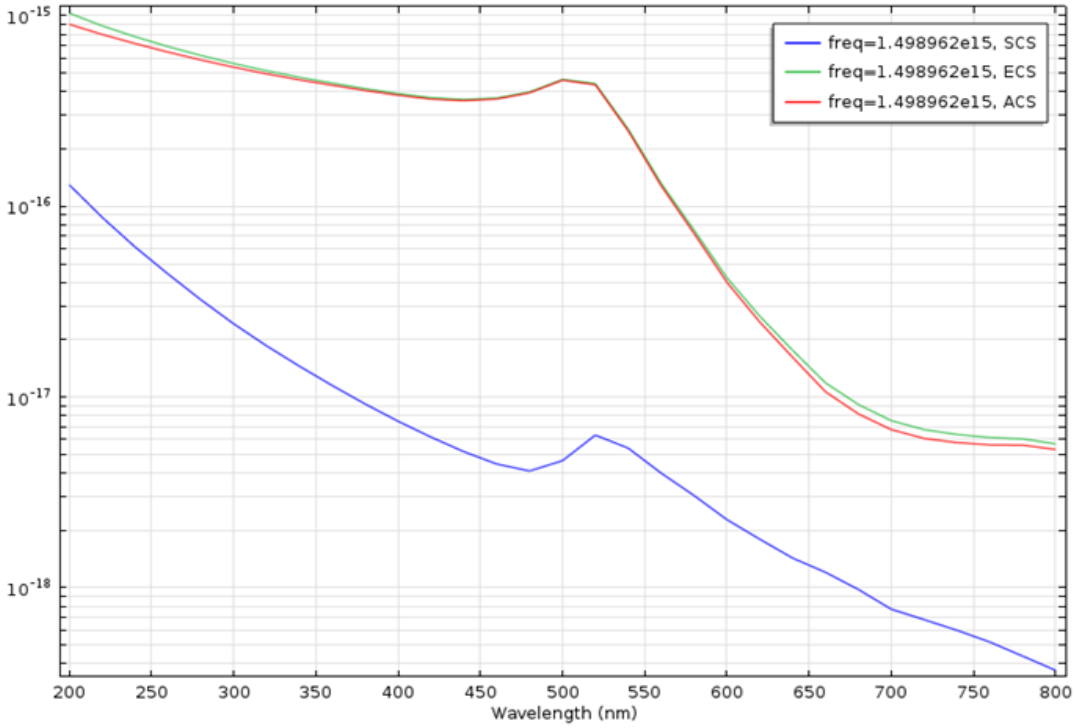

Fig. 3.14 Numerical cross-section simulation of a single gold sphere (15 nm diameter) using FEM model. ACS: absorption cross section (m^2); SCS: scattering cross section (m^2); ECS=ACS+SCS, extinction cross section (m^2)

Besides, the electromagnetic fields models of these two nanoparticles are also simulated with COMSOL (see figure 3.15 and 3.16). Single particle and two particles models are simulated for nanosphere and nanorod, respectively. The results indicate that 1) isotropic particle shows lower electromagnetic filed, therefore the Raman enhancement, compared with anisotropic particle; 2) two particles model shows stronger electromagnetic field when the distance between the two particles is close to 2 nm. In order to validate the simulation results, nanosphere is functionalized with 4-ATP as well as multi-histidine proteins and the SERS measurement results are compared with nanorod-4ATP complex (see figure 3.17). It clearly shows that the enhancement of GNR-4ATP-protein is much larger than the nanosphere-4ATP-protein complex.

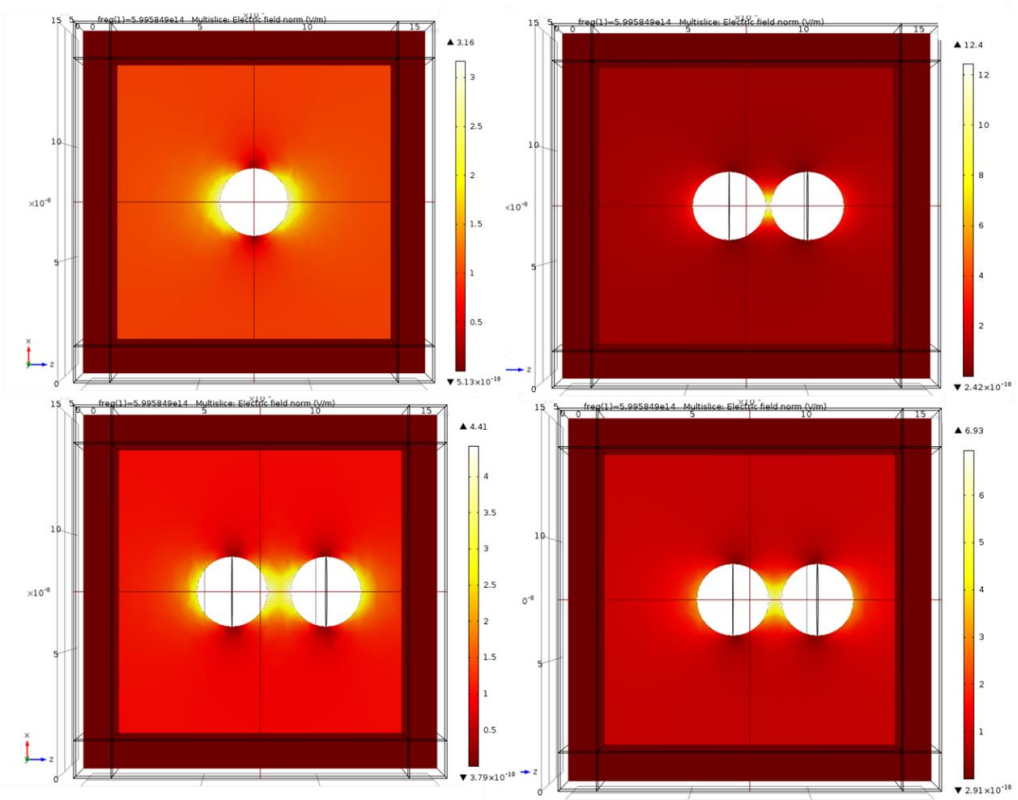

Fig. 3.15 Electromagnetic field simulation of single gold nanosphere, two sphere with 2nm, 5nm 10 nm distance

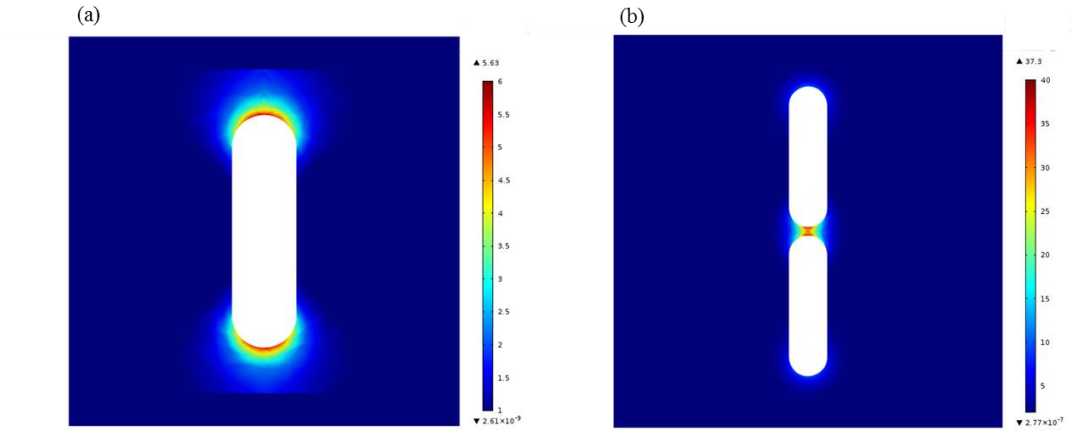

Fig. 3.16 Electromagnetic field simulation of single gold nanorod (a) two rods with 2nm distance

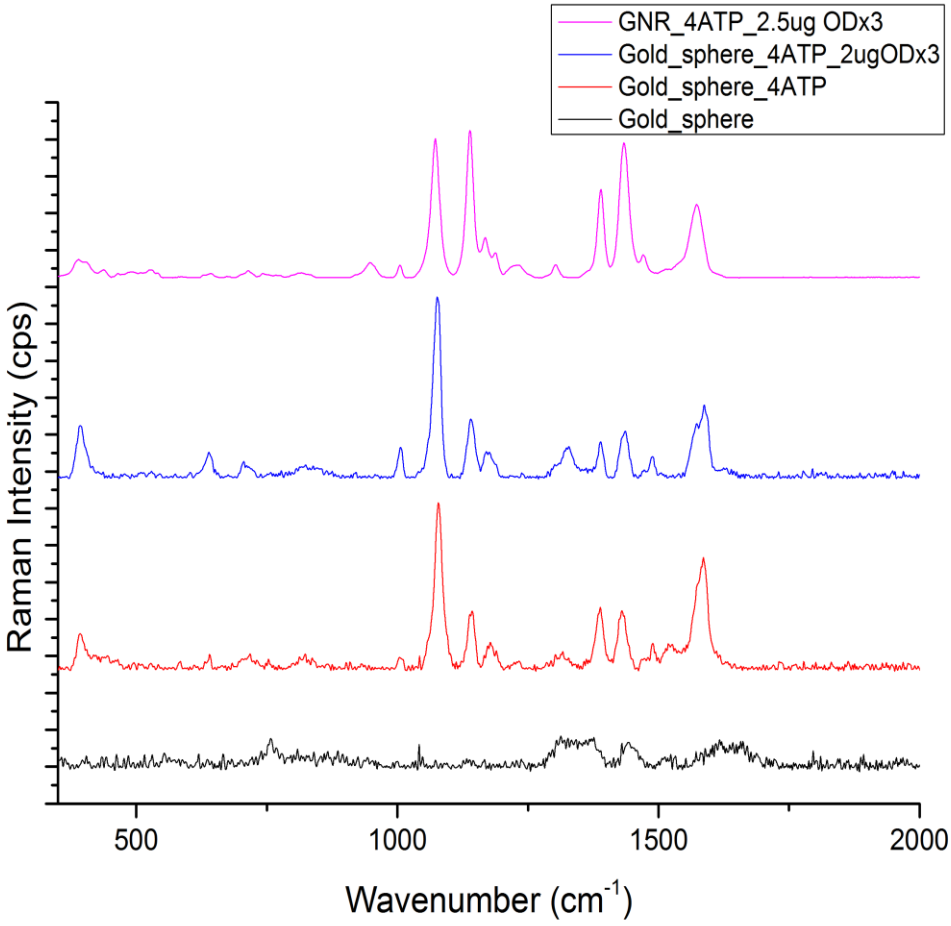

Fig. 3.17 SERS spectra of nanosphere complex and nanorod complex

3.5. Reference

Asano S, Yamamoto G 1975 Light scattering by a spheroidal particle *Appl. Opt* 14 29

Barber PW, Hill SS 1990 Light scattering by particles: Computational methods *Singapore: World Scientific*

Barhoumi A, Zhang D, Tam F, Halas N 2008 Surface Enhanced Raman Spectroscopy of DNA *J. Am. Chem. Soc.* 130 5523-5529

Bendinger B, Kroppenstedt RM, Klatte S, Altendorf K 1992 Chenotaxonomic differentiation of coryneform bacteria isolated from biofilters *Int. J. Systematic Bacteriology*. 42 474-486

Bizzarri A, Cannistraro S 2007 SERS detection of thrombin by protein recognition using functionalized gold nanoparticles *Nanomedicine NBM* 3 306-310

Brade H, Brade L, Rietschel ET 1988 Structure-activity repationships of bacterial liqopolysaccharides (endotoxins). Current and future aspects *Zentralbl Bakteriol Mikrobiol Hyg*

Chen J, Wiley B, Li Z, Campbell D, Saeki F, Cang H, Au L, Lee J, Li X, Xia Y 2005 Gold Nanocages: Engineering their structure for Biomedical Applications *Adv. Mater*. 17 2255-2261

De Gelder J 2008. Raman spectroscopy as a tool for studying bacterial cell compounds *PhD dissertation in sciences*, Chemistry. Gent University

Ding H, Yong KT, Roy I, Pudawar HE, Law WC, Bergey EJ, Prasad PN 2007 Gold nanorods coated with multilayer polyelectrolyte as contrast agents for multimodal imaging *Journal of Physical Chemistry C.* 111 12552-12557

Draine BT, Flatau PJ 1994 Discrete-dipole approximation for scattering calculations *J. Opt. Spc. Am. A.* 11 1491

Frey S, Stadler V, Heister K, Eck W, Zharnikov M, Grunze M, Zeysing B, Tertort A 2001 Structure of thioaromatic self-assembled monolayers on gold and silver *Langmuir* 17 2408-2415

Ghosh SK, Pal T 2007 Interparticle coupling effects on the surface plasmon resonance of gold nanoparticles: from theory to applications *Chem Rev.* 107 4797

Grosges T, Vial A, Barchiesi D 2005 Models of near-field spectroscopic studies: comparison between finite-element and finite-difference methods *Opt. Expr*. 13 8483

Jiao L, Niu L, Shen J, You T, Dong S, Ivaska A 2005 Simple azo derivatization on 4-aminothiophenol/Au monolayer *Electrochem. Comm.* 7 219-222

Johnson PB, Christy RW 1972 Optical constants of the noble metals *Physical Review* B. 6 4370-4379

Lin-Vien D, Colthup NB, Fateley WG 1991 The handbook of infrared and Raman characteristic frequencies of organic molecules *Academic Press*, San Diego

Liz-Marzán L, Pérez-Juste J, and Pastoriza-Santos I 2008 Plasmonics of Gold Nanorods. Considerations for Biosensing, in Nanomaterials for Application in Medicine and Biology 103-111, *Springer, Netherlands*

Meschenko MI, Travis LD, Mackowski DW 1999 T-matrix computations of light scattering by non-spherical particles: a review *J. Quant. Spectrosc. Radiat. Transfer*. 55 535

Mishchenko M, Travis L, Lacis A 2002 Scattering, Absorption, and Emission of Light by small Particles *New York: Cambridge University Press*

Neacsu CC, Steudle GA, Raschko MB 2005 Plasmonic light scattering from nanoscopic metal tip. *Appl. Phys. B* 80 295-300

Nlkoobakht B, El-Sayed M 2003 Preparation and Growth Mechanism of Gold Nanorods (NRs) Using Seed-Mediated Growth Method *Chem. Mater*.15 1957-1962

Rycenga M, Kim M, Camargo P, Cobley C, Li Z, Xia Y 2009 Surface-enhanced Raman scattering: Comparison of three different molecules on single-crystal nanocubes and nanospheres of silver *J. Phys. Chem. A* 113 3932-3939

Skrabalak S, Chen J, Au L, Lu X, Li X, Xia Y 2007 Gold Nanocages for Biomedical Applications *Adv. Mater.* 19 3177-3184

Wang X, Li Y, Wang H, Fu Q, Peng J, Wang Y, Du J, Zhou Y, and Zhan L 2010 Gold nanorod-based localized surface plasmon resonance biosensor for sensitive detection of hepatitis B virus in buffer, blood serum and plasma *Biosens. Bioelectron.* 26 404-410

Yee K 1996 Numerical solution of initial boundary value problems involving Maxwell's equations in isotropic media *IEEE. Ant. Propag*. 14 302

Zhang Z, Chen S, Liang Y, et al. 2010 An intelligent background-correction algorithm for highly fluorescent samples in Raman spectroscopy *Journal of Raman Spectroscopy* 41 659-669

Zheng J, Zhou Y, Li X, Ji Y, Lu T, Gu R 2003 Surface-enhanced Raman scattering of 4-aminothiophenol in assemblies of nanosized particles and the macroscopic surface of silver *Langmuir* 19 632-636

CHAPTER 4. A SELF-REFERENCING DETECTION OF MICROORGANISMS USING SURFACE ENHANCED RAMAN SCATTERING NANOPROBES IN A TEST-IN-A-TUBE PLATFORM

Modified from a peer-reviewed article published in Biosensors 2013, 3, 312-326

4.1. Abstract

Anisotropic nanoparticles (i.e., silver nanocubes) were functionalized with target-specific antibodies and Raman active tags to serve as nanoprobes for the rapid detection of bacteria in a test-in-a-tube platform. A self-referencing scheme was developed and implemented in which surface enhanced Raman spectroscopic (SERS) signatures of the targets were observed superimposed with the SERS signals of the Raman tags. The assessment through the dual signals (superimposed target and tag Raman signatures) supported a specific recognition of the targets in a single step with no washing/separation needed to a sensitivity of 10^2 CFU/mL, even in the presence of non-target bacteria at a 10 times higher concentration. The self-referencing protocol implemented with a portable Raman spectrometer potentially can become an easy-to-use, field-deployable spectroscopic sensor for onsite detection of pathogenic microorganisms.

Keywords: surface enhanced Raman scattering; self-referencing; microorganism; nanoparticles

4.2. Introduction

The presence of pathogenic bacteria in food and drinking water poses a threat to both public health and security; approximately 9.4 million illnesses, 56,000

hospitalizations and 1,300 deaths occur annually in the U.S. (Scallan et al., 2011). To deal with this threat, an early-warning surveillance system is needed to detect bacteria at the earliest possible moment, preferably in-field. However, traditional biochemical and nutritional analysis for microorganisms, such as analytical profile index (API), requires a series of biochemical tests for cultured microbes that takes days to finish (Jarvis and Goodacre. 2008). A molecular assay, such as sandwiched Enzyme-linked immunosorbent assay (ELISA), cuts the experimental time to hours; however, in ELISA assay, multiple washing steps are needed to separate bound antibodies from unbound ones, which still limits their in-field deployability (Lam and Kostov. 2010). Surface enhanced Raman scattering (SERS)-based signaling is emerging as an alternative to fluorescence-based detection (Sun et al., 2007; Sun et al., 2008). In recent years, the advances in SERS-based biosensing have enabled detection of targets at even single molecule sensitivity (Le et al., 2007; Haran. 2010; Neacsu et al., 2006). SERS-based molecular probes typically contain nanoscale metallic structures such as the SERS enhancer, organic Raman tags as quantitative reporters for the presence of the probes, and capturing molecules (i.e., antibodies, single strand DNAs, RNA aptamers) to interact with bio-targets (Bizzarri and Cannistraro. 2007; Drachev et al., 2004; Tripp et al., 2008; Wang et al., 2010). Their application bears great similarity to fluorescence-labeled antibodies, with the advantage of broader reporter library (theoretically, any molecule with a specific spectrum can be used as a Raman reporter, hence the restriction on selecting a Raman reporter is quite limited), supreme multiplexing due to sharp Raman bands (~10 nm vs. fluorescence band of ~50–300 nm) (Sun et al., 2007; Sun et

al., 2008), and no photobleaching. A detection limit of 10 cells/mL has been reported by Wang and coworkers with the SERS-active labeling technique (Wang et al., 2010). However, to utilize the SERS-probes for target detection, separation of target-bound probes from unbound ones through multiple washing steps is still needed, which reduces its field deployability.

An alternative to SERS probe-based detection is to directly identify bio-targets using their own inherent Raman fingerprints. Utilizing self-assembled monolayers of metallic nanoparticles, well-controlled nanostructures can be fabricated to yield reproducible SERS substrates for biosensor applications (Tripp et al., 2008; Wang et al., 2010; Kahraman et al., 2009; Patel et al., 2008; Jarvis et al., 2004; Kahraman et al., 2008; Premasiri et al., 2005; Javis and Goodacre. 2004; Efrima and Bronk. 1998; Efrima and Zeiri. 2009). Kahraman et al. reported a limit of detection (LOD) of 10^3 CFU/mL for E. coli in water (Kahraman et al., 2009). With SERS and a novel barcode data processing procedure, Ziegler et al. reported more than 10 bacteria could be differentiated (Patel et al., 2008). However, direct differentiation/identification of microbial targets through their unique Raman spectroscopic signatures requires high-quality and highly reproducible spectral data in conjunction with statistical analysis built upon known spectral fingerprints of the microbial species. Well-defined and controlled nano-SERS substrates used in these spectroscopic sensors usually only provide moderate enhancement (Le et la., 2007), and highly-sensitive benchtop Raman spectrometers are needed to produce the required high-quality spectral data, which limits the field depolyability of these approaches. Besides, SERS decays exponentially

away from the surface of the nanostructures, in nanoprobes where surfaced-immobilized antibodies (or other capturing molecules) are used, biotargets are usually not in direct contact with the metallic surface, and the enhancement to the biotarget Raman spectral signals is therefore much weaker, and further increases the difficulty to acquire high-quality SERS spectra directly from the bio-targets.

Another concern over SERS-based microorganism detection and identification is that SERS signals from microorganisms are highly dependent on the types of the SERS substrates (Jarvis et al., 2004; Kahraman et al., 2008; Premasiri et al., 2005), how SERS substrate are brought into contact with the microbial targets (Javis and Goodacre. 2004; Efrima and Bronk. 1998; Efrima and Zeiri. 2009), and the excitation laser wavelengths (Javis and Goodacre. 2004; Efrima and Bronk. 1998; Efrima and Zeiri. 2009). Variations in these factors may lead to a lack of consistency and poor reproducibility across measurements, which limit the application of SERS-based detection.

In this study we introduced a concept of self-referencing mechanism that utilizes SERS molecular probes to achieve bacteria detection in one single step in a test-in-a-tube platform, which would be more suitable for in-field applications. As shown in Figure 4.1, in the dual-recognition mechanism, Raman-labeled and antibody-functionalized anisotropic nanostructures (e.g., silver nanocubes) are fabricated as SERS nanoprobes that display specific probe signatures (probe signal), and through covalently-bound antibodies they could bind to their target bacterial cells specifically. The selection of silver nanocube as the SERS probe is to take advantage of the superior electromagnetic enhancement of anisotropic nanoparticle to Raman scattering of target

molecules in their vicinity, due to the geometrical singularity of these nanoparticles (Murphy et la., 2005; Potara et al., 2010; Qian and Nie. 2008; Liand Xia. 2010). The antibody-antigen binding ensures that the target cells would bind to enough nanoprobes, and measureable SERS signals from the bacterial cells would be generated (non-target would NOT have enough nanoprobes bound to them, and their SERS signal would be non-measurable due to weak or no enhancement). Observation of superimposed SERS signals of the probe and the target indicates the binding events, and subsequently definitely identifies the target in one single step; no washing or separation is needed. Furthermore, since the specificity of the target detection is provided by the antibodies, only a few key signature peaks from the bacterial cells are needed for the target recognition, a positive identification of the target can be reached without relying on multivariate analysis throughout a broad spectral range. A portable Raman sensor thus becomes feasible under the self-referencing dual-recognition scheme for target detection, as shown in this study.

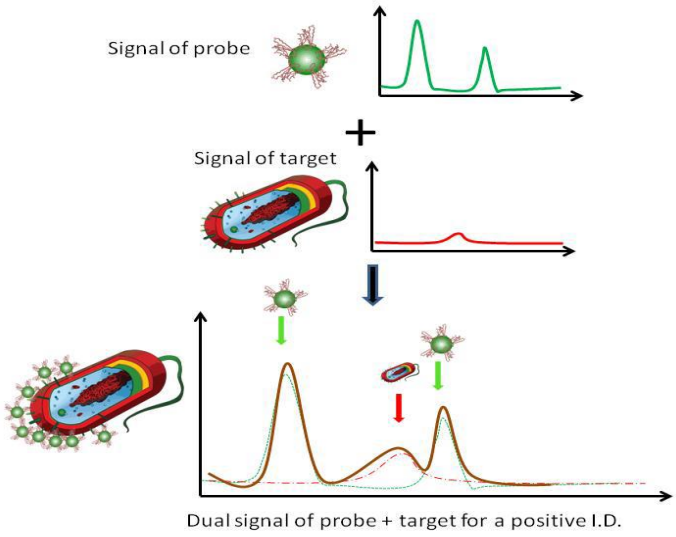

Fig. 4.1 Schematic illustration of a dual recognition mechanism for surface enhanced Raman spectroscopic (SERS) pathogen detection; the superimposed bacterial signature peaks and probe signatures peaks indicate the binding between the bacterial target and the nanoprobes

For this self-referencing scheme to work properly, the selection of proper Raman tags to label the nanoprobes is critical. The scheme relies on the observation of Raman peaks from the microbial cells to confirm binding between the nanoprobes and the microbes. Since microbial cells are further away from the nanoparticle surface, enhancement to microbial Raman signal is not as strong as to the Raman tags. Hence, if the peaks from the Raman tags are in the same spectral range as the peaks from the microbes (primarily cell walls), the weaker microbial signal may be overwhelmed by the stronger Raman tag signal, and fail to provide the self-referencing confirmation of the binding events. In an earlier report (Xiao and Yu. 2010), we used 11-mercaptoundecaonic acid (MUDA) as the Raman tag. The strong peaks of MUDA overlap with that of microbial cells to a great extent; only two weak microbial peaks were identified for the self-reference. In this study, a different Raman tag (4-aminothiophenol, 4-ATP) was used, which only has weak signals below 900 cm^{-1}. Microbial Raman peaks below 900 cm^{-1} hence can be easily recognized for self-reference.

4.3. Experimental section

Reagents and Antibodies

Ethylene glycol (99%), sodium sulfide (Na_2S, 99%), Polyvinylpyrrolidone (PVP, 99%), silver nitrate (>99%), 4-aminothiophenol (4-ATP, >99%), sodium nitrite (>99%), sodium hydroxyl (>99%) were all purchased from Sigma-Aldrich (St. Louis, MO, USA) and used without further purification. Nanopure deionized and distilled water (18.2 MΩ) was used for all experiments. Polyclonal anti-E. coli (Pierce®) antibodies (Lot#

LC1293681) were purchased from Thermo Scientific (Rockford, IL, USA) for E. coli molecular detection. E. coli and L. monocytogenes cultures were provided by a colleague (Brehm-Stecher).

4.3.1. Nanoprobe fabrication and functionalization

To take advantage of the superior surface enhancement performance of anisotropic nanoparticles due to the stronger local electromagnetic field around the singular features (sharp corners and edges) of these particles (Le et al., 2007; Efrima and Zeiri. 2009), we chose to use Ag nanocubes (as shown in Figure 4.2 a) to make nanoprobes.

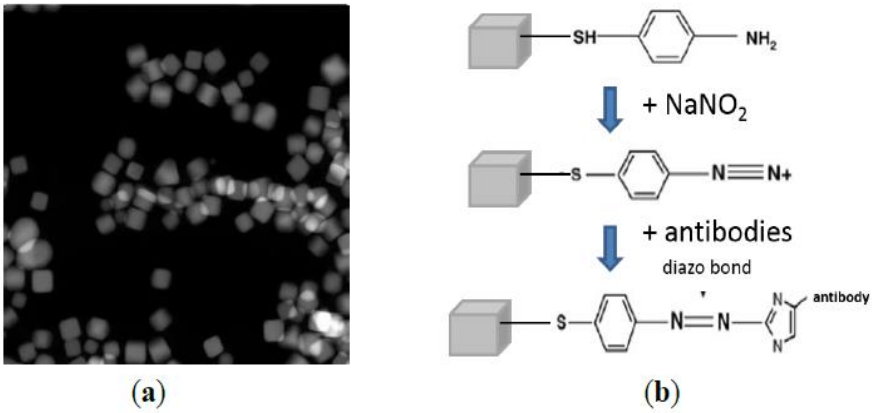

Fig. 4.2 a Silver nanocubes used to make molecular probes (STEM image); b Reaction scheme to functionalize silver nanocubes with anti-E. coli antibodies

Silver nanocubes were synthesized following the method of Skrabalak et al. (Skrabalak et al., 2007). Typically, in 20 mL glass reaction vial, 6 mL of ethylene glycol were added. The vial was incubated at 150 °C for 1 h to evaporate the water in the system. After heating, 70 μL of 3 mM Na2S in ethylene glycol was pipetted to each vial. The vial was then heated for 10 min before 1.5 mL of 0.02 g/mL PVP (Polyvinylpyrrolidone) in ethylene glycol was added together with 0.5 mL of 0.048

g/mL $AgNO_3$ in ethylene glycol. Finally, the whole mixture was heated for up to 20 min until the solution became ochre-colored.

The reaction was quenched by putting the vial in water bath at room temperature. The nanocubes were subsequently rinsed with acetone and then washed with nanopure water for three times and finally resuspended in 4 mL of nanopure water.

The PVP coating of the Ag cubes was then replaced with 4-ATP for antibody attachment. The 4-ATP molecules also serve as Raman tag for the nanoprobes. To replace the PVP coating with 4-ATP, 4 mL of 3 nM Ag-PVP were reacted with 0.5 mL of 10 mM 4-ATP dissolved in acidic water (pH = 2) under vigorously stirring at 60 °C for 3 h. The solution was then centrifuged and washed with water-free ethanol once and acidic water (pH = 4) twice to remove the extra PVP and unbound 4-ATP. Finally, Ag-4-ATP nanocubes were redispersed in 2.5 mL of acidic water (pH = 4).

To covalently conjugate antibodies with the Ag-4-ATP nanocubes, diazonium salt of Ag-4-ATP was obtained by reacting 1 mL of as made Ag-4-ATP solution with 10 mL of 10–3 M sodium nitrite at pH 4 at 0 °C for 30 min (Bizzarri and Cannistraro. 2007). Then the Ag-4-ATP-azo solution was neutralized by addition of 300 μL 1 M sodium hydroxyl and 1 mL of 100 mM phosphate buffer (pH = 7.4). Finally, antibodies were incubated with Ag-4-ATP solution at 0 °C for 4 h to form diazo bonds between the electron-rich aromatic lateral chains of antibody molecules and the diazonium moiety of the Ag-4-ATP-azo (Bizzarri and Cannistraro. 2007), the unbound antibodies were successively removed by centrifugation, and the Ag-4-ATP-Abs were collected and resuspended in 10 mM phosphate buffer (pH = 7.4) and stored at 4 °C. The

functionalization reaction scheme is illustrated in Figure 4.2 b. The final concentration of the nanoprobe was 5 nM.

They remain stable for up to 1 month.

4.3.2. Bacterial cell culture

Two bacterial strains (E. coli and L. monocytogenes) were grown in LB medium at 37 °C for 18 h. The bacterial cells were then centrifuged and washed with PBS buffer twice and finally redispersed in PBS buffer. The final bacterial cell concentration was determined by optical density (OD) measurement at 600 nm (the concentration of the bacterial cells for both strains was ~10^9 CFU/mL at OD = 1.0) 1 mL of the PBS solution with various cell concentrations was then incubated with proper nanoprobes over ice for around 30 min in an eppendorf tube (1.5 mL) to allow the nanoprobes to bind to their targets, respectively.

4.3.3. One-Step Raman spectroscopic measurement

To acquire SERS spectra of the bacteria-nanoprobe sample, 10 μL of the sample was withdrawn from the eppendorf tube and put into a cap of an eppendorf tube (removed from a tube). The cap was used as a sampling container. It was put at the focal point (6 cm measuring from the tip of the i-Raman spectrometer (B&W Tek, Inc., Newark, DE, USA) as shown in Figure 4.3) of the i-Raman laser beam (15 mW, 785 nm NIR laser, 3 cm^{-1} spectral resolution, 400–2,000 cm^{-1} range). The focal point of the laser beam was pre-set by the manufacturer. Raman spectra of the sample were hence obtained directly with no washing being performed after the mixing of the bacterial suspension and the nanoprobes in one single step. 60 s integration time was used at 15

mW laser power for spectral acquisition. 10 spectra were collected from each sample to calculate an average spectrum, which was used for further analysis.

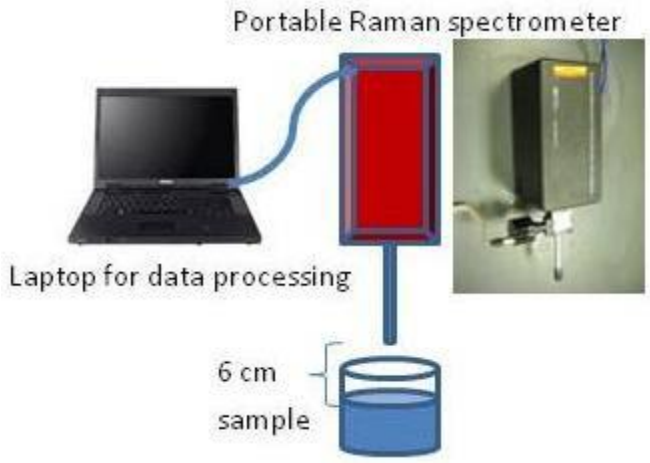

Fig. 4.3 Schematic illustration of the experimental setup

4.3.4. Spectral data processing

Using near infrared excitation (785 nm) radically reduces the observance of sample auto-fluorescence. To further reduce the remaining fluorescence, a polynomial background subtraction method was implemented (Zhao et al., 2007; Wang et al., 2013). Another challenge in spectral pre-processing is to capture important patterns in the spectra while removing noise or other fine-scale structures. The 10-point moving average method was used in this study to smooth the spectra. Finally all spectra were area-normalized for intensity consistency at the region between 400 to 2,000 cm^{-1}. All data processing was conducted using R, a widely used language and software tool for statistical computing and graphics. Peak intensity is calculated based on the integration of the peak area.

4.4. Results and discussion

4.4.1. Self-Referencing detection of target bacteria in a test-in-a-tube platform

The diazo-conjugation strategy utilizes aromatic side chains of the antibodies for their immobilization onto the Ag-cubes (Rycenga et al., 2009; Frey et al., 2001; Zheng et al., 2003; Jiao et al., 2005; Xiao and Yu. 2010). As the side chains that are reactive can be at the Fc segment as well as the Fab segment of the antibody molecule, the orientation of the immobilized antibody molecules on the Ag-cube surface is uncertain. In certain cases the antigen binding sites might be brought in close vicinity to the Ag-cube surface; when such antibody molecules bind to their target cells, the cell walls are also being brought into close distance to the Ag-cube surface, and SERS signals can be observed from these cells.

Figure 4.4 shows the Raman spectra of Ag-4-ATP-Abs probe (Ag-nanocube functionalized with anti-E. coli antibodies) binding with E. coli and L. monocytogenes, respectively. Since bacteria cells were suspended in aqueous solution, they are constantly drifting in and out of the focal volume of the laser beam. To assure a meaningful SERS spectrum is acquired, the integration time was set to be 60 s, with the laser power set at 15 mW. Earlier reports suggested that at this power level and integration time, microbial samples tend to become graphitic and their spectroscopic characteristics may change dramatically (Ferima and Zeiri. 2009). However, in our experiment the cells were suspended in aqueous solution, and the SPR-induced heat damage seems to be alleviated. Also the cells were drifting in and out of the focal

volume, and the actual laser exposure of individual cells seems not to have gone over the graphitic limit; evidenced by the lack of the D and G bands of graphene in the spectra.

Peaks at 735 cm^{-1} and 1,330 cm^{-1} have been widely reported as characteristic SERS peaks that can be observed from microbial cells (Jarvis et al., 2004; Kahraman et al., 2008; Premasiri et al., 2005; Javis and Goodacre. 2004; Efrima and Bronk. 1998; Efrima and Zeiri. 2009). Due to the nature of surface enhancement, only molecules that are in close vicinity to the SERS substrate can be affected by the surface-plasmon based enhancement. The 735 cm–1 and 1,330 cm–1 peaks are typical of adenine (Efrima and Zeiri. 2009). They can come from the adenine part of the fully reduced FAD (Zheng et al., 2004) or from other adenine-bearing molecules (NAD, ATP, DNA, etc.). No matter what molecular species that contributes to the adenine peaks, they can only come from the cells. The 735 cm^{-1} peak only appeared upon the binding of nanoprobes to their specific bacterial targets (E. coli). For samples with only probes or with a non-target bacteria L. monocytogenes, the 735 cm^{-1} peak is missing. Hence, this peak was used subsequently as the fingerprinting peak for E. coli in the self-referencing mechanism.

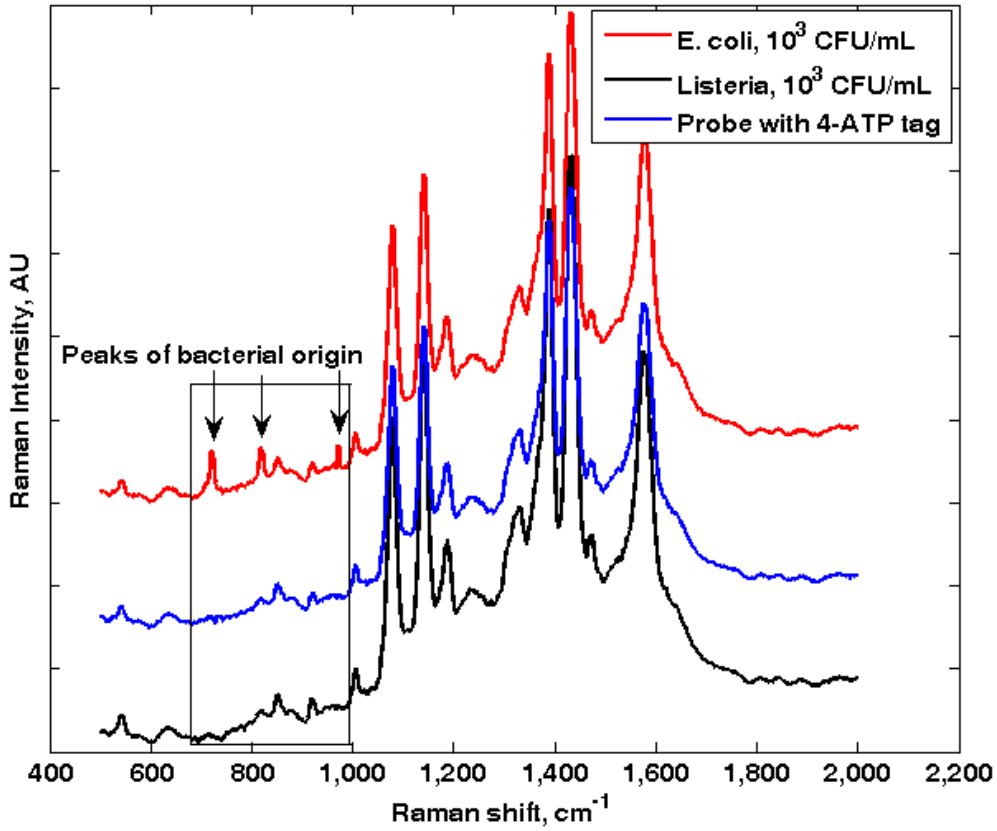

Fig. 4.4 SERS spectra of silver nanoprobes functionalized with anti-E. coli antibodies (blue) incubated with E. coli (red) and Listeria (black). No bacterial-originated peaks can be observed when non-target species is integrated with the nanoprobes

It has been reported that the 1,330 cm^{-1} peak in bacteria is usually stronger than the 735 cm^{-1} peak, hence should be a better indicator of probe-bacteria binding. However, 4-ATP itself displays a strong peak at 1,335 cm^{-1}, which completely overwhelms the — could-be ‖ bacterial peak at the same wavelength region. As shown in Figure 4.4, a peak is always visible at 1,330 cm^{-1}, regardless of samples. Hence, in our experiment the 1,330 cm^{-1} adenine peak cannot be used as a bacterial marker.

Two other peaks (825 cm^{-1} and 985 cm^{-1}) also appeared to be associated with the presence of target bacteria (E. coli) in a sample, also their exact biological origins are less clear and more investigation is needed. In a summary, as illustrated in Figure 4.1,

the observation of bacteria-originated Raman peaks in the superimposed probe-target spectrum clearly indicated the presence of the targets in a sample.

The absence of bacteria-originated peaks in control samples as well as non-target samples showed that the self-referencing detection scheme is highly specific and accurate.

Our observation was consistent with what has been previously reported (Efrima and Zeiri. 2009): Although colloidal nanoparticles can be absorbed onto microbial cell wall from all directions due to non-specific electrostatic interaction, simply mixing bacterial cells with nanoparticles usually do not bring enough particles to the surface of bacterial cells to generate measurable SERS signals. With our specifically functionalized nanoprobes, however, significantly more nanoprobes were attached to the surface of the target cells due to the antibody-antigen binding, and in certain cases the molecules located at the inner side of the cell walls come into close proximity to the Ag-cubes that are bound on the surface, and the 735 cm^{-1} peak becomes detectable.

Due to the usual longer distance between the cellular originated molecular species (i.e., FAD, NAD etc.) and the nanoparticle surface (i.e., no direct contact) than that between the Raman tag

(4-ATP molecules) and the nanoparticle surface (direct contact), the enhancement to the Raman tag is more effective and the observed spectra were dominated by the signatures of the 4-ATP molecules. However, the dual-recognition mechanism only requires a few identifiable signature peaks from the microbial cells to serve as spectral markers, as demonstrated in Figure 4.4.

4.4.2. Limit of Detection of the Dual-Recognition Probing Scheme

The limit of detection (LOD) and specificity of the self-referencing detection scheme were investigated. A detectable signal is recorded when the peak intensity measured from a sample is significantly higher ($\geqslant$Mcontrol + 3 σ) than the peak intensity of a control, where Mcontrol is the mean of the peak intensity of the control (10 replicates), and σ is the standard deviation of the peak intensity of the control at the same wave number.

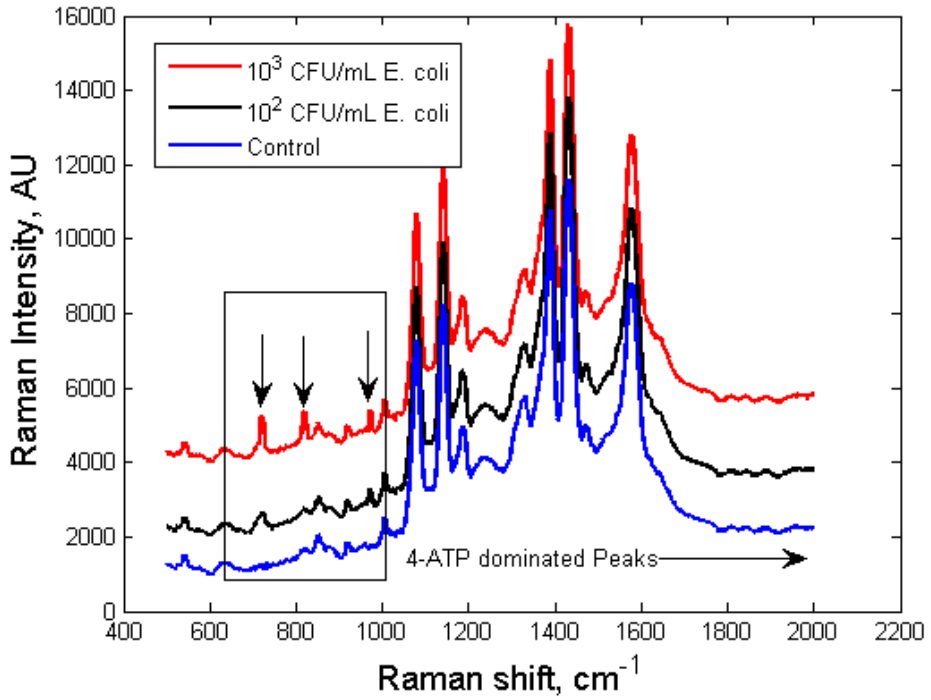

Fig. 4.5 SERS spectra of silver nanoprobes functionalized with anti-E. coli antibodies, incubated with E. coli (red and black) at different concentrations (blue: control sample with no E. coli cells)

As shown in Figure 4.5, the 735 cm^{-1} bacterial peak became detectable at 10^2 CFU/mL E. coli concentration, comparable to that of high-end ELISA assay, without going through any washing steps. When E. coli concentration was lower than 102 CFU/mL (three were tested, 50 CFU/mL, 30 CFU/mL,

10 CFU/mL, respectively), the 735 cm^{-1} peak was not significantly different from that of the control (within Mcontrol ± 3σ), hence it was considered as indistinguishable from the control. The relative intensity of the 735 cm^{-1} peak, calculated with reference to the 1,079 cm^{-1} peak (representative peak of 4-ATP, which is determined by the number of nanoprobes, not the number of bacterial cells, stayed within Mcontrol ± 3σ for all samples investigated), is exponentially correlated to the concentration of bacterial cells in the sample, between 10^2 CFU/mL to 10^6 CFU/mL. A second peak at 985 cm^{-1} was also investigated. Similarly, the relative intensity of the 985 cm^{-1} peak calculated with reference to the 1,079 cm^{-1} peak, is exponentially correlated to the concentration of bacterial cells in the sample. Experiments were replicated five times with each concentration, and the standard errors of the mean for each concentration are also shown in Figure 4.6. The self-referencing assay potentially can be developed into a fast semi-quantitative assay for bacterial targets.

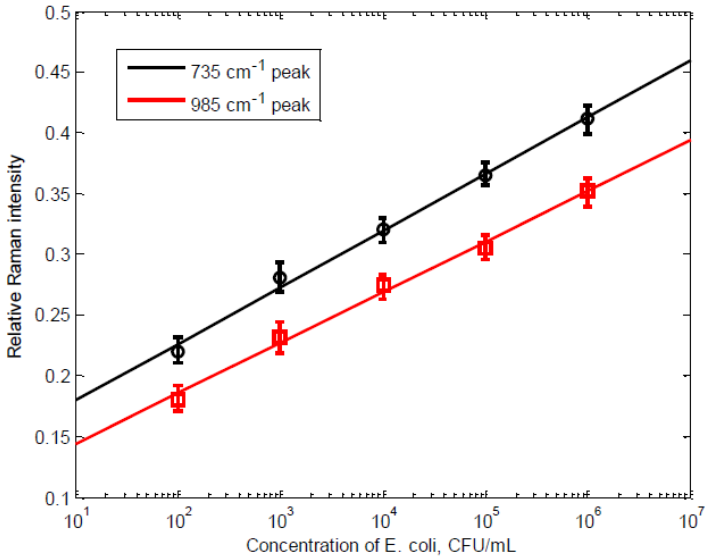

Fig. 4.6 The correlation between the relative Raman intensity of the 735 cm^{-1} peak and the concentration of E. coli cells in the sample. The relative Raman intensity was calculated using the 4-ATP peak at 1,079 cm^{-1} as internal reference, error bar indicates the standard errors of the mean from five independent runs

To further improve the LOD of the self-referencing scheme, more effective SERS enhancers should be used. The Ag nanocubes are good SERS enhancers, due to their sharp corners and edges that generate singularity in electromagnetic field around the particles which enhances the Raman scattering electronically. Nano-enhances with more extreme singularity, such as nanostars or nano-prisms, may provide stronger enhancement that would result in better LOD.

4.4.3. Specificity of the Dual-Recognition Probing Scheme

The specificity of the self-referencing dual-recognition scheme is determined by the specificity of the antibodies. As illustrated in Figure 4.7, when a sample with non-targets (L. monocytogenes,

10^3 CFU/mL) was integrated by the nanoprobes (specifically E. coli), no self-referencing signatures (735 cm^{-1}, 825 cm^{-1} and 985 cm^{-1}) were observed which resulted in a correct negative I.D. For a sample with a 10-fold higher non-targets (L. monocytogenes, 10^3 CFU/mL) concentration than target (E. coli, 10^2 CFU/mL), the specific E. coli peaks could still be identified, as shown in Figure 4.7. Relatively high level of interferences from other bacteria (L. monocytogenes) did not diminish the accuracy of the self-referencing dual-recognition scheme, indicating that this scheme would be extremely attractive to in-field pathogen detection applications, where interference from other co-existed microorganism species will be omnipresent.

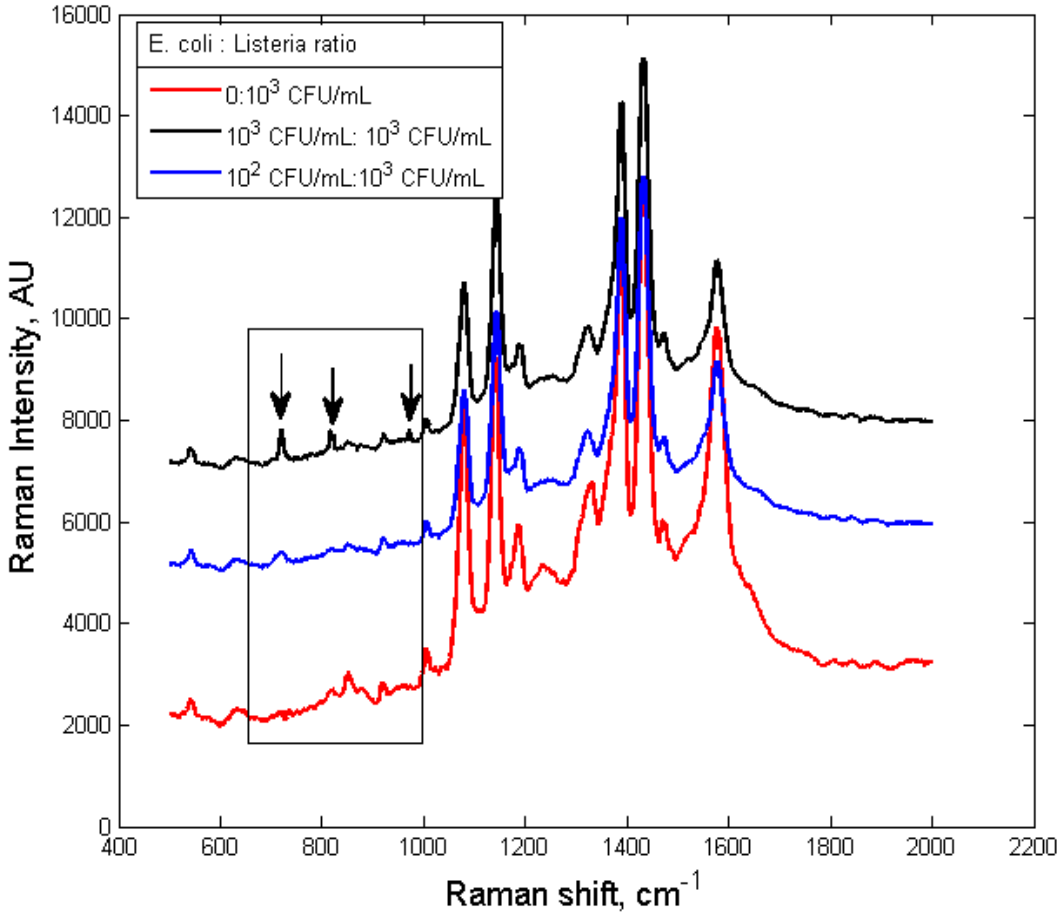

Fig. 4.7 SERS spectra of silver nanoprobes with anti-E. coli antibodies interacted with E. coli and Listeria mixture sample solutions with different E. coli:Listeria ratio

4.5. Conclusions

A self-referencing mechanism was successfully developed for single-step detection of bacterial target in a lab-in-a-tube setting using SERS spectroscopic sensing. The detection time, about 30 min, is relatively short compared to alternative methods. The sensitivity of the self-referencing probing scheme is high (10^2 CFU/mL), and it was demonstrated that interference from other sources was minimal even at high concentrations (10 times higher than the targets). As the binding efficiency between nanoprobes and target bacteria is further improved through the optimization of the nanoprobe design and functionalization, stronger SERS enhancement of the

fingerprinting peaks of the bacterial targets could be expected. In addition, by deploying nanoprobes with molecular recognition agents targeting different motifs (e.g., antibodies binding to different epitopes), a multiplexing self-referencing scheme can be further developed to improve the detection specificity. With the self-referencing mechanism, a multiplexing field-deployable biosensor can soon be developed for onsite detection of pathogenic bacteria with high sensitivity and selectivity.

Acknowledgments

The authors would like to acknowledge Byron Brehm-Stecher from Iowa State University for providing the microorganism cultures used in this study.

4.6. References

Bizzarri AR, Cannistraro S 2007SERS detection of thrombin by protein recognition using functionalized gold nanoparticles *Nanomedicine NBM* 3 306–310

Drachev VP, Thoreson MD, Khaliullin EN, Davisson J, Shalaev VM 2004 Surface-enhanced Raman difference between human insulin and insulin lispro detected with adaptive nanostructures *J Phys Chem B.* 108 18046–18052

Efrima S, Bronk BV 1998 Silver colloids impregnating or coating bacteria *J Phys Chem B.102* 5947–5950

Efrima S, Zeiri L 2009 Understanding SERS of bacteria *J Raman Spectrosc. 40* 277-288

Frey S, Stadler V, Heister K, Eck W, Zharnikov M, Grunze M, Zeysing B, Tertort A 2001 Structure of thioaromatic self-assembled monolayers on gold and silver *Langmuir. 17* 2408–2415

Haran G 2010 Single-molecule Raman spectroscopy: A probe of surface dynamics and plasmonic fields *Acc. Chem. Res.* 43 1135–1143

Javis RM, Goodacre R 2004Discrimination of bacteria using surface-enhanced Raman spectroscopy *Anal Chem*. *76* 40–47

Jarvis RM, Goodacre R 2008 Characterisation and identification of bacteria using SERS *Chem. Soc. Rev.* 37 931–936

Jarvis RM, Brooker A, Goodacre R 2004 Surface-enhanced Raman spectroscopy for bacterial discrimination utilizing a scanning electron microscope with a Raman spectroscopy interface *Anal Chem. 76* 5198–5202

Jiao L, Niu L, Shen J, You T, Dong S, Ivaska A 2005 Simple azo derivatization on 4-aminothiophenol/Au monolayer *Electrochem Comm.7* 219–222

Kahraman M, Yazici MM, Sahin F, Culha M 2008 Convective assembly of bacteria for surface-enhanced Raman scattering *Langmuir. 24* 894–901

Kahraman M, Zamaleeva AI, Fakhrullin RF, Culha M 2009 Layer-by-layer coating of bacteria with noble metal nanoparticles for surface-enhanced Raman scattering Anal Bioanal Chem. 395 2559–2567

Lam H, Kostov Y 2010 Optical instrumentation for bioprocess monitoring *Adv. Biochem. Eng. Biotechnol*. 116 125–142

Le Ru EC, Blackie E, Meyer M, Etchegoin PG 2007 Surface Enhanced Raman Scattering enhancement factors: A comprehensive study *J. Phys. Chem*. 111 13794–13803

Li ZY, Xia Y 2010 Metal nanoparticles with gain toward single-molecule detection by surface-enhanced Raman scattering *Nano Lett. 10* 243–249

Murphy CJ, Sau TK, Gole AM, Orendorff CJ, Gao J, Gou L, Hunyadi SE, Li T 2005 Anisotropic metal nanoparticles: Synthesis, assembly, and optical applications *J Phys Chem B.109* 13857–13870

Neacsu CC, Dreyer J, Behr, N, Raschke, MB 2006 Scanning-probe Raman spectroscopy with single-molecule sensitivity *Phys. Rev. B* 73 193406, doi:10.1103/PhysRevB.73.193406.

Patel IS, Premasiri WR, Moir DT, Ziegler LD 2008 Barcoding bacterial cells: A SERS based methodology for pathogen identification *J Raman Spectrosc. 39* 1660–1672

Potara M, Baia M, Farcau C, Astilean S 2012 Chitosan-coated anisotropic silver nanoparticles as a SERS substrate for single-molecule detection *Nanotechnology. 23* doi:101088/0957-4484/23/5/055501

Premasiri WR, Moir DT, Klempner MS, Krieger N, Jones G, II, Ziegler LD 2005 Characterization of the surface enhanced Raman scattering (SERS) of bacteria *J Phys Chem B. 109* 312–320

Qian, XM Nie SM 2008 Single-molecule and single-nanoparticle SERS: From fundamental mechanisms to biomedical applications *Chem Soc Rev. 37* 912–920

Rycenga M, Kim MH, Camargo PHC, Cobley C, Li Z, Xia Y 2009 Surface-enhanced Raman scattering: Comparison of three different molecules on single-crystal nanocubes and nanospheres of silver *J Phys Chem A. 113* 3932–3939

Scallan E, Hoekstra RM, Angulo FJ, Tauxe RV, Widdowson MA, Roy SL, Jones JL, Grifin, PM 2011 Foodborne illness acquired in the United States—Major pathogens *Emerg. Infect. Dis*. 17 7–15.

Skrabalak SE, Au, L, Li XD, Xia Y 2007 Facile synthesis of Ag nanocubes and Au nanocages *Nat Protocol. 2* 2182–2190

Sun L, Yu C, Irudayaraj I 2007 Surface-enhanced Raman scattering based nonfluorescent probe for multiplex DNA detection. *Anal. Chem*. 79 3981–3988

Sun L, Yu C, Irudayaraj I 2008 Raman multiplexers for alternative gene splicing. *Anal. Chem*. 80 3342–3349

Tripp R, Dluhy R, Zhao Y 2008 Novel nanostructures for SERS biosensing *Nano Today* 3 31–37

Wang Q, Grozdanic SD, Harper MM, Hamouche K, Hamouche N, Kecova H, Lazic T, Yu C 2003 Detection and characterization of glaucoma-like canine retinal tissues using Raman spectroscopy *J Biomed Opt.18* doi:101117/1JBO186067008

Wang Y, Lee K, Irudayaraj J 2010 Silver nanosphere SERS probes for sensitive identification of pathogens *J Phys Chem C*. 114 16122–16128

Xiao N, Yu C 2010 Rapid-response and highly sensitive non-crosslinking colorimetric nitrite sensor using 4-aminothiophenol modified gold nanorods *Anal Chem. 82* 3659–3663

Xiao N, Yu C Dual Recognition Mechanism for Bacteria Detection Using Surface Enhanced Raman Spectroscopic Nanoprobes In Proceedings of ASABE Annual International Meeting, Pittsburgh, PA, USA, 20–23 June 2010

Zhao J, Lui H, McLean DI, Zeng H 2007 Automated autofluorescence background subtraction algorithm for biomedical Raman spectroscopy *Appl Spectros. 61* 1225–1232

Zheng J, Zhou Y, Li X, Ji Y, Lu T, Gu R 2003 Surface-enhanced Raman scattering of 4-aminothiophenol in assemblies of nanosized particles and the macroscopic surface of silver *Langmuir. 19* 632–636

Zheng Y, Carey PR, Palfey BA 2004 Raman spectrum of fully reduced flavin *J Raman Spectrosc. 35* 521–524

4.7. Appendix: Synthesis and Bio-Functionalization of Silver Nanocubes

The silver nanocubes synthesized in this study have a average size of 41 nm, with a standard deviation of 7.8 nm, measured over 437 particles imaged using STEM. Typical STEM image is shown in Figure S4.1.

Extinction spectra of silver nanocube (PVP coated, right after synthesis), 4-ATP-coated silver nanocube, and antibody-functionalized silver-nanocube probes are shown in Figure S4.2. After replacing the PVP coating with 4-ATP, the plasmonic peak blue-shifted, due to the change of refractive index (a reduction) and the thickness of the surface coating; the thinkness of the 4-ATP coating, which is a monolayer of small molecules, is much smaller than that of the PVP coating. After antibodies are conjugated to the 4-ATP linker, the plasmonic peak re-shifted slightly, due to the addition of the antibody molecules further increased the refractive index of the surface layer on the nanoparticles.

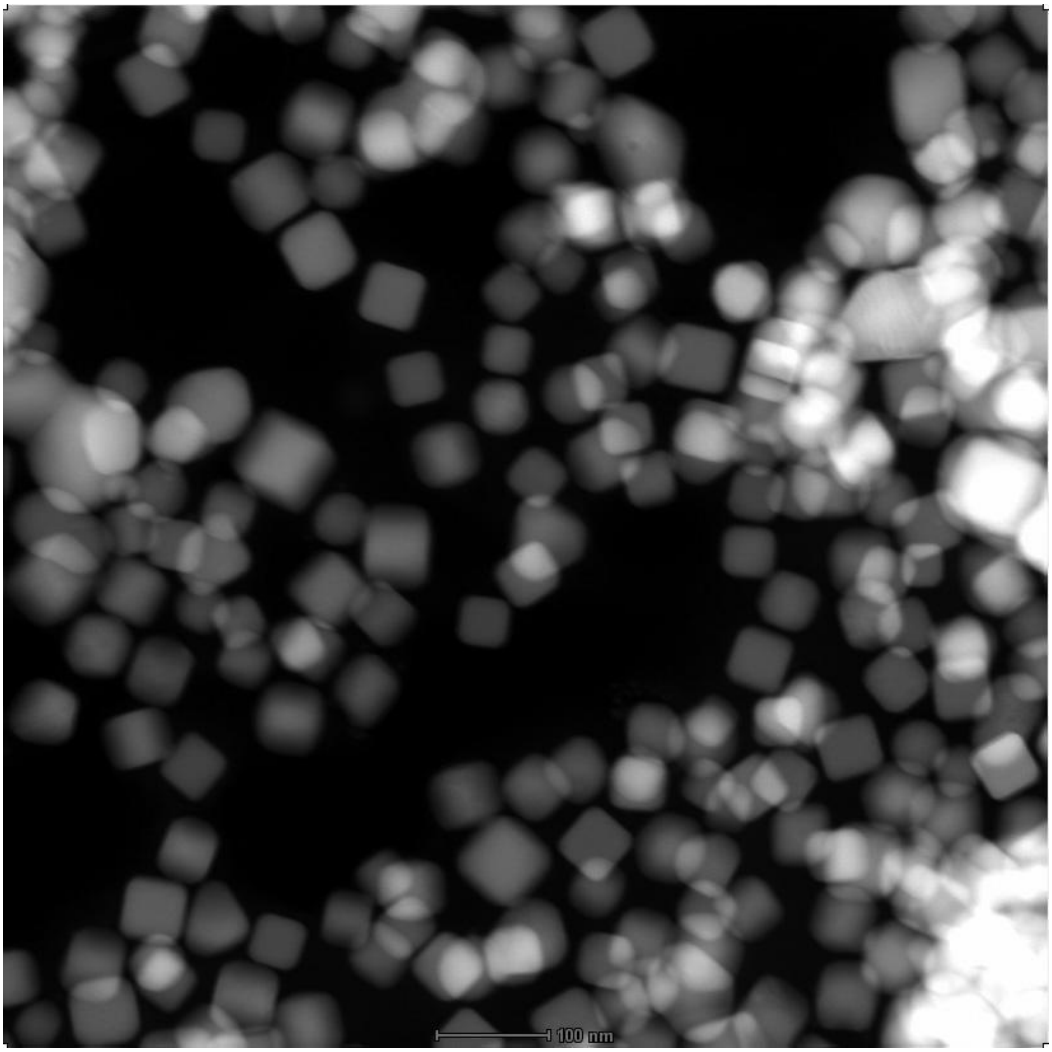

Fig. S4.1 STEM image of the silver nanocube

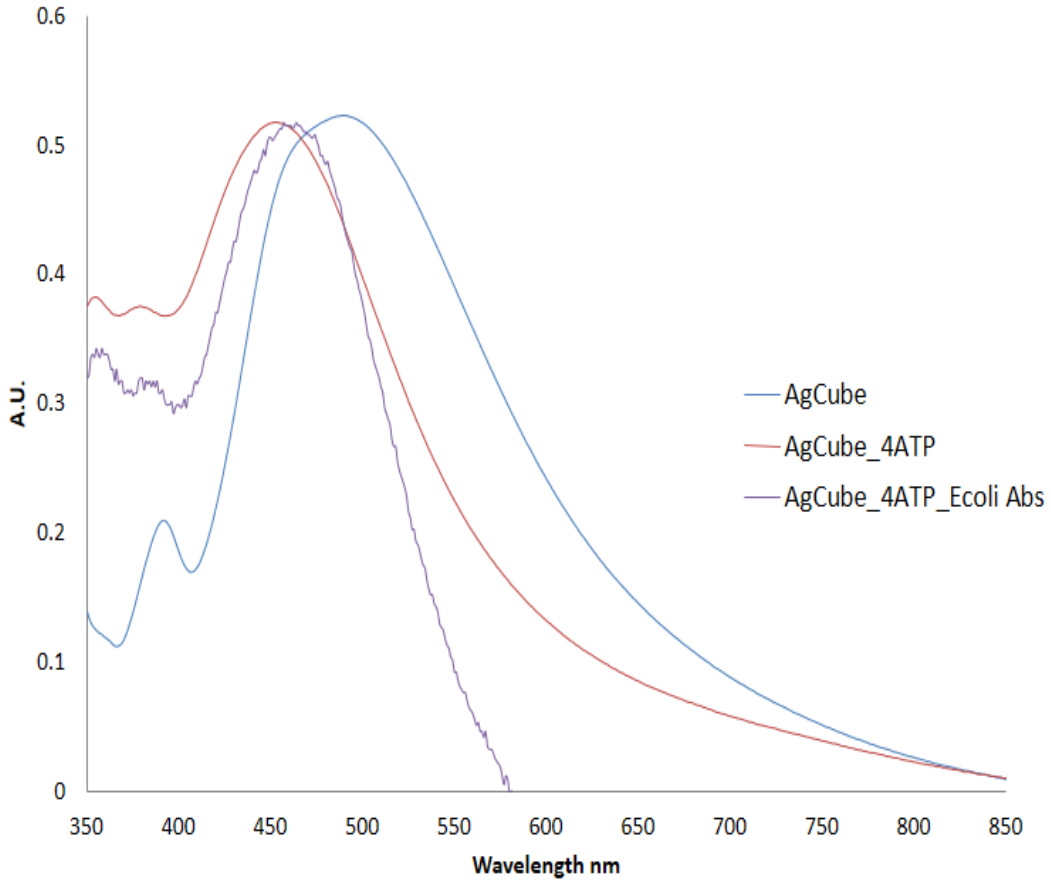

Fig. S4.2 Extinction spectra of silver nanocube (PVP coated), 4-ATP-coated silver nanocube, and antibody-functionalized silver-nanocube probes

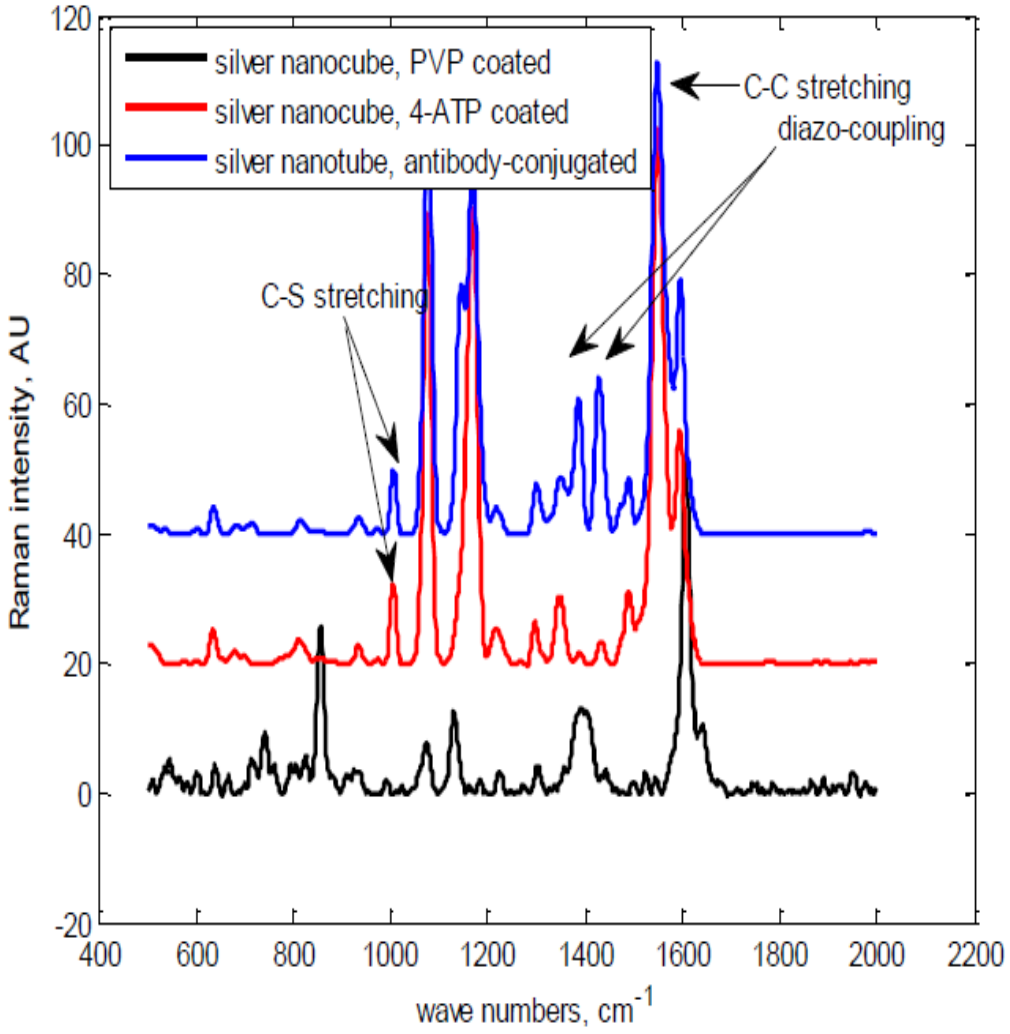

Fig. S4.3 Raman spectra of Ag nanocube with antibodies conjugated to them

Figure S4.3 shows the Raman spectra of PVP-coated silver nanocube, 4-ATP-coated silver nanocube and anti-E. coli antibody-conjugated silver nanocube. A layer of 4-ATP molecules were anchored on the surface of the silver nanotubes after incubation with the Ag-cube solution due to Ag–S bonding. As shown in Figure S2, band at 1,090 cm^{-1} is the stretching vibration of C–S bond and band at 1,590 cm^{-1} is the C–C stretching vibration of benzene ring in 4-ATP (Rycenga et al., 2009; Frey et al., 2001;Zheng et al., 2003; Jiao et al., 2005; Xiao and Yu. 2010). The appearance of these bands, replacing the original PVP bands, indicated the successful replacement of PVP with 4-ATP on the Ag-cube surface. Another notable difference between the

spectra of pure 4-ATP and that of 4-ATP labeled Ag-cube is the intensity of 4-ATP characteristic peak at 1,590 cm^{-1}. The apparent enhancement of the mode at 1,590 cm^{-1} can be ascribed to a charge transfer between the metal and the 4-ATP molecules (Bizzarri and Cannistraro. 2007), further confirms the binding of 4-ATP to the Ag-cube surfaces. The Ag-4-ATPs were then reacted with nitrite ions in acid condition to form diazonium salt, which subsequently reacted with histidine residues of the antibodies. The stengtherning of the 1,394 cm^{-1} and 1,435 cm^{-1} diazonium peaks (N=N stretching) proved the conjugation of the antibodies, as shown in Figure S4.3 (Bizzarri and Cannistraro. 2007; Rycenga et al., 2009; Frey et al., 2001;Zheng et al., 2003; Jiao et al., 2005; Xiao and Yu. 2010).

CHAPTER 5. DEVELOPMENTOF A MULTIPLEXING SELF-REFERENCING SERS MICROFLUIDIC BIOSENSOR FOR WATERBORNE PATHOGEN DETECTION

5.1. Abstract

Conventional methods for the detection of pathogens are time-consuming and labor-intensive. Molecular methods (e.g., PCR, ELISA) are more sensitive and selective. But they often need pre-enrichment of the bacterial targets, or are susceptible to interference from other water components. In this study, a microfluidic approach is developed to allow enrichment of bacterial cells in water at extremely low levels, and a multiplexing dual recognition SERS scheme is developed that allows one-step detection of bacterial targets with elevated reliability and accuracy. The limit of detection (LOD) of the SERS scheme reached single cell level. Experiments with a mixture of E.coli O157:H7 and E.coli K12 demonstrated that this method could be used for identification of pathogenic bacteria from mixed samples at sub-species level. SERS coupled with statistical analyses was shown to be an effective way for pathogen detection.

5.2. Introduction

Pathogen detection and identification is of the utmost importance for medicine, food safety, public health and security, and water and environmental quality control (Leonard et al., 2003). The World Health Organization (WHO) identified that contaminated water serves as a mechanism to transmit communicable diseases such as diarrhea, cholera, dysentery, typhoid and guinea worm infection. Except for poor water,

sanitation and hygiene services (WASH) conditions in communities and institutional settings, slow detection strategies has also been exacerbating the spread of those infectious diseases (WHO and UN-Water. 2014). Timing is extremely important in pathogen detection and the delay or inaccurate diagnosis of the pathogenic infection is always the primary cause of mortality or serious illness. Traditional and standard pathogen detection methods rely on off-line laboratory procedures (consist of multiple cultural enrichment steps, isolation of bacterial colonies, identification) and may take up to 8 days to yield an answer (Lazcka et al., 2007). This slow process clearly can't provide a sufficient protection from exposure to water borne pathogens within public water systems. Furthermore, this processing time-lag can negatively affect tracking of contamination sources because the contamination signal can dissipate or disperse while the initial samples are being processed. In addition, temporal changes in indicator bacteria levels are shorter than the incubation period, which limits the immediacy of posting accurate information to the public.

Outside traditional culturing, molecular assays such as PCR and ELISA are becoming popular tools for pathogen detection (Gibbs. 1990; Lam and Kostov. 2010). These techniques provide high selectivity and reliability; however they usually require intensive sample preparation and special equipment and trained users (Straub et al., 2005). Furthermore, in reality, the debris and competitor organisms in water samples can cross-react with detection systems, rendering false-positive results, or can grow to levels that will mask target organisms (Benoit and Donahue. 2003). That is the main reason why most of these methods are still far from being real-time and online, and

most still require cultural enrichment to enhance sensitivity before the analysis is carried out. Besides, the difficulty of sample handling at extreme low concentrations, and the lack of consistency in highly sensitive detection are still significant problems for pathogen detection and identification. Hence, there is a compelling need for the development of easy-to-use biosensors that could give highly sensitive and reliable detection results, and even allow on-site field monitoring (Kim et al., 2014).

Portable stand-alone biosensors, especially those utilize with coin-size microfluidic chips, are suitable for rapid on-site pathogen detection with accurate diagnostic results.

Electrochemical and optical signal transduction are the most commonly utilized signaling mechanisms in biosensor field over the last 30 years (Ahmed et al., 2014). Electrochemical biosensors comprise of potentiometric, amperometric, and impedimetric sensors. Amperometric biosensors are the earliest and most widely available commercially, especially for glucose detection (Korotcenkov 2010). Although amperometric biosensors possess distinct advantages, such as simplicity and ease of miniaturization, the simple signaling mechanism depending on the applied potential shows low specificity in presence of other redox-active species, inaccurate results are often produced due to the large interference (Higson 2012). Optical biosensors are usually divided into two categories, labeled, or label free. The fluorescence-labeling is the most widely used labeling technique which evolved from the traditional sandwich immunoassays. However, secondary reagents, such as a fluorescence-labeled antibody, are required, and it adds time and cost to the procedure. Surface plasmon resonance (SPR) is a label-free method of optical sensing. By using

various bioreceptors, such as antibodies, bacteriophages, aptamers and lectins, various kinds of SPR biosensors have been developed for the detection of whole bacterial cells. However, the detection sensitivity of SPR biosensor is low because the refractive index changes between bacterial cytoplasm and the aqueous medium are similar, and the interference from biological samples threatens the accuracy of SPR detection (Torun et al., 2012). Surface-enhanced Raman spectroscopic (SERS) is another kind of label-free optical technique and has been widely used in pathogen discrimination. The distinct "fingerprinting" SERS spectra from analytes similar in structures could be acquired, which is essentially important in pathogen detection since discrimination of different bacterial species and strains is difficult. However, as a detection tool, SERS could not been directly used in real on-site cases because SERS requires relatively high concentration of bacteria to obtain detectable spectra (Wu et al., 2013; Grow et al., 2003).

In this study, we developed the concept of self-referencing mechanism that utilizes SERS molecular probes to achieve target bacteria detection in one single step with high reliability brought by a novel multiplex targeting scheme, and integrated the detection methodology with a microfluidic sample preparation platform for easy interrogation of water samples (see figure 5.1).

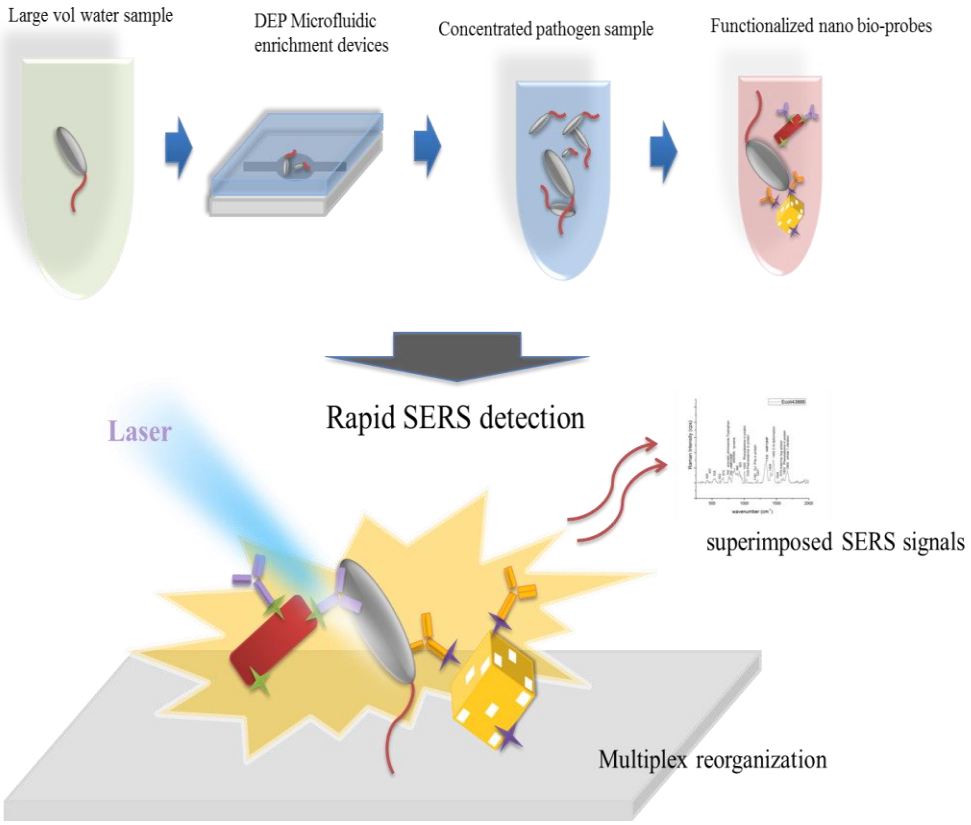

Fig. 5.1 Schematic routine describing the rapid enrichment step using microfluidic device and detection step using the multiplex self-referencing SERS strategy

In the self-referencing scheme, only specific binding of nanoprobes to targets will yield detectable signal, non-specific binding or no-binding will not yield a signal in this scheme, because of the specially designed SERS probes, made from functionalized anisotropic nanoparticles. In Chapter 4, one epitope recognition scheme was designed and tested. Even though the unique vibrational signatures could be identified in the previous experiment design, the reliability and reproducibility seems not consistent enough for distinguishing biotargets in water samples for practical applications. Another consideration is that potential mutation to the binding epitope can render the single-epitope detection scheme completely useless. Expanding the single epitope mechanism, multiple nanoparticle-antibody assemblies are used here in our detection

system for improvement of stain level specificity and signal enhancement. Here, we build up a three-epitope detection scheme (see figure 5.2) to avoid the antibody-antigen binding failure in only one assembly. Briefly, three different types of monoclonal antibodies binding to three different epitopes on the same pathogen cell, the binding events become more distinctive and specific by introducing the different SERS tags with various enhanced signature peaks. Three different Raman tag molecules are selected as probe reporters for nanoparticle functionalization, because of their large Raman cross section, and favorable chemistry for antibody conjugation. The three selected Raman tag molecules have weak signals in the microbial spectral range. Hence, the microbial signals would not be overwhelmed by the enhanced Raman tags peaks in SERS spectra analysis. Obviously, the result would be more credible and the binding events become more distinctive and specific by inducing the different Raman tags with various enhanced signature peaks. In our preliminary test, the limit of detection (LOD) could be improved to 10^1 CFU/mL by using the multiple epitopes self-referencing recognition strategy. Even though this SERS-based scheme could already provide such ultrasensitive and rapid detection results, the required sensitivity needs further improvement. It is reported that the infectious dose of E.coli O157:H7 bacteria is only 10 cells per gram of food, or 0.2 CFU/mL in environmental sample, which underlines the desirability for extremely sensitive and specific pathogen detection (Johnson et al., 1995; Buehler et al., 2004).

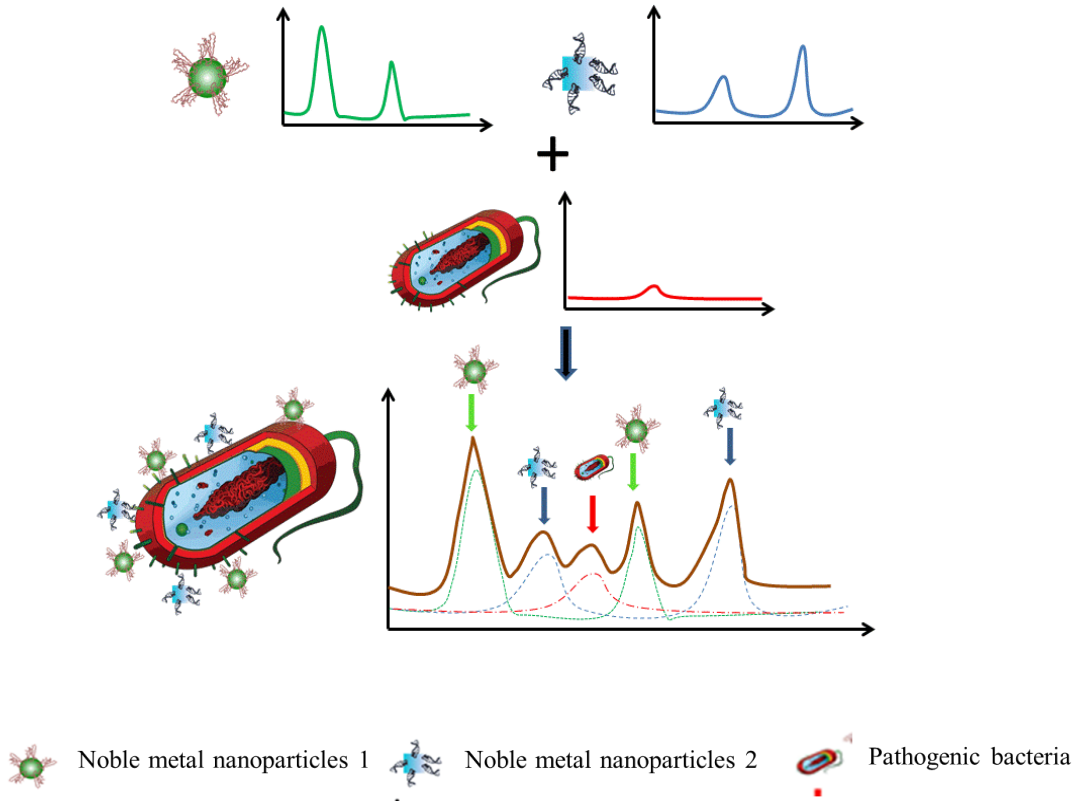

Fig. 5.2 schematic of Multiplex self-referencing pathogen recognition using SERS molecular probes

In order to further improve the LOD in the pathogenic bacteria detection strategy, a novel concentrating technique is also developed in our study by using a nano-Dielectrophoretic (Nano-DEP) microfluidic device. In several studies, DEP has been used to concentrate and separate various types of cells, especially microorganisms. Results obtained by Markx et al. (1996) suggest that E. coli can be separated from M. luteus or B. subtilis with the use of various medium conductivities. As shown in figure 5.3, carbon nanofiber (CNF) nanoelectrode arrays (NEAs) are embedded into this AC nano-DEP microfluidic device for single cell trapping. In this lab-on-a-chip setup the integrated nanoelectrode (NE) tip (in the square position) displays an extremely high electric field gradient (10^{20} V^2 m^{-3}) when applied a voltage source, generating the so called DEP force, a force exerted on a suspended dielectric particle in the presence of

a non-uniform electric field. The DEP is strong enough to achieve cells trapping at high throughput by overcoming the hydrodynamic drag influence. Hence, the DEP microfluidic device is used in our system for low concentration biotargets (10 or below CFU/mL) enrichment. By passing through the bacteria-containing water samples into the device for certain time periods when voltage turning on, the number of the cells trapped on the electrodes increase gradually. After a certain duration of enrichment, the trapped target cells are released in one burst when the voltage is turned off, and they can be collected at a much concentrated level.

The combination of SERS, molecular probes, and microfluidics makes a major step forward towards developing a real field-deployable biosensor for rapid pathogen detection. This approach could be adapted for the detection of a wide variety of bacterial pathogens in food and environmental samples.

5.3.Materials and methods

5.3.1. Nanoprobe fabrication

Materials and methods for bacteria handling and nanoprobes fabrication could be found in Chapter 3.

The SERS spectra of three nanoprobes are shown in Figure 5.4. By comparing the Raman intensities of these three probes, the enhancement factors from diazo bonding conjugation (4-ATP-antibody and ATT-antibody) are larger than EDC/NHS bonding (3-MPA-antibody). The nanorod-4ATP-antibody showing the highest enhancement factor is due to the 2 or 3 nanorod cluster formation through DMAB which has been explored in the appendix.

5.3.2. Testing of the microfluidic device

By using the microfluidic device, cell enrichment could be achieved in a continuous sample preparation step. Two different *E.coli* strains were mixed: *E.coli* O157:H7 (pathogenic) and *E.coli* K12 (non-pathogenic) and used to test the efficiency of the microfluidic device. The mixture was used so that the specificity of the self-referencing mechanism in the following SERS measurement can be investigated. Two E. coli strains were diluted to extremely low concentrations and mixed together uniformly. 1 mL of the mixed cell suspension at ~10^0 CFU/mL was passed through the microfluidic device. At a flow rate of 1 μL per min, it took about 17 hours for the 1 mL sample to be processed. We then collected the concentrated samples (1 mL→ 100 μL, 10X, a concentration of ~10^1 CFU/mL). As a result, the LOD of the multiple nanoprobes (10 CFU/mL) could be improved to 1 CFU/mL by using microfluidic device. Two different mixed cell suspensions with different concentration ratios (between *E.coli* O157:H7 and *E.coli* K12) were chosen in the testing. One was 1 CFU/mL (*E.coli* O157: H7) : 1 CFU/mL (*E.coli* K12); the other was 1 CFU/mL (*E.coli* O157:H7) : 10 CFU/mL (*E.coli* K 12). The concentration of original mixed cell suspension and the concentrated suspension were validated by plate counting. The results are shown in figure 5.5.

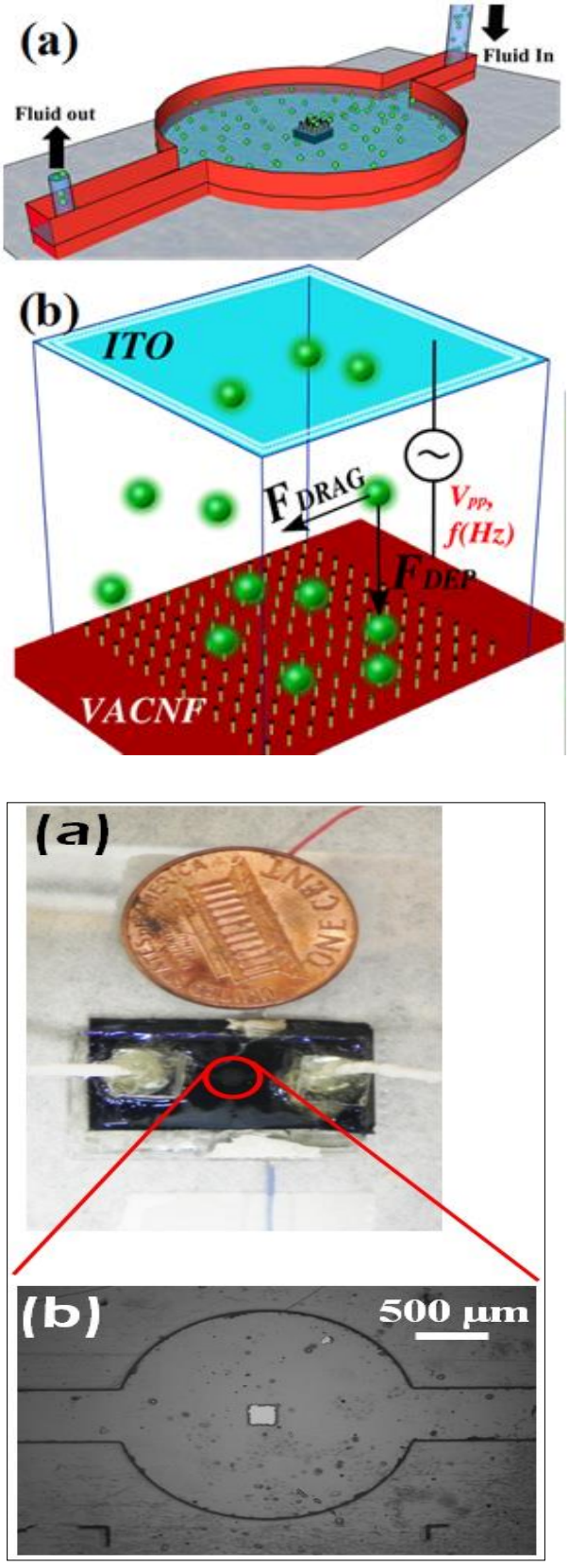

Fig. 5.3 Schematic illustration of nano-DEP microfluidic device and the actual dimension under microscope

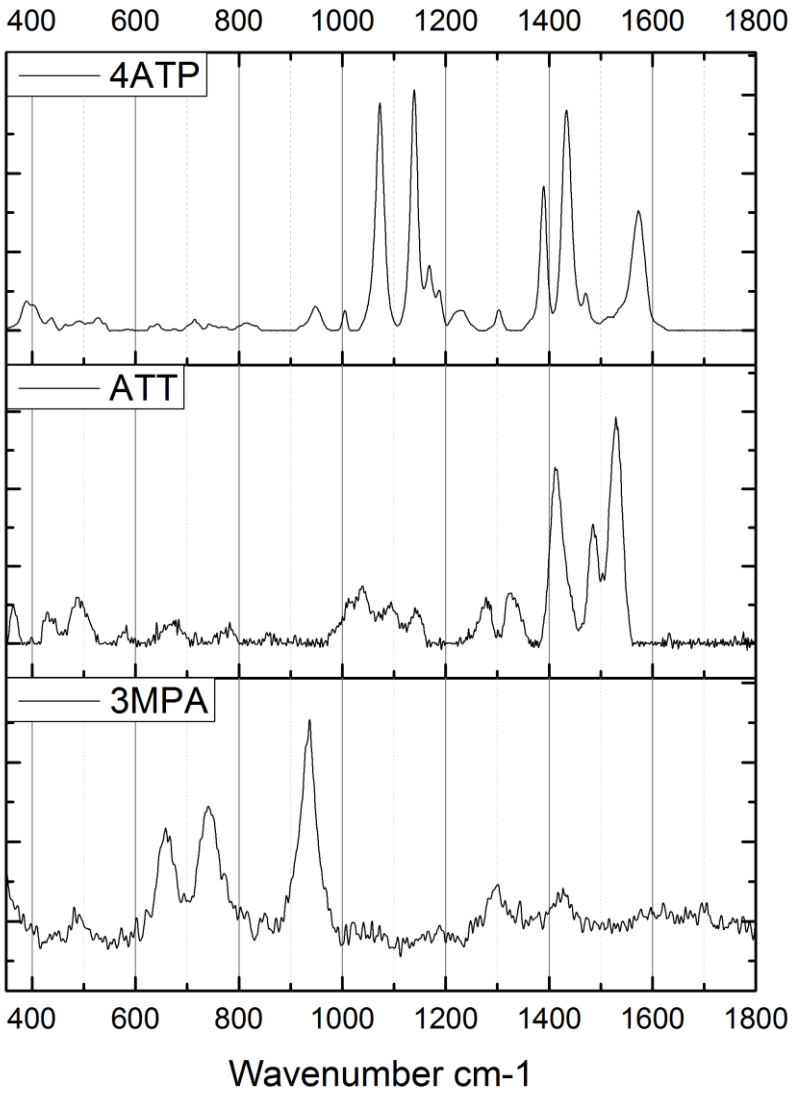

Fig. 5.4 SERS spectra of three nanoprobes: nanorod-4ATP-monoclonal antibody; nanorod-ATT-monoclonal antibody; nanocage-3MPA-polyclonal antibody.

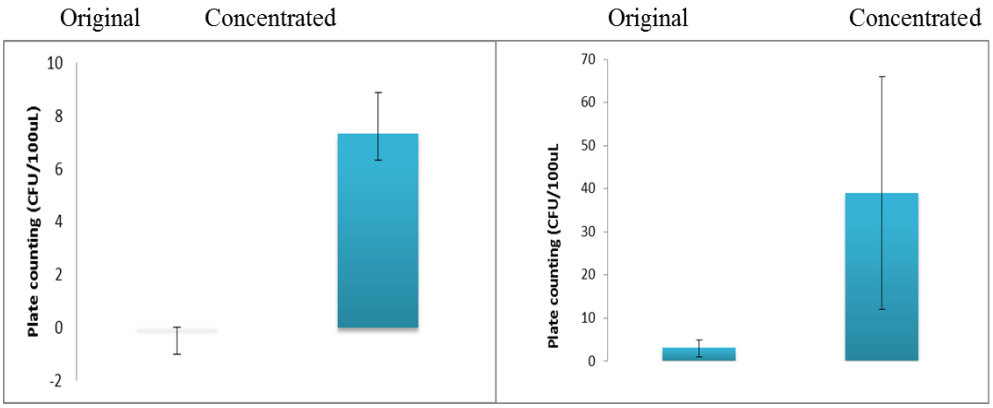

Fig. 5.5 Plate counting results for two concentration ratios: left: O:K=1:1 (CFU/mL in original solution); right: O:K=1:10 (CFU/mL in original solution)

Even though the low concentration bacterial sample enrichment could be achieved using a Nano-DEP microfluidic device, the processing is too time-consuming to make it implementable on-site and establish a dynamic monitoring routine. To resolve this problem, parallel packing of thousands Nano-DEP devices will be utilized in the future experimental design. As we observed, processing 1 mL water sample using single Nano-DEP device demands 17 hours; however, if we pack 1000 devices and pass the water solution in a parallel mode (see figure 5.6, only 1 second is needed to concentrate 1 mL water sample. The dimensions of single device and a thousand devices are $20mm \times 20 \times 1.5mm$ and$100mm \times 100mm \times 60mm$, respectively.

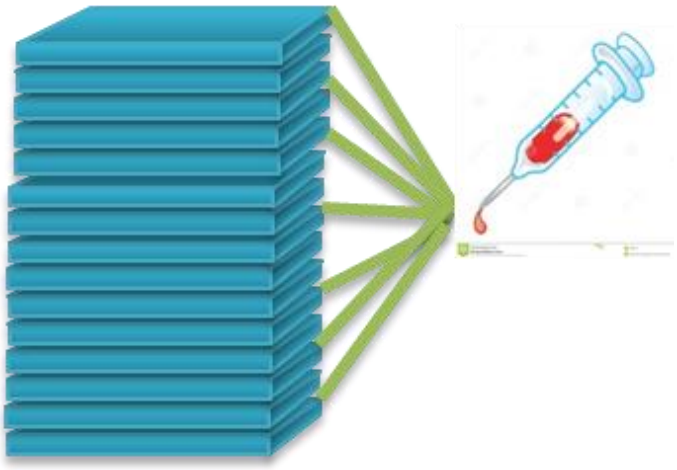

Fig. 5.6 schematic of parallel packing of thousands of DEP microfluidic devices

5.3.3. SERS measurement

Different batches of nanoprobes were used for each mixed sample to test the reproducibility of the SERS measurement. Several droplets of sample solutions were placed on gold-coated microscope slide, and multiple SERS spectra were obtained from different positions on each droplet.

All experiments were conducted in Biosafety level 2 approved facilities with proper safety training and approval in place.

5.4. Result and Discussion

In our self-referencing scheme, the SERS signatures of the target bacteria are observed superimposed with the SERS signals of the Raman tags. The assessment through the dual signals (superimposed target and tag Raman signatures) support a specific recognition of the targets in a single step with no washing/separation needed. Nevertheless, the observation of the dual signals could only be observed when the conjugated bacterial cell wall components fall into the hotspot regions of the nanoprobes. Hot spots are highly localized regions of intense local field enhancement believed to be caused by local surface plasmon resonances. It has been claimed that the hot spots could provide extraordinary enhancement of up to 10^{15} orders of magnitude to SERS signal (Michaels et al., 2000; Xu et al., 2000; Futamata. 2006; Jiang et al., 2003). Additionally, the effective enhancement regions on anisotropic nanoparticle surfaces usually locate at the sharp edges and corners. Therefore, the enhanced type of spectra are not expected in every single measurement. Besides, the focusing point in the colloidal state liquid sample is randomly selected for all collection in order to obtain a big and random database to fulfill the requirement in the following statistical data analysis chapter.

Among all the spectra collection, most are non-enhanced Raman spectra (data not shown) in which the significantly enhanced Raman fingerprint signatures are not identifiable from both Raman tag and bacteria; and 20% of the acquired spectra are

considered as SERS spectra. Among the enhanced spectra, two types of SERS spectra could be identified: one is non-binding (probe signal) type in which only the featured peaks from three Raman tag molecules could be found, indicating that the probes are not bound to bacterial cells; the other is binding (dual signal) type in which both Raman tags' peaks and bacterial peaks are significantly enhanced. From the non-binding SERS type, two subtypes are identified because of the variation of the amount of three different nanoprobes at the random measurement focus spots. Most of the featured peaks from three Raman tags could be found in both subtypes; however, the intensities of those peaks are different. The average SERS spectra of these two subtypes are shown in Figure 5.7. The non-binding and binding types SERS spectra are shown in figure 5.8. The peaks from Raman tags are assigned at the top of this figure. Besides the Raman tags SERS peaks, some weak-intensity peak could be identified in the microbial information rich region (500-1000 cm^{-1}). The peak assignment for bacterial components in binding type SERS spectra is shown in figure 5.9. The pure and high-concentration *E.coli* O157:H7 is also exhibited in this figure for reference. As we know, the surface enhancement of nanostructures is highly distance dependent and the electromagnetic field decays exponentially away from the nanoparticle's surface. Hence, the Raman tag molecules, as the nearest conjugated layer, exhibit the highest Raman peaks intensity. In contrast, the outside layer bacterial cell wall components show relatively weaker peak intensity (see figure 5.9). Additionally, some of the important microbial components (marked as red color wavenumber) peaks could not be clearly identified due to the overlapping with the Raman tags featured signals. Hence,

it is necessary to investigate proper data mining techniques for bacterial pathogens in strain level pattern recognition, employing reference libraries due to the similarity between the spectra of different E.coli strains. Thus, different statistical analysis methods are utilized for data analysis, which are described in the next chapter.

5.5. Conclusion

This novel multiplex self-referencing SERS pathogen detection scheme offers high sensitivity (10^1 CFU/mL) and strain level discrimination by measuring the superimposed SERS signatures with multiple characteristic peaks. Multiple epitopes being assessed simultaneously could avoid false negative results due to mutations to any of the binding epitopes. Furthermore, the superimposed spectra could be obtained directly with no washing being performed. Compared to the ELISA kits, this platform can isolate and identify bacteria in water samples without the need for repeated wash steps and secondary antibody reporting, hence significantly reducing the operation processes, detection time and the cost. In addition, this platform demonstrated excellent separation and concentration capacities by using DEP microfluidic devices and further improves the sensitivity to single cell per mL. The miniaturized microfluidic device potentially can be used to concentrate the extremely low concentration target pathogen to a detectable level in short period of time.

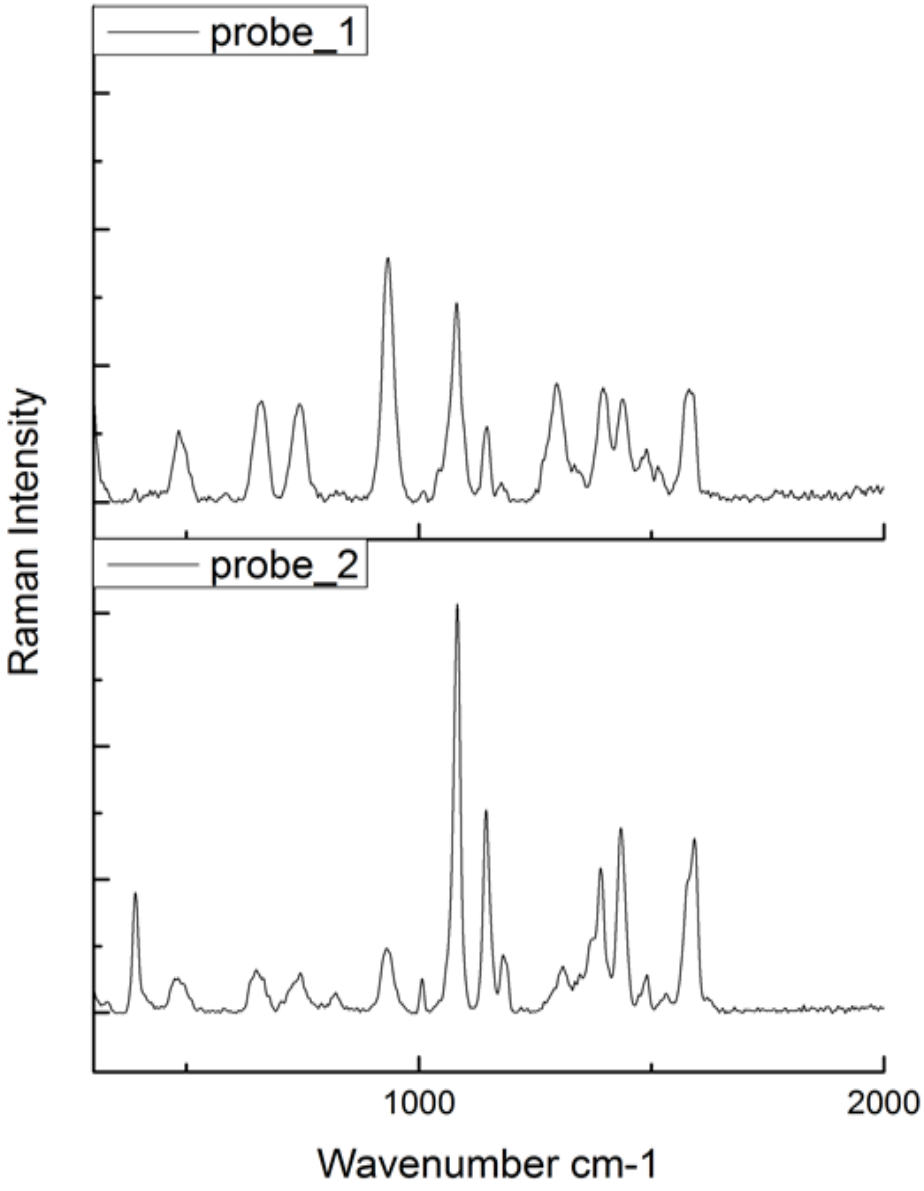

Fig. 5.7 SERS spectra of two subtypes of non-binding (probe signal)

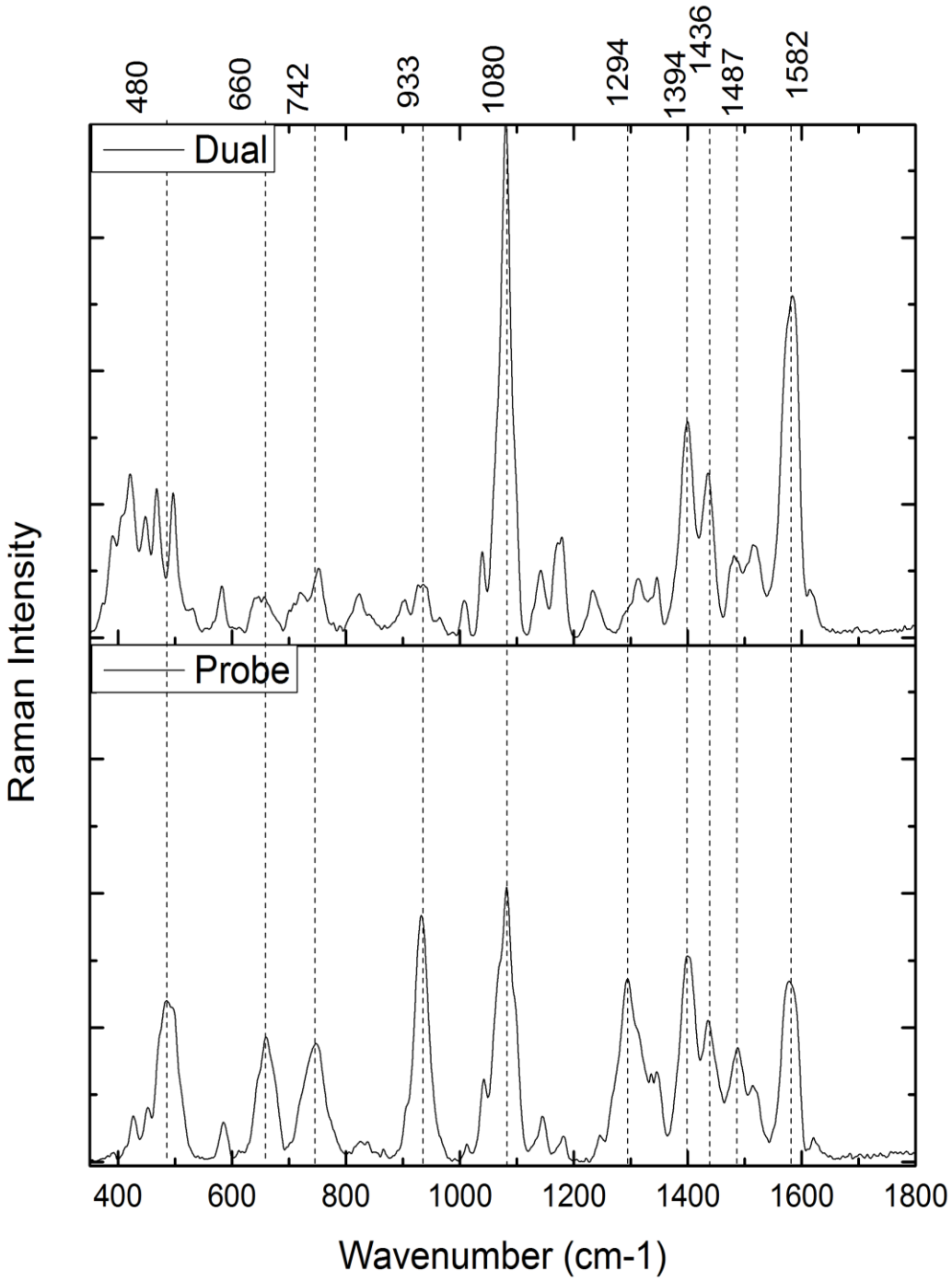

Fig. 5.8 SERS spectra and peak assignment of non-binding (probe signal) type and binding (dual signal) type; the marked peaks are the featured Raman peaks from three Raman tag molecules

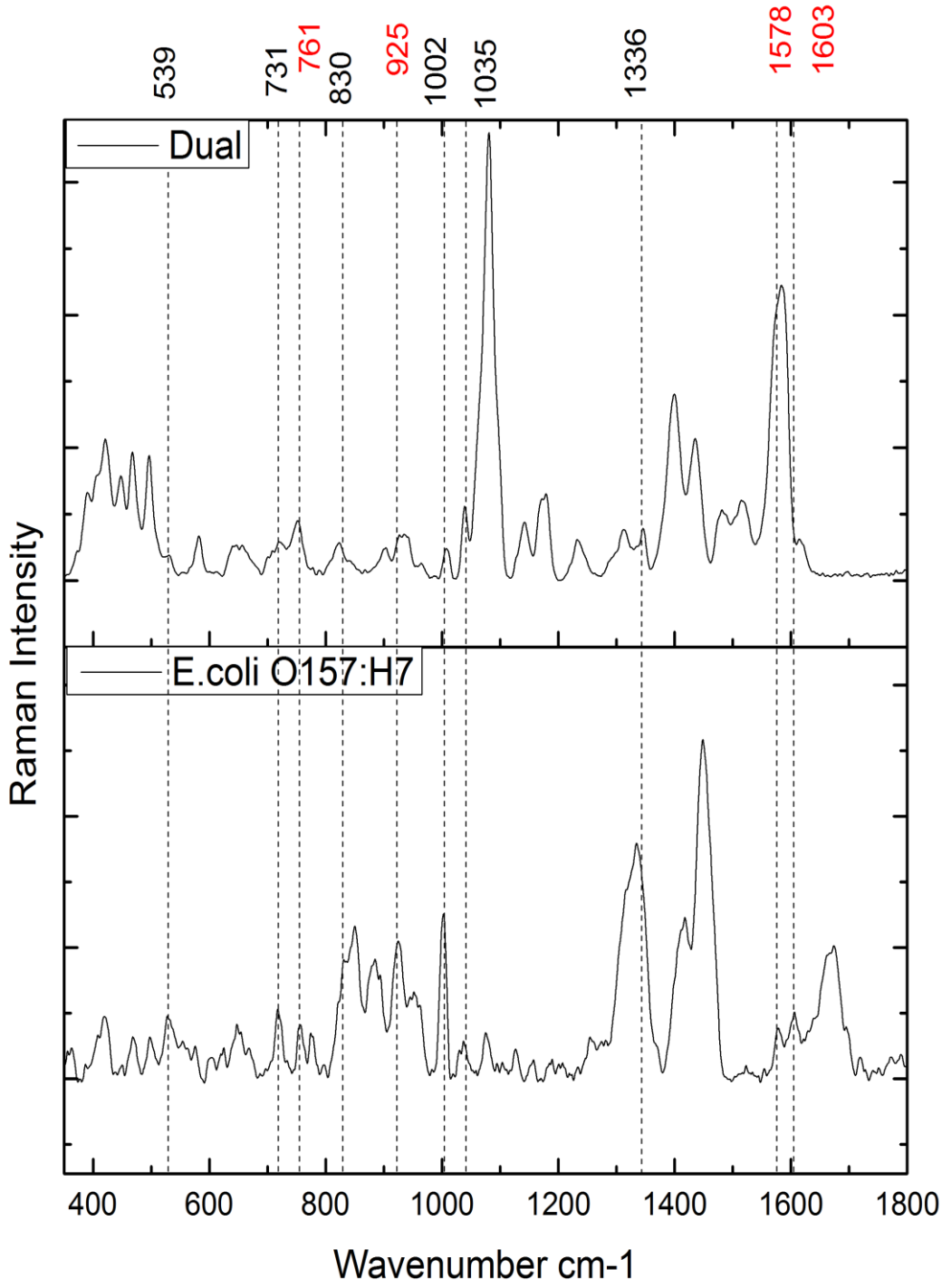

Fig. 5.9 SERS spectra and peak assignment of binding type and normal Raman spectra of pure & high-concentration *E.coli* O157: H7 bacteria

5.6. Reference

Ahmed A, Rushworth JV, Hirst NA, Millner PA 2014 Biosensors for Whole-Cell Bacterial Detection *Clin. Microbiol. Rev*. 27(3) 631

Benoit PW, Donahue DW 2003 Methods for Rapid Separation and Concentration of Bacteria in Food that Bypass Time-Consuming Cultural Enrichment. *J. Food Protection*. 66 1935-1948.

Buehler S, Dindal A, Willenberg Z, Riggs K 2004 Environmental Technology Verification Report-- Applied Biosystems TaqMan® E. coli O157:H7 Detection System *USEPA. Battelle. Columbus 43201*

Cheng H, Huan S, Wu H, Shen G, and Yu R 2009 Surface-enhanced Raman spectroscopic detection of a bacteria biomarker using gold nanoparticle immobilized substrates *Analytical Chemistry* 81 9902-9912

Cheng IF, Lin CC, Lin DY, Chang HC 2010 A dielectrophoretic chip with a roughened metal surface for on-chip Surface Raman Enhanced Scattering analysis of bacteria *Biomicrofluidics.* 4 034104

Culha M, Adigüzel A, Yazici M, Kahraman M, Sahin F, Güllüce M 2008 Characterization of thermophilic bacteria using surface-enhanced Raman scattering *Applied Spectroscopy* 62 1226-32

Eghtedari M, Liopo A, Copland J, Oraevsky A, and Motamedi M 2009 Engineering of hetero-functional gold nanorods for the in vivo molecular targeting of breast cancer cells *Nano Lett*. 9 287-91

Fan C, Hu Z, Mustapha A, Lin M 2011 Rapid detection of food-and waterborne bacteria using surface-enhanced Raman spectroscopy coupled with silver nanosubstrates *Appl. Microbiol. Biotechnol.* 92 1053-1061

Futamata M 2006 Single molecule sensitivity in SERS: importance of junction of adjacent Ag nanoparticles *Faraday Discuss*. 132 45–61

Gibbs R 1990 DNA amplification by the polymerase chain reaction. *Anal. Chem*. 62 1202-1214.

Grow AE, Wood LL, Claycomb JL, Thompson PA 2003 New Biochip technology for label-free detection of pathogens and their toxins *J. Microbiol*. *Methods*. 53 223-233

Hasan J, States S, Deininger R 2004 Safeguarding the security of public water supplies using early warning systems: A brief review *Water Res. Ed.* 129 27-33

He L, Liu Y, Lin M, Mustapha A, Wang Y 2008 Detecting single Bacillus spores by surface enhanced Raman spectroscopy *Sens & Instument Food Qual*. 2 247-253

Higson SP 2012 Biosensors for medical applications *Woodhead Publishing, Cambridge, United Kingdom*

Huelseweh B, Ehricht R, Marschall H 2006 A simple and rapid protein array based method for the simultaneous detection of biowarfare agents *Proteomics* 6 2972-2981

Ibelings M, Maquelin K, Endtz H, Bruining H, and Pupples G 2005 Rapid identification of Candida spp. in peritonitis patients by Raman Spectroscopy *Clinical Microbiology and Infection* 11 353-358

Jarvis R and Goodacre R 2004 Discrimination of bacteria using surface enhanced Raman spectroscopy *Analytical Chemistry* 76 40-47

Jiang J, Bosnick K, Maillard M, Brus L 2003 Single molecule Raman spectroscopy at the junctions of large Ag nanocrystals *J Phys Chem B.* 107 9964–9972

Johnson JL, Rose BE, Sharar AK, Ransom GM, Lattuada CP, Mcnamara AM 1995 Methods used for detection and recovery of Escherichia coli O157h7 associated with a food-borne disease outbreak *J. Food Prot.* 58 597-603

Kim J, Ko S, Yun G Kim J 2014 Disposable chemical sensors and biosensors made on cellulose paper *Nanotech.* doi:10.1088/0957-4484/25/9/092001

Korotcenkov G 2010 Chemical sensors, vol 1. General approaches. *Momentum Press, New York, NY.*

Lam H, Kostov Y 2010 Optical instrumentation for bioprocess monitoring Adv. Biochem. Eng. Biotechnol. 116 125-142

Lazcka O, Campo F, Munoz F 2007 Pathogen detection: A perspective of traditional methods and biosensor *Biosensors and Bioelectronics*. 22 1205-1217

Leonard P, Hearty S, Brennan J, Dunne L, Quinn J, Chakraborty T, O'kennedy R, 2003. Enzyme *Microb. Technol*. 32, 3-13

Lopez M, Bertolini E, Olmos A, Caruso P, Gorris M, Llop P, Penyalver R, Cambra M 2003 Innovative tools for detection of plant pathogenic viruses and bacteria *Int. Microbiol*. 6 233-243

Lopez-Diez K and Goodacre R 2004 Characterization of microorganisms using UV resonance Raman spectroscopy and chemometrics *Analytical Chemistry*. 76 585-591

Magliulo M, Simoni P, Guardigli M, Michelini E, Luciani M, Lelli R, Roda, A A Rapid multiplexed chemiluminescent immunoassay for the detection of *Escherichia coli* O157:H7, *Yersinia enterocolitica*, *Salmonella typhimurium*, and *Listeria monocytogenes* pathogen bacteria *J. Agric. Food Chem*. 55 4933-4939

Maquelin K, Kirschner C, Choo-Smith L, van den Braak L, Endtz H, Naumann D, and Pupples G 2002 Identification of medically relevant microorganisms by vibrational *spectroscopy J. of Microbiological Methods* 51 255-271

Markx GH, Dyda PA, Pethig R 1996 Dielectrophoretic separation of bacteria using conductivity gradient *J. Biotechnol*. 51 175-180

Michaels AM, Jiang J, Brus L 2000 Ag nanocrystal junctions as the site for surface-enhanced Raman scattering of single rhodamine 6 G molecules *J Phys Chem B.* 104 11965–11971

Mühlig S, Cialla D, Cunningham A, März A, Weber K, Bürgi T, Lederer F, Rockstuhl C 2014 Stacked and Tunable Large-Scale Plasmonic Nanoparticle Arrays for Surface-Enhanced Raman Spectroscopy *J. Phys. Chem. C.* 118 10230-10237

Nielsen U, Geierstanger B 2004 Multiplexed sandwich assays in microarray format *Immunol. Methods.* 290 107-120

Nikoobakht B, El-Sayed M 2003 Preparation and Growth Mechanism of Gold Nanorods (NRs) Using Seed-Mediated Growth Method *Chem. Mater*.15 1957-1962

Petry R, Scmitt M, and Popp J 2003 Raman spectroscopy - a prospective tool in the life sciences *Chemical and Physical Chemistry* 4 14-30

Sengupta A, Brar N, and Davis E 2007 Bioaerosol detection and characterization by surfaceenhanced Raman spectroscopy *Journal of Colloid and Interface Science* 30936-43

Sharma S, Sachdeva P, Virdi J 2003 Emerging water-borne pathogens *Appl. Microbiol. Biotechnol.* 61 424-428

Straub T, Dockendorff B, Quinonez-Diaz M, Valdez C Shutthanandan J Tarasevich B, Grate J, Bruckner-Lea C 2005 Automated methods for multiplexed pathogen detection, *J Microbiol Methods J. Microbiol. Methods* 62 303-316

Torun O, Boyaci IH, Temur E, Tamer U 2012 Comparison of sensing strategies in SPR biosensor for rapid and sensitive enumeration of bacteria. *Biosens. Bioelectron*. 37 53-60

Tsien R and Waggoner A 1995 Fluorophores for confocal microscopy J.B. Pawley, Handbook of biological confocal microscopy, New York, Plenum Press 267-274

UN-water global analysis and assessment of sanitation and drinking-water (GLAAS) report 2014

http://apps.who.int/iris/bitstream/10665/139735/1/9789241508087_eng.pdf?ua=1

Wu X, Xu C, Tripp R, Huang Y, Zhao Y 2013 Detection and differentiation of foodborne pathogenic bacteria in mung bean sprouts using field deployable label-free SERS devices *Analyst*. 138 3005-3012

Xu HX, Aizpurua J, Kall M, Apell P 2000 Electromagnetic contributions to single-molecule sensitivity in surface-enhanced Raman scattering *Phys Rev E*. 62 4318–4324

Yang K and Trewn J 2004 Multivariate Statistical Methods in Quality Management, New York

Ye J, Wen F, Sobhani H, Lassiter JB, Van Dorpe P, Nordlander P, Halas NJ 2012 Plasmonic Nanoclusters: Near Field Properties of the Fano Resonance Interrogated with SERS *Nano Lett*. 12 1660-1667

Zhao J, Pinchuk AO, McMahon JM, Li S, Ausman LK, Atkinson AL, Schatz GC 2008 Methods for Describing the Electromagnetic Properties of Silver and Gold Nanoparticles *Acc. Chem. Res.* 41 1710-1720

5.7. Appendix: Nano-DEP microfluidic device capture ability test and The conversion of 4-ATP to DMAB happened on the surface of GNRs

Nano-DEP microfluidic device capture ability test

Before the enrichment testing, we demonstrated the capture ability of the DEP device as well as the optimal parameters of the device for trapping our specific pathogenic target. Briefly, GNR-ATP was conjugated with Anti-*E.coli* antibody labelled with Fluorescein isothiocyanate (FITC) fluorescein and then the complex was perfectly mixed with 10^3 CFU/mL *E.coli* bacteria solution. After passing the mixed sample into microfluidic device, the fluorescence imaging were achieved (see Fig. S5.1) under microscope. The optimized condition of microfluidic device for pathogenic *E.Coli* ATCC 43888 was also found: 200 KHz frequency, 10 V_{pp} AC voltages, and 1.0 ul/min passing speed. Besides, the concentrating efficiency was inspected by plate culturing the bacteria samples before/after concentrating within the microfluidic

devices. Even though we successfully trapped the labelled bacteria cells in the microfluidic device, we didn't conduct direct SERS measurement on chip. In fact, on-chip single step detection is the ideal strategy to utilize SERS-microfluidic detection system. However, it is a great challenge to accurately focus laser spot through the cover of the microchannel on the trapped the target bacteria cell with nanoprobes complex. Additionally, the TIO and Polydimethylsiloxane (PDMS) materials used in microfluidic device are Raman active materials which have their own Raman scattering signals. As a result, the strong background in the measured spectra dramatically decreased the detection sensitivity of the target. In the future, in situ SERS measurement is required to be implemented because the integration of a microfluidic device provides a well-defined detection environment, leas to constant aggregation behavior and processes more reproducible SERS spectra. It would increase the consistent enhancement of nanoprobes.

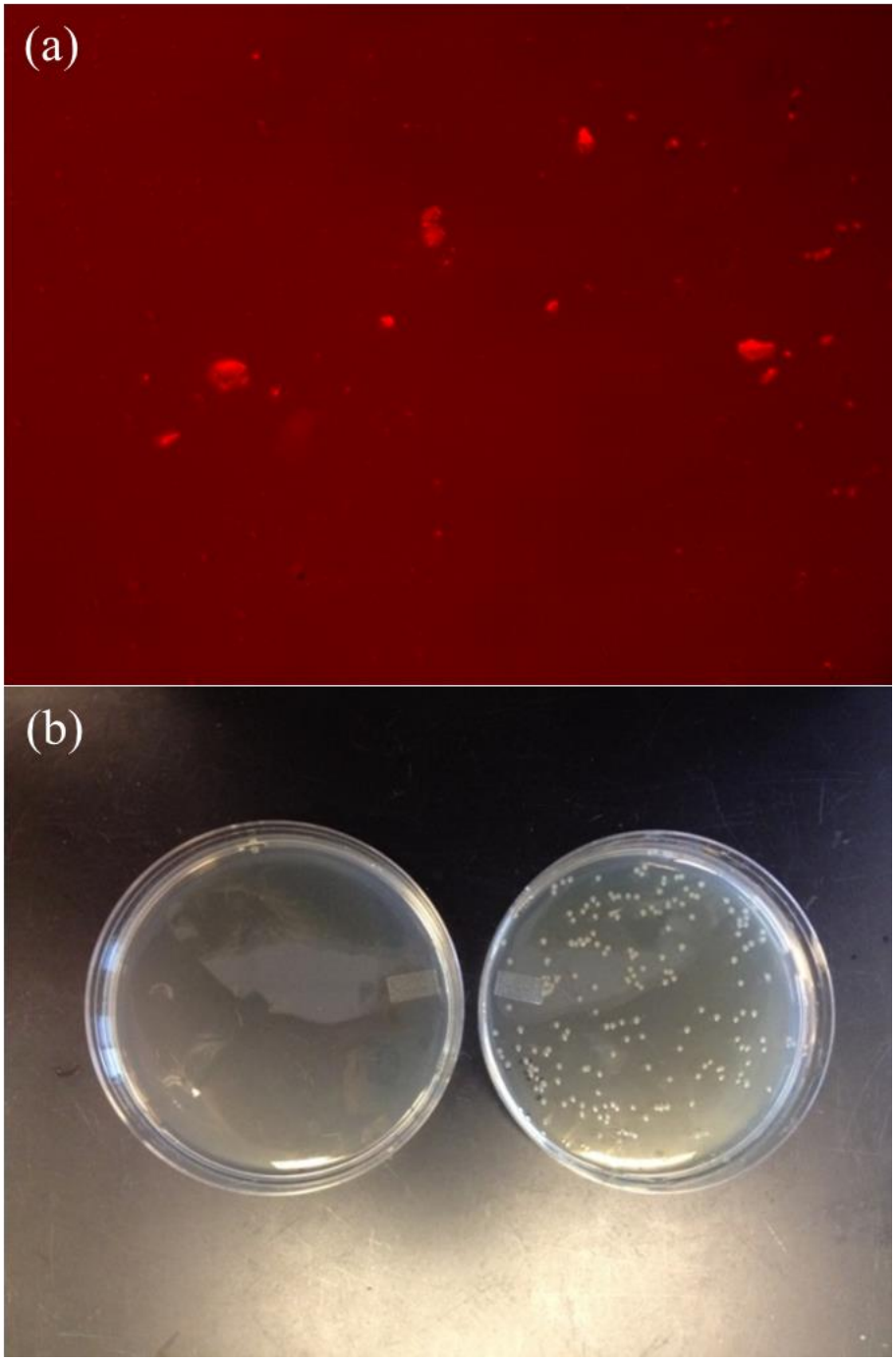

Fig. S5.1 (a) Fluorescence imaging of nanoprobes-FITC-Antibody mixing with bacteria (b) the contrast before/after passing low concentration bacteria into microfluidic device (passing 3mL 30 CFU/mL bacteria into device and 30 μL enriched solution was collected).

The conversion of 4-ATP to DMAB happened on the surface of GNRs

It is a novel functionalization method to form 4,4-dimercaptoazobenzene (4,4-DMAB) from 4-aminothiophenol (4-ATP) in the process of gold nanorods surface modification. The formation of 4,4-DMAB could dramatically enhance the Raman scattering of conjugated molecules using Surface-enhanced Raman scattering (SERS) technique. After GNRs are synthesized through seed-mediated growth method with aspect ratios of 3~4 (Nikoobakht and El-Sayed, 2003) in our lab, 4-ATP is chosen as the covalent-bonding linker molecules to functionalize GNRs through thiol-Au linkage. The main reason of selecting 4-ATP is that 4-ATP could efficiently immobilize his-tags rich proteins by forming diazo coupling between diazonium moiety in 4-ATP molecule and histidine tags (Wu et al., 2006, Eghtedari et al., 2009). Besides, 4-ATP is also a Raman active molecule which could be called “SERS tags” showing distinguishable Raman spectral signatures.

Anisotropic gold or silver nanostructures (i.e., rods, cube and cages) are known to cause strong local electric field enhancement compared with isotropic structures (nanosphere), therefore highly improve the SERS signals. Gold nanorods represent one class of nanostructures with tunable LSPR peaks in the NIR region by controlling the size and shape. These versatile nanostructures can be prepared in large quantities with a remarkably simple protocol. In addition, the local fields can be further enhanced by near-field coupling between neighboring NPs (Mühlig et al., 2014). It has been demonstrated that complex resonances resulting from NPs clusters can exhibit huge local field enhancement to yield high intensity of SERS signals (Ye et al., 2012).

However, it is still challenging to fabricate suitable resonance coupling SERS substrates in biosensing platforms. As a nanocarrier, particles or clusters have been synthesized using wet-chemistry methodologies rather than electron beam lithography, hence it is difficult to deposit nanostructures and control the interparticle space between neighboring NPs to obtain the maximum enhancement. Besides, an ideal candidate of nanomaterial carriers should not aggregate at high concentrations in phosphate buffered saline (PBS) or in the circulation after intravenous injection in animals. To mitigate these two problems, the optimization of GNR synthesis is necessary. In this study, we designed and implemented a new surface modification method using anisotropic gold nanorods to build up the SERS substrates. DMAB/4-ATP is used as the functional linker molecules to both form stable 3-particle nanoclusters and to further enhance the SERS spectral signals.

DMAB is considered showing remarkable SERS spectral features after conjugating with nanostructures. However, only limited data are available on DMAB spectral exploration because it has to be custom synthesized. In this study, we discovered a novel protocol to generate DMAB from 4-ATP through simple long-period oil bath heating. Furthermore, the local fields as well as the SERS signals intensities can be further enhanced by near-field coupling between neighboring nanoparticles, forming the so-called “hotspots” (Mühlig et al., 2014; Ye et al., 2012). Therefore, when analytes molecules are entrapped by two or more nanoparticles aggregate, the Raman spectroscopic signals of target cells would be significantly enhanced. The hypothetical mechanism of the DMAB synthesis guaranteed the generation of stable nanoparticles

aggregate. As a result, Raman signals from target cells could be further enhanced even at extremely low concentration.

Recently, Xu et al. (2013) investigated the mechanism of surface plasmon assisted catalysis reactions of 4-ATP to and back from 4,4-DMAB. Briefly, hot electrons generated during long incubation period are regarded as the species that mediate the conversion of 4ATP to DMAB, which is a chemically reduction reaction (Sun and Xu. 2013; Kim et al. 2010). In particular, GNR surface provided rich electrons which transferred from the $–NH_2$ groups to give $–NH^{2+}$ radial cations and then a diphenylhydrazine intermediate, Ar-NH-NH-Ar was induced. After a second two-electron loss and deprotonation steps, the DMAB were formed on GNR particles surface (The schematics could be found in figure S5.2). We also found the existing of oxygen and water is necessary to act as the electron acceptor and deprotonation agent, respectively. In order to prove this hypothesis, N_2 atmosphere is introduced to deprive O_2. Results showed no conversion of 4-ATP to DMAB occurring after long time period of incubation due to the lack of electrons acceptors (data not shown).

The Raman spectra (Fig. S5.3) between the shorter and longer incubation times can be clearly distinguished from the new Raman bands at 1390 and 1432 cm^{-1} (azo bond, N=N) as well as the band at 1140 cm^{-1} (β(CH) from DMAB).

Following this mechanism, we optimized the GNR-4-ATP functionalization process and successfully fabricated the stable and suitable SERS colloids, dimer and/or trimer GNR clusters.

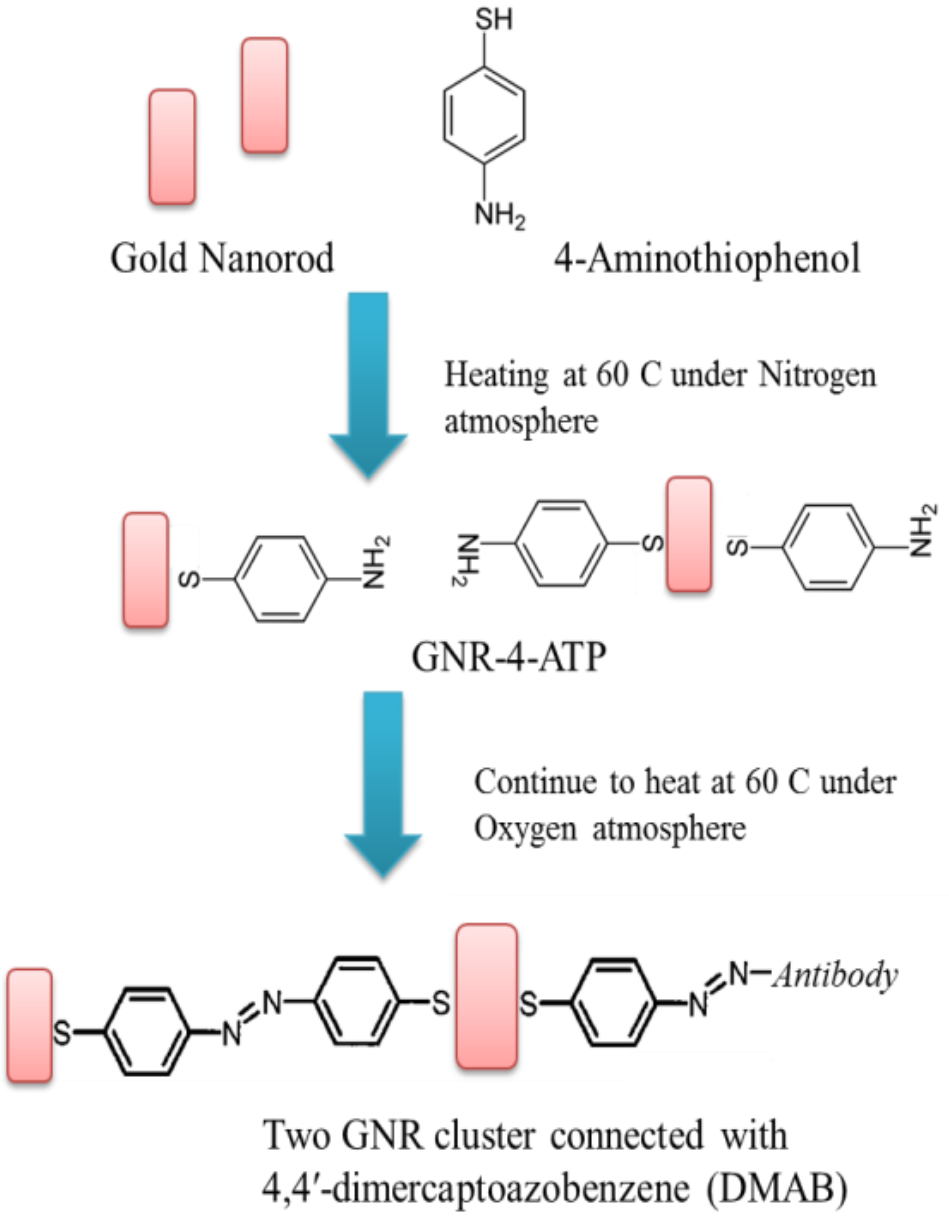

Fig. S5.2 Schematic illustration of conversion from 4-ATP to DMAB occurred on the nanorods surface.

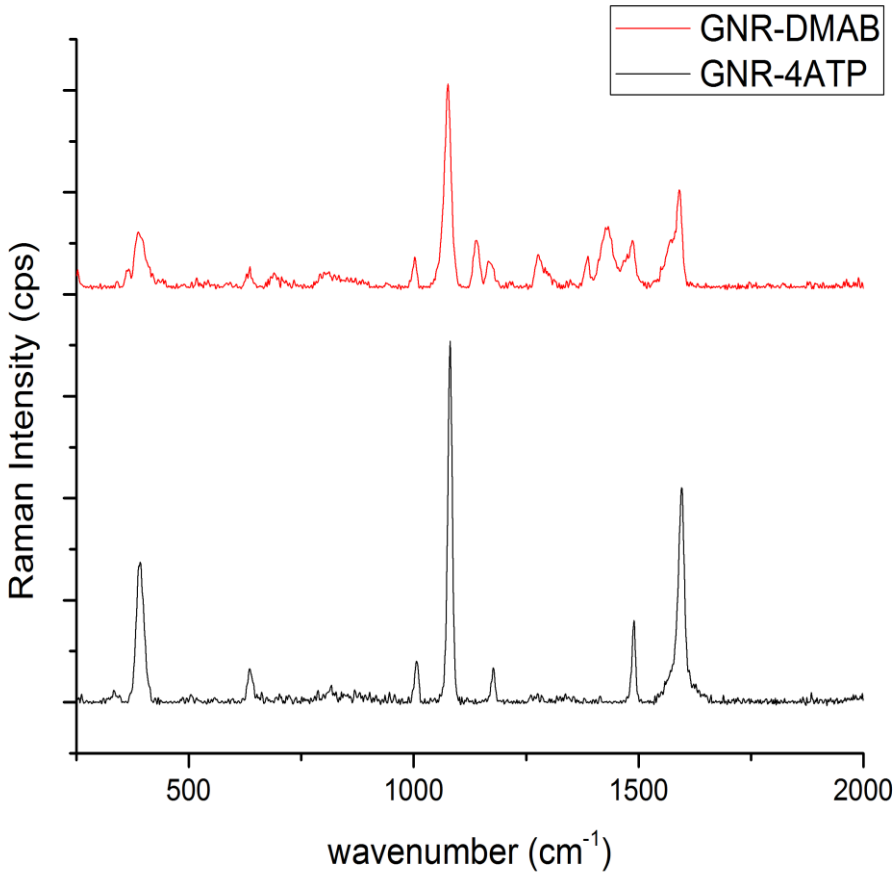

Fig. S5.3 SERS spectra of GNR-4ATP. Red: DMAB signatures found spectrum with longer incubation time; Black: 4-ATP signatures shown with shorter incubation time

CHAPTER 6. IDENTIFICATION OF TARGET BACTERIA BY STATISTICAL AANALYSIS OF DUAL-RECOGNITION RAMAN FINGERPRINTS

Although the SERS spectra of the sample can be easily differentiated from the non-enhanced Raman spectra of the control, the reproducibility of the SERS-based analysis is still not ideal. The variations could be due to the nature of the SERS process, where even the same analyte (i.e., chemically heterogeneous bacterium) cannot be expected to repeatedly satisfy all of the criteria for SERS, namely, orientation, and presence within the range of the enhanced local optical field (Jarvis and Goodacre. 2004). Improvement of the reproducibility could be achieved by optimizing the uniformity of the coverage of nanoprobes onto the analyte in binding process, or extending the collection time to obtain more spectral data that satisfy the SERS conditions, or by implementing statistical analysis to the data to highlight SERS-specific patterns in the data acquired.

6.1. Data preprocessing

Data analysis was conducted using R studio software. Preprocessing algorithms were employed to the data, including smoothing, baseline correction, area normalization, and mean centering in order to compensate for variations in experimental conditions, and to develop accurate calibration models. The regions above 2000 and below 350 cm^{-1} were excluded to minimize noise effects. The information in the lower wavenumber region cannot be completely recorded due to the limitation of bandwidth of the filter applied to suppress the Rayleigh line. The microbial Raman

fingerprinting region is usually from 300-1900 cm^{-1}, therefore the higher wavenumber region is also excluded to reduce the non-essential spectral changes, and numbers of variables.

Measurement variables are subject to scaling effect which are due to properties of samples (e.g., concentration). In spectroscopic applications, the measured variables usually experience a different level of scaling because of a multiplicative factor. The multiplicative factor resulting from scattering effects, source or detector variations, or other general instrumental sensitivity effect. Normalization is a critical preprocessing step in Raman spectra analysis in order to correct those effects by identifying some aspect of each measurement which should be essentially constant from one measurement to the next. The excellent normalization should separate the scaling effects from the interfering systematic effect (Rinnan et al., 2009; Afseth et al., 2006). Available algorithms include maximum intensity normalization, spectra area normalization and specific peak area normalization. Area normalization is used in our study. Briefly, it is produced by setting the area under the spectrum to unit one. That is, the content of all chemicals are considered as the same and their composition could be examined afterwards.

As discussed earlier, the spectra of biological samples suffer from strong fluorescence background. The strong background signals could obscure the real Raman signals from target cells. To suppress the background in order to obtain further qualitative or quantitative analysis of the spectra, some methods using experimental techniques have been developed. A drop-coating deposition Raman method was

described to reduce the fluorescence of commercial amino acid and protein samples (Zhang et al., 2004). Oshima et al., (2006) developed a shifted excitation method to decrease the protein fluorescence background. Liquid-core optical fiber waveguides was also used in Raman spectra collection in order to suppress the fluorescence (Pelletier and Altkorn. 2000). In this study, NIR laser of 780 nm wavelength was used to photobleach initially strong fluorescent background, then reduce the sample fluorescence. Even though these methods perform well in rejecting the background, the costs of equipment and sample preparation are expensive to implement. Especially when considering on-site monitoring, it is difficult to miniaturize these methods into the portable Raman spectrometers. Therefore, using computational methods to preprocess the raw Raman spectra might be a more efficient and cheaper way to reject the fluorescence influence. Various mathematical models have been utilized to separate the background signals from the Raman signals, such polynomial fitting (Jirasek et al., 2004; Mazet et al., 2005; Leger and Ryder. 2006; Zhao et al., 2007); wavelet transformation (Ramos and Ruisanchez. 2005; Camerlingo et al., 2006; Hu et al., 2007); and derivatives (O'Grady et al., 2001; Zhang and Ben-Amotz. 2000; Leger and Ryder. 2006). Even though these methods have shown effectiveness in certain situations, they are still suffering some limitations. For instance, the polynomial fitting is not accurate enough and might show poor signal-to-noise ratio (Zhao et al., 2007). The derivatives algorithms change the original spectra shapes which may lead to wrong interpretation of the bioanalytes' structures (Leger and Ryder. 2006). Wavelet algorithms usually transform the signals to different frequency components, and remove the low-frequency

background to rebuild the signal from the wavelet coefficient. As a result, some important spectral information might get lost (Hu et al., 2007). An intelligent background correction algorithm was implemented in our study to remove general-purpose background, including fluorescence from the Raman spectral data (Zhang et al., 2010). This method combines the three major algorithms together to overcome the shortcomings. Briefly, wavelet and wavelet derivative calculation are used to detect peak as well as estimate peak width to obtain a low signal-to-noise/signal-to-ground environments; then the penalized least squares algorithm is used in background fitting, which simulates the background-correction procedure (linear and/or curved). Finally, the corrected Raman spectrum is obtain by subtracting the fitted background. One example of Raman spectrum background correction by using this method is shown in figure 6.1.

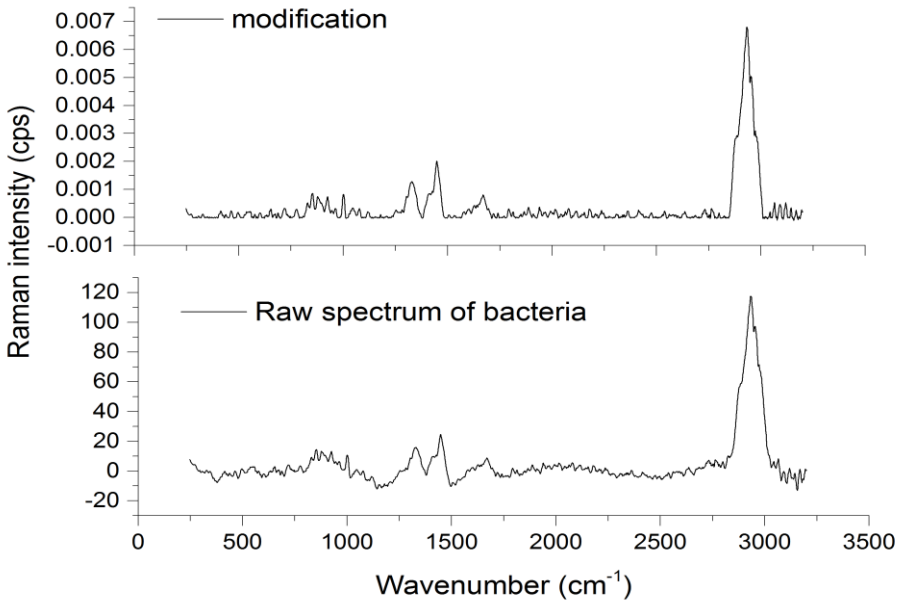

Fig. 6.1 The comparison between the raw bacteria spectrum and the background-correction spectrum of bacteria using the iterative polynomial background removal algorithm

6.2. Multivariate statistical methods

Even though Raman spectroscopy and SERS have been considered as potentially powerful whole-organism fingerprinting techniques, limitations still exist in specific cases. First of all, SERS spectra could suffer inconsistency between measurements due to the uncontrollable nature of quantum effect at nanoscale that leads to variation in enhancement (Shanmukh et al., 2008). Therefore, large database is needed for mathematically reliable results in statistical evaluation. Secondly, it is still challenging to detect and identify bacteria at the strain level because the differences between the spectra obtained from different bacterial strains can be quite subtle. Zeiri et al. (2002) performed SERS by simply conjugating sodium borohydride-reduced silver colloids with target bacterial cells. Very little difference between SERS from the surface of chemically diverse Gram-positive and gram-negative bacteria could be identified. In addition, the complexity of the bacterial chemical composition in single strain is large. Its Raman spectrum usually consists of many overlapping features. It is hence not straightforward to extract species and/or strain specific information (both quantitative and qualitative) from the measured spectra. In recent Raman and SERS research, multivariate statistical techniques have been applied, and shown to be excellent computational tool to automatically handle big database, compress the multi-variable spectra, identify specific bacteria strain, and discriminate between different bacterial strains and species as well. The common multivariate statistical methods include principal components analysis (PCA), discriminant function analysis (DFA), Support

Vector Machines (SVM), and hierarchical cluster analysis (HCA) (Manly. 1994; Jarvis and Goodacre. 2004; Kotsiantis S et al., 2007).

6.2.1. Principle Component Analysis (PCA)

In a Raman spectrum, each wavenumber represents a dimension or variable, which means one Raman spectrum consists over 3 thousands of dimensions. Dealing with data with such high dimensions is usually computationally ineffective. Hence, the first step in statistical analysis of Raman spectral data is usually dimension reduction. PCA is a common statistical technique that is used to reduce the number of dimensions of data with a minimum loss of information. The goal of PCA is to determine the data patterns and underlying factors that cause the similarities and differences of the original data without any prior knowledge. Those factors are orthogonal basis and called principal components (PCs) (He et al., 2008; Yang and Trewn. 2004).

Mathematically, the original spectroscopic data matrix (spectra, Raman intensities) is decomposed into two new matrices, the scores matrix (S) and the loading matrix (L). The relationship between the original matrix and these two new matrices could be shown in the equation $X = L \times S^T$. The variables in the scores matrix are linearly weighted combination of the original X. The PCs are the eigenvectors of the S matrix and the eigenvalues represent the data variance captured by the PCs. The first PC is associated with the highest eigenvalue so it has the largest variance and so on. For each PC score, the influence (weight) of the original spectral data is found in its corresponding loading profile L (matrix of loading). An example of the loading plot is given in figure 6.2 and figure 6.3. PCA is basically the first step for other multivariate

analyses which would use PCs values instead of the original spectral data, and the subsequent analysis can be simplified (Jolliffe. 1986; Davies. 2005; Yang and Trewn. 2004; Brereton. 2007).

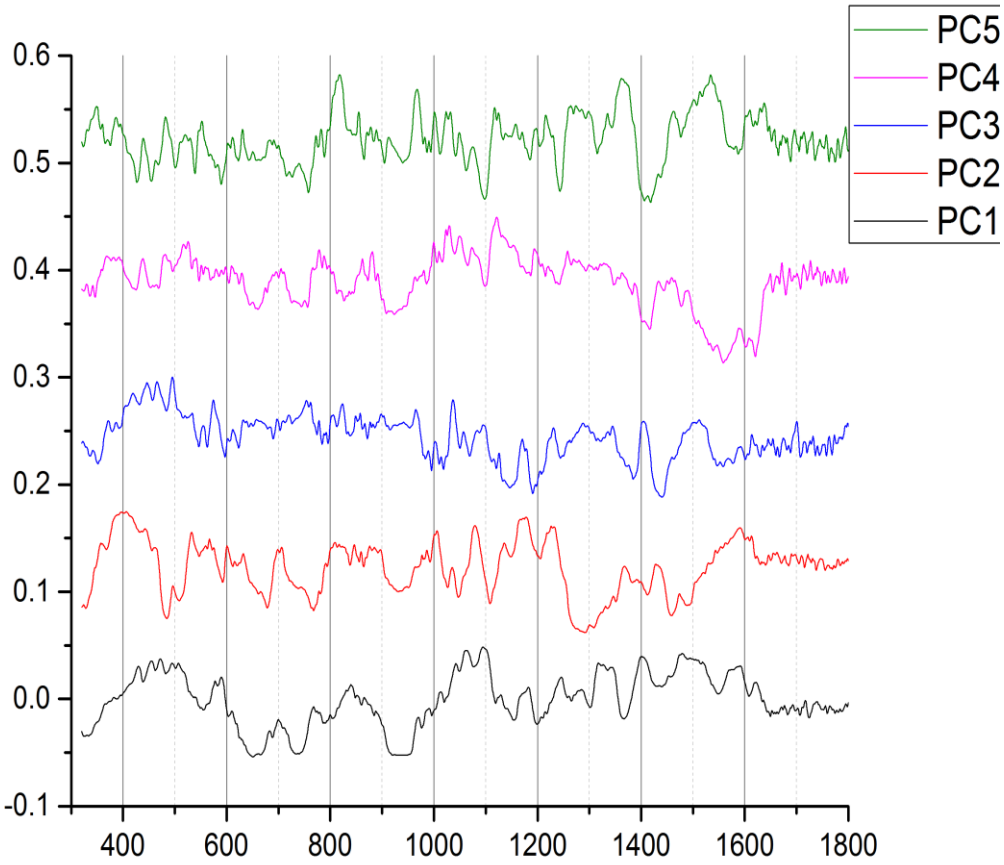

Fig. 6.2 The first 5 principal component loadings of the PCA performed on the SERS spectra acquired from multiplex antibodies functionalized Nanoprobes conjugating with *E.coli* O157: H7 bacteria sample

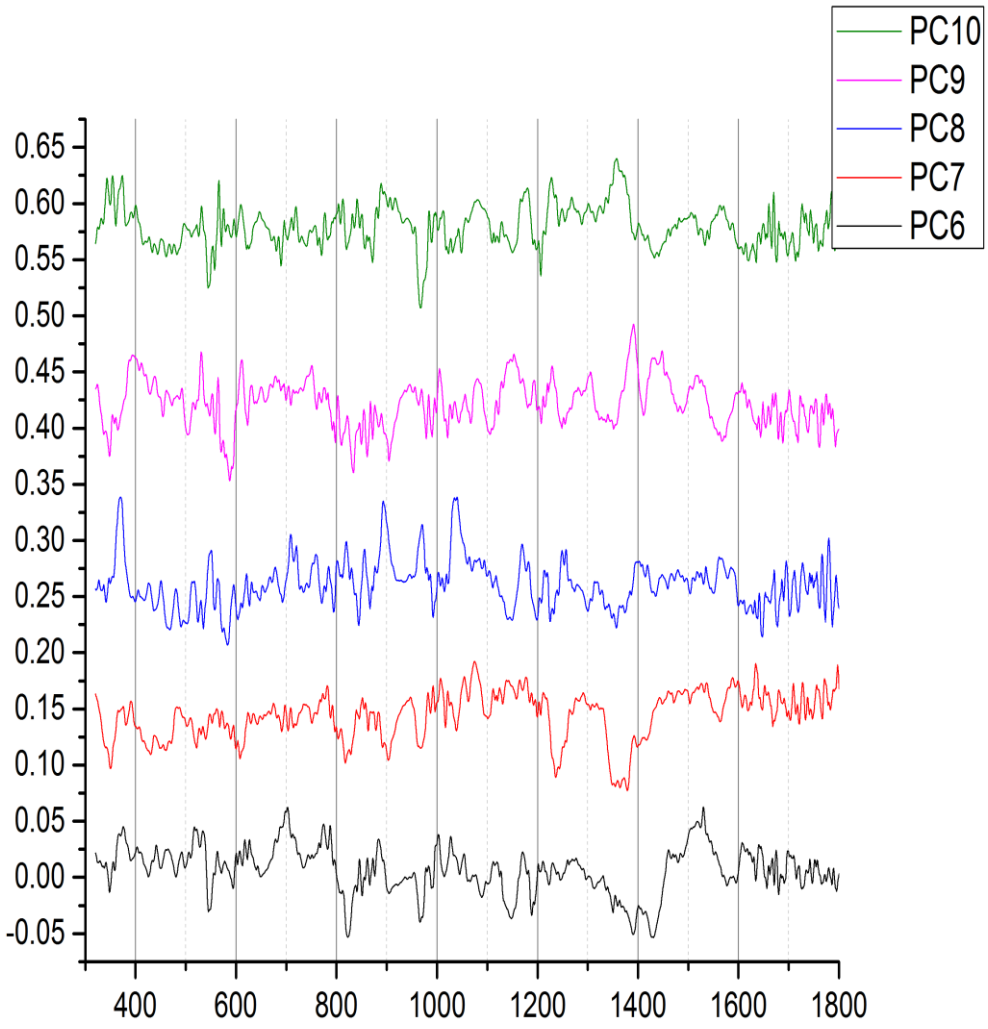

Fig. 6.3 The 5 to 10 principal component loadings of the PCA performed on the SERS spectra acquired from multiplex antibodies functionalized Nanoprobes conjugating with *E.coli* O157: H7 bacteria sample

The peak identification of pure and high-concentration target bacteria cells could be found in Chapter 3. In our study, however, due to the variations of the binding events on the bacterial cell surface, not all the surface chemical components could be enhanced uniformly, and not all featured peaks could be identified in the binding-type (dual signal) spectra. The detectable Raman signals in the binding-type spectra were summarized in Table 3.1. As shown in Fig. 5.9, even though certain amount of microbial peaks could be assigned in the binding-type SERS spectra when the bacteria concentration is at an

extremely low level, the peak intensities of the microbial information are weak compared with Raman tag signals. It compromises the reliability of detecting pathogenic bacteria strains by directly using the multiplex self-referencing SERS strategy. To extract the microbial information from the binding-type spectra and discriminate the featured signals from pathogenic strains, data mining and classification are needed. As we mentioned above, PCA is often used as the first step in multivariate statistical analysis to reduce the data dimensions. And then the component scores will be used in the following discrimination processes instead of original dataset, therefore it will speed up the subsequent analysis. In our study, the first 58 PCs, represented 80% variance in the data, are used in the following analysis to simplify the data processing and increase the classification accuracy.

To quantify the spectral differences responsible for discrimination, the first 10 PC loadings (see figure 6.2 and figure 6.3) were compared to find the most representative loading spectra of bacterial target. It is considered that the second PC loading spectrum showed the highest matching with the bacterial Raman spectra. The spectral contribution from the second PC loading is assigned in figure 6.4. Figure contains the band assignments according to the Raman spectra of the high concentration and pure *E.coli* O157:H7 solution. The 2^{nd} PC loading shows band matching at 731, 850, 1002, 1035, 1093, 1331, 1603, 1660 cm^{-1}. Hence, it is reasonable to assume the 2^{nd} loading represents the main contribution to the superimposed spectra from the target bacteria.

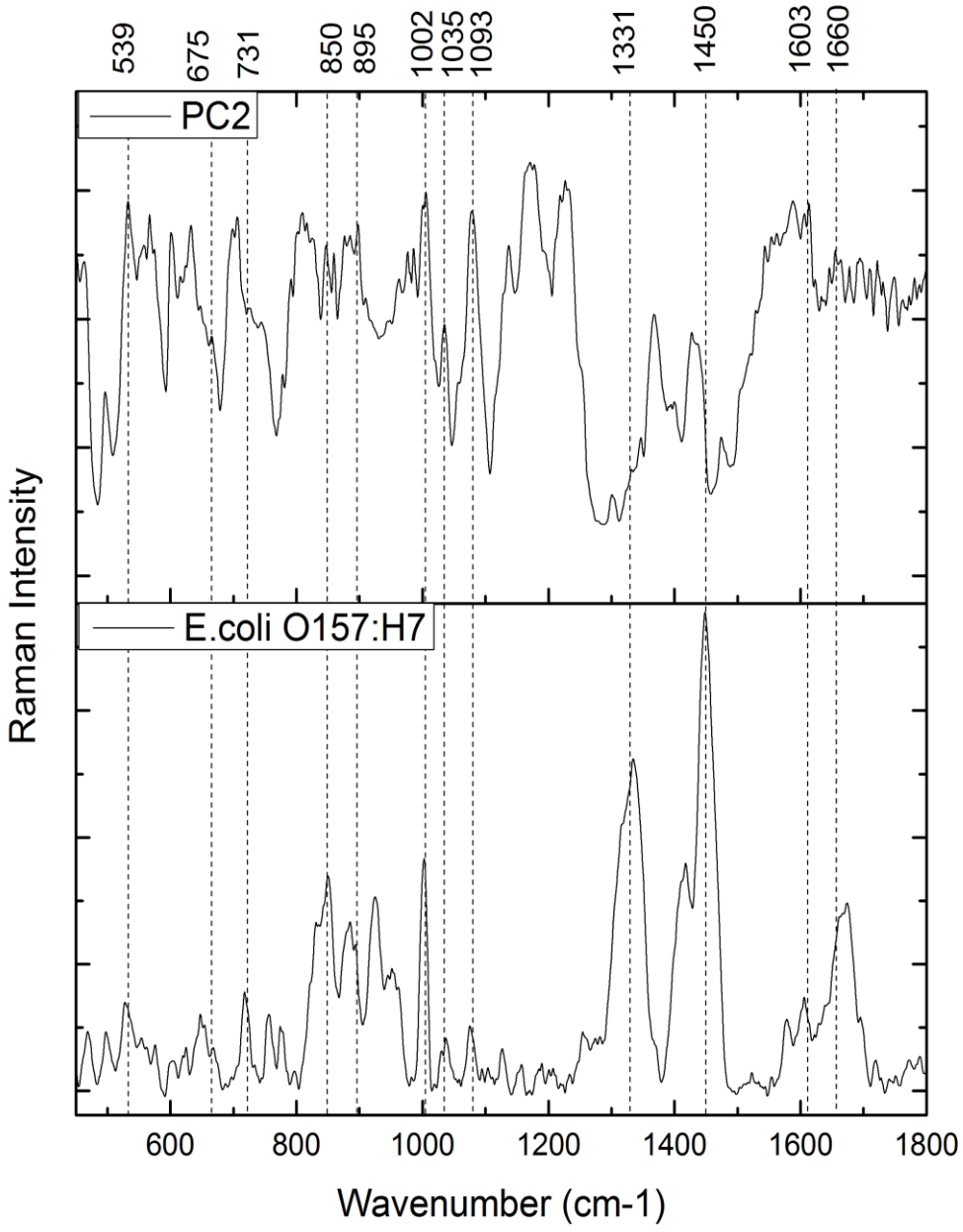

Fig. 6.4 The peak identification of PC2 spectral loading and the normal Raman spectrum of pure & high-concentration Bacterial target cells

6.2.2. Support Vector Machine (SVM)

As we explained in Chapter 4, the purpose of self-referencing scheme is to detect the binding events between SERS-nanoprobes and their target bacterial cells. Only specific binding to targets will yield detectable signal, non-specific binding or no-binding will not yield a signal in this scheme. Therefore, the classification could be

realized by using binary-based algorithm. Among various prediction models, the Support Vector Machine (SVM) is only directly applicable for two-class tasks, which is appropriate to be used in our case. In addition, SVM also shows excellent performance in high dimensional spaces.

SVM is a supervised learning machine. Machine learning is about learning structure from data. Supervised learning is the machine learning task of inferring a function from labeled training data. The training data consist of a set of training examples. In supervised learning, each example is a pair consisting of an input object (typically a vector) and a desired output value (also called the supervisory signal). SVMs are such kinds of learning algorithms that analyze data and recognize patterns, used for classification and regression analysis. Given a set of training examples, each marked as belonging to one of two categories, an SVM training algorithm builds a model that assigns new examples into one category or the other, making it a non-probabilistic binary linear classifier. An SVM model is a representation of the examples as points in space, mapped so that the examples of the separate categories are divided by a clear gap that is as wide as possible. New examples are then mapped into that same space and predicted to belong to a category based on which side of the gap they fall on. In SVMs, the classifier's evaluation is based on prediction accuracy (the percentage of correct prediction divided by the total number of predictions). In linear model, SVM algorithm will construct a separating hyper plane in that space, which maximizes the margin between the two data sets, the smallest distance between the decision boundary and any of the samples. Intuitively, a good separation is achieved by the hyper plane

that have the largest distance to the neighboring data points of both classes, since in general larger the margin, better the classification. The SVM algorithm also assigns a weight to each input point, but most of these weighs are equal to zero. The points having non-zero weight are called support vectors and they can be bounded support vectors (if they take a maximum possible value C) or unbounded support vectors (if their absolute value is smaller than C). The separating hyper plane is defined as a weighted sum of supported vectors.

In addition to performing linear classification, SVMs can efficiently perform a non-linear classification using what is called the kernel trick, implicitly mapping their inputs into high dimensional feature spaces.

Rather than performing prediction analysis using all of the spectroscopic information in the dataset, we use only those spectroscopic components with the strongest estimated correlation with bacterial target. After dimension reduction with PCA, we need to decide which principle components are important. Apparently, we let the computer do most of the work to extract PCs, which is considerable. Among all PCs values, the first 58 PCs, represented 80% data variance, are used for the following SVMs calculation. Linear kernel is used in our SVM model. The two types of SERS spectra (probe and dual) were collected from three separated batches experiments. A sum of 166 spectra are used in the SVM testing, 79 are dual type; 87 are probe type SERS spectra. In this experiment the dataset is randomly split into two subsets: one containing 124 spectra is used to train the SVM model and the second dataset containing 42 spectra is used for the evaluation to validate the established SVM model

by rotating the tested dataset into the same coordinate system as the first dataset. The validation (see Table 6.1) is evaluated by the accuracy percentage (> 95%). The discrimination can be observed by drawing a 2D plot of the first and second principal components scores for each spectrum (see figure 6.5).

Table 6.1 Result of the probe & dual spectra validation with a SVM model (the first 58 PCs are used only)

	SVM testing	
prediction	Probe	Dual
Probe	22	0
Dual	1	19

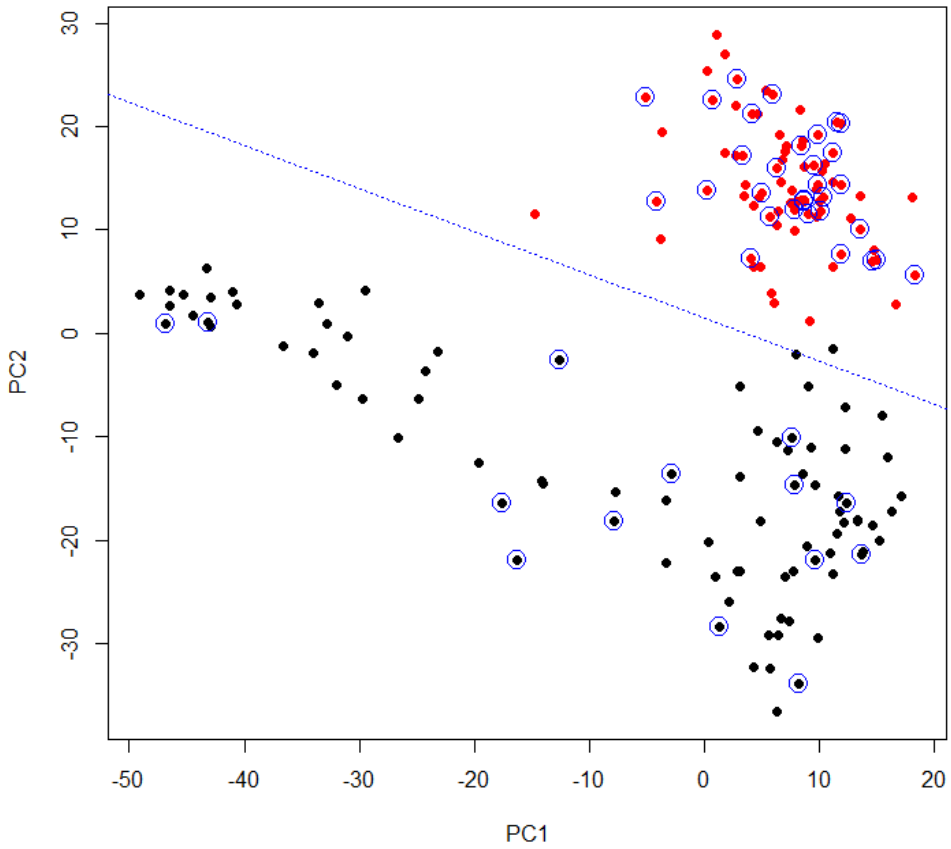

Fig. 6.5 Classification of binding (red dot) and non-binding (black dot) type spectra using SVM. The dash line is the hyperplane showing the optimal linear separation. The blue circles indicate the support vectors.

6.3. Conclusion

To summarize, the statistics based analysis methods, such as preprocessing methods and multivariate methods, are important in analyzing Raman spectra because the spectra usually have many features (background influence, scaling differences, high dimensions interference) which render the complicity of reading and identifying the spectral results. In our statistical analysis scheme, background correction and area normalization are utilized to preprocess the raw data. Then PCA reduces the dimensions

from 3000 wavenumbers to 60 PC values. Then a SVM is performed on the PC scores to discriminate between groups.

6.4. Reference

Afseth NK, Segtnan VH, Wold JP 2006 Raman spectra of biological samples: A study of preprocessing methods *Appl Spectrosc.* 60 1358-1367

Brereton RG. 2007. Applied chemometrics for scientists. Chapter 5 "Pattern recognition". *John Wiley & Sons Ltd.*, Chichester

Camerlingo C, Zenone F, Gaeta GM, Riccio R, Lepore M 2006 Wavelet data processing of micro-Raman spectra of biological samples *Meas. Sci. Technol*. 17 298-303

Davies AMC. 2005 Back to the basics: applications of principal component analysis. Spectroscopy Europe. 17 30-31

Hu YG, Jiang Y, Shen AG, Li W, Wang XP 2007 A background elimination method based on wavelet transform for Raman spectra *Chemometrics Intell. Lab. Syst*. 85 94-101

Jolliffe IT. 1986 Principal Component Analysis. *Springer-Verlag*. New York.

Kotsiantis S, Zaharakis I, et al. 2007 Emerging Artificial Intelligence Applications in Computer Engineering: Supervised Machine Learning: A review of Classification Techniques. *IOS Press. Lansdale PA*

Leger MN, Ryder AG 2006 Comparison of Derivative Preprocessing and Automated Polynomial Baseline Correction Method for Classification and Quantification of Narcotics in Solid Mixtures *Appl. Spectrosc*. 60 182-193

Manly BFJ.1994 Multivariate Statistical Methods: A Primer. *Chapman & Hall*. London

Mazet V, Carteret C, Brie D, Idier J, Humbert B 2005 Background removal from spectra by designing and minimising a non-quadratic cost function *Chemometrics Intell. Lab. Syst.* 76 121-133

Oshima Y, Komachi Y, Furihata C, Tashiro H, Sato H 2006 Fluorescence-Suppressed Raman Technique for Quantitative Analysis of Protein Solution Using a Micro-Raman Probe, the Shifted Excitation Method, and Partial Least Squares Regression Analysis *Appl. Spectrosc*. 60 964-970

O'Grady A, Dennis AC, Denvir D, McGarvey J, Bell SE 2001 Quantitative Raman Spectroscopy of Highly Fluorescent Samples Using Pseudosecond Derivatives and Multivariate Analysis *Anal. Chem*. 73 2058–2065

Ramos PM, Ruisanchez I 2005 Noise and background removal in Raman spectra of ancient pigments using wavelet transform *J. Raman Spectrosc*. 36 848-856

Rinnan A, Van den Berg F, Engelsen SB 2009 Review of the most common pre-processing techniques for near-infrared spectra *Trends in Anal. Chem.* 28 1201-1221

Yang K. Trewn J. 2004 Multivariate Statistical Method in Quanlity Management. New York

Zhang Z, Chen S, Liang Y, et al. 2010 An intelligent background-correction algorithm for highly fluorescent samples in Raman spectroscopy. *Journal of Raman Spectroscopy* 41 659-669

Zhang DM, Ben-Amotz D 2000 Enhanced Chemical Classification of Raman Images in the Presence of Strong Fluorescence Interference *Appl. Spectrosc*. 54 1379-1383

Zhang DM, Mrozek MF, Xie Y, Ben-Amotz D 2004 Chemical Segregation and Reduction of Raman Background Interference Using Drop Coating Deposition *Appl. Spectrosc.* 58 929-633

Zhao J, Lui H, McLean DI, Zeng H 2007 Automated Autofluorescence Background Subtraction Algorithm for Biomedical Raman Spectroscopy *Appl. Spectrosc*. 61 1225-1264

Zeiri L, Bronk BV, Shabtai Y, Czege J, Efrima S 2002 Silver metal induced surface enhanced Raman of bacteria *Colloids Surf. A.* 208 357-362

CHAPTER 7. CONCLUSION AND FUTURE PERSPECTIVE

7.1. Conclusion

In this dissertation, I successfully developed the multiplex self-referencing SERS pathogen (*E.coli* O157: H7) detection biosensor platform which offers high sensitivity (10^1 CFU/mL) and strain level discrimination by measuring the superimposed SERS signatures with multiple characteristic peaks. Furthermore, the superimposed spectra could be obtained directly with no washing being performed. One of the most critical challenging in this scheme is the fabrication of Raman molecular probes with high enhancement factor. To harvest the effective Raman molecular probes, I developed methods to fabricate anisotropic metallic nanoparticles to serve as SERS enhancers, and more importantly, I developed surface modification methodology to add functionality to the SERS enhancers so that they can bind specifically to their pathogen targets for highly accurate and sensitive detection. Gold nanorods (GNRs) and gold/silver nanocages are successfully fabricated with high particle yield. Three highly effective linker molecules (4-Aminothiophenol (4-ATP), 3-Amino-1,2,4-triazole-5-thiol (ATT), and 3-Mercaptopropionic acid (3-MPA)) are identified and designed to conjugate on gold nanostructures, and then different monoclonal antibody molecules are designed to bond to the different linkers through diazo-histine binding (4-ATP and ATT) and EDC/NHS bonding (3-MPA-antibody).

In addition, this platform demonstrated excellent separation and concentration capacities by using DEP microfluidic devices and further improves the sensitivity to 10^0 CFU/mL. The integration of microfluidic devices with SERS detection has yielded

simple and miniaturized instrumentation that is suitable for the detection and characterization of small volume of chemical and biological analytes with high sensitivity and specificity.

Another challenging in my study is spectral data analysis. Raman spectra always suffer the limitation of reliability and reproducibility. Since our Raman molecular probes are at nanoscale, it is difficult to avoid the quantum effect during measurement. Therefore, the inherent inconsistency of SERS spectral signal needs to be dealt with for reliable and reproducible detection results. Various preprocessing methods are used for spectral background removal, baseline correction, smoothing, and normalization. Principle Component Analysis (PCA) is applied to reduce the variable dimensions. A Support Vector Machine (SVM) discriminant analysis model based on statistical multivariate model is being developed for superimposed spectra classification. The validation of spectral classification model (target binding VS no target binding) is evaluated by the accuracy percentage, which is above 95%.

7.2. Future perspective

Despite this novel biosensor platform significantly increase the sensitivity and specificity of waterborne pathogen detection; a few challenges remain to be addressed before this approach can truly become an alternative to the existing techniques. In the future, the optimization of this work would be focusing on integration of SERS measurement within microfluidic device. Although the Nano-DEP device shows high efficiency of trapping microbial cells, the strong fluorescent background effect from Polydimethylsiloxane (PDMS) and Indium tin oxide (ITO) materials used in the device

fabrication limits the possibility of measuring the trapped target bacterial cells inside the device directly. Hence, the microfluidic device is only used for bacterial cells enrichment and the concentrated cells solution is then mixed with Raman probes followed by regular Raman spectroscopic measurement in current stage. In the next step, confocal Raman microscopy is considered to be used to remove the signals of those Raman active materials (Sarrazin and Salmon. 2008). Alternatively, new materials and new molding techniques might be involved in the device fabrication processes to limit the background effect (Luecha et al., 2011). After resolving this challenge, the step of mixing water sample and Raman probes could be implemented at first, then the Nano-DEP device is used to trap the target cells on which surface the multiple probes are conjugated. Focusing points of SERS measurement would be aligned within the device channels. It would significantly increase the possibility of finding the accurate "hot spot" as well as collecting the enhanced spectra. As a result, the time-consuming problem in the data collection would be resolved.

The second challenge we are facing in this scheme is how to mix the bacterial cells solution with Raman probes to obtain a quick and effective conjugation. Furthermore, a complete mixing of sample and probes could improve the SERS signal reproducibility and reliability. Hence, the collection time could be dramatically reduced. A successful microfluidic device design could provide a high-efficient control of the Reynolds number in the microscale channels and increase the turbulence and the dominance of laminar flow, therefore creating an *in situ* mixing function without any other equipment (Schulte et al., 2002). Among the various device design strategies (West et al., 2002;

Yang et al., 2001), 3D passive mixing is one of the most efficient mixing mechanisms (Yasui et al., 2012). In addition, no extra equipment, such as magnetic stir and ultrasonic wave generators would be used in passive mixers. To sum up, in order to provide the potential of a high precise-controlled manipulation of biological samples a real-time portable pathogen detection platform, the future work should pay more attention to the design of microfluidic device, including background Raman signals removing and channels design for complete passive mixing.

The third challenge is to build up a complete database of standard SERS spectra of compounds, or biological samples of interests (e.g., pathogenic microorganisms, biological toxins, pollutants) for more accurate classification and discrimination analysis. Even though the difference between target bacteria binding Raman spectra and non-binding Raman spectra could be identified and classified using multivariate statistical analysis, the enhanced fingerprinting peaks of target bacterial cells observed in the results do not completely match the current reference. The reason might be the lack of the standard spectra of the whole possible components on the bacterial cell surface. From this perspective, our multiplex self-referencing SERS detection mechanism could be considered as an optimized method to obtain a more complete fingerprinting Raman spectral database of target bacteria due to the significant enhancement of the specific surface epitopes paired to the selective antibodies on the Raman molecular probes. One advantage of our multiplex epitopes scheme is unlimited Raman linkers and anti-target antibodies can be functionalized on different nanostructures to facilitate multiple Raman molecular probes. Therefore the Raman

signals of a large amount of epitopes on the same target bacteria cell surface could be enhanced simultaneously. In the future, more than three epitopes scheme are expected to be developed to further increase the sensitivity of detection and complete the database of standard spectra of target microbial structures.

7.3. Reference

Luecha J, Hsiao A, Brodsky S, Liu G, Kokini J 2011 Green microfluidic devices made of corn proteins *Lab Chip*. 11 3419-3425

Sarrazin F, Salmon J 2008 Chemical Reaction Imaging within Microfluidic Devices Using Confocal Raman Spectroscopy: The Case of Water and Deuterium Oxide as a Model System *Anal. Chem*. 80 1689-1695

Schulte T, Bardell R, Weigl B 2002 Microfluidic technologies in clinical diagnostics *Clin. Chim. Acta.* 321 1-10

West J, Karamata B, Lillis B, Gleeson J, Alderman J, Collins J, Lane W, Mathewson A, Berney H 2002 Application of magnetophydrodynamic actuation to continuous flow chemistry *Lab Chip*. 2 224-230

Yang Z, Matsumoto S, Goto H, Matsumoto M, Maeda R 2001 Ultrasonic micromixer for microfluidic systems *Sensors and Actuators* A. 93 266-272

Yasui T, Omoto Y, Osato K, Kaji N, Suzuki N, Naito T, Okamoto Y, Tokeshi M, Shamoto E, Baba Y 2012 Confocal Microscopic Evaluation of Mixing Performance for Three-Dimensional Microfluidic Mixer *Analytical Sciences* 28 57-59

ACKNOWLEDGEMENTS

I would like to thank my supervisor, Dr. Chenxu Yu, for his support, guidance and trust in me. Almost 5 years of research under supervision of someone who knows a lot, but lets you choose your own destiny taught me the wisdom of decisions making.

Additionally, I would like to thank my committee members for advising and questioning me on my project: Dr. Kurt A. Rosentrater, Michelle L. Soupir, Jacek A. Koziel, and Xinwei Wang.

Furthermore, I would like to thank all members of my groups: Qi Wang, Nan Xiao, Shaowei Ding, Tianjian Tong for their support and inspiration.

Special words of appreciation to the collaborators: Dr. Jun Li and his graduate student, Foram Madiyar, in Kansas State University.

I would also like to thank my friends, and the ABE department for making this journey joyful and fun.

And finally I would like to dedicate all my work and experiences here to my family.